

---

Dissertation zur Erlangung des Doktorgrades der  
Naturwissenschaften (Dr. rer. nat.) an der Fakultät für Biologie  
der Ludwig-Maximilians-Universität München

# Cellular functions of the kinase- coupled TRPM6/TRPM7 channels



durchgeführt am

Walther-Straub-Institut für Pharmakologie und Toxikologie der  
Ludwig-Maximilians-Universität München

vorgelegt von

**Silvia Ferioli**

aus Cento (FE), Italien

München, November 2017

---

Die vorliegende Dissertation wurde von März 2012 bis November 2017 unter der Leitung von Prof. Dr. med. Thomas Gudermann und Dr. Vladimir Chubanov am Walther-Straub-Institut für Pharmakologie und Toxikologie der Ludwig-Maximilians-Universität München durchgeführt.

---

Erster Gutachter: **Prof. Dr. Barbara Conradt**

Zweiter Gutachter: **Prof. Dr. med. Thomas Gudermann**

Datum der Abgabe: 23.11.2017

Datum der mündlichen Prüfung: 27.04.2018

---

*Alla mia famiglia...*

# Eidesstattliche Erklärung

Ich versichere hiermit an Eides statt, dass die vorgelegte Dissertation mit dem Titel "Cellular functions of the kinase-coupled TRPM6/TRPM7 channels" von mir selbstständig und ohne unerlaubte Hilfe angefertigt wurde.

München, den 23.11.2017

Silvia Ferioli

## Erklärung

Hiermit erkläre ich,

- dass die Dissertation nicht ganz oder in wesentlichen Teilen einer anderen Prüfungskommission vorgelegt worden ist.
- dass ich mich anderweitig einer Doktorprüfung ohne Erfolg nicht unterzogen habe.

München, den 23.11.2017

Silvia Ferioli

# Abstract

TRPM6 and TRPM7 are bifunctional proteins containing an ion channel segment covalently linked to a kinase domain. Both proteins function as divalent cation-selective channels highly permeable to  $Mg^{2+}$  and  $Ca^{2+}$ , whose activity is regulated by intracellular levels of  $Mg^{2+}$  and Mg-ATP. TRPM7 has been found in all mammalian cells investigated so far, while expression of TRPM6 is restricted to epithelial cells of the kidney, intestine and placenta. TRPM6 and TRPM7 have been proposed to be required for cellular  $Mg^{2+}$  homeostasis. However, the exact role of TRPM7 in the regulation of  $Mg^{2+}$  metabolism remains poorly understood and discussed controversially. Loss-of-function mutations in the human *TRPM6* gene give rise to an autosomal recessive disorder called hypomagnesemia with secondary hypocalcemia (HSH). It has been suggested that in epithelial cells TRPM6 functions primarily as a constituent of heteromeric TRPM6/M7 channel complexes, but this concept has not been thoroughly examined. Therefore, the main goal of this work was to define the cellular function of TRPM6 and TRPM7 in cells either expressing only TRPM7 or co-expressing both proteins, TRPM6 and TRPM7. In the first line of our experiments, we generated and functionally characterized three different cell lines deficient in TRPM7 such as mouse trophoblast stem (TS) cells, human haploid leukaemia (HAP1) cells and primary isolated mouse megakaryocytes (MKs). Using the patch-clamp approach, we showed that all three cell lines lacked endogenous TRPM7 divalent cation-selective currents. We also found that TRPM7 deficient TS and HAP1 cells developed  $Mg^{2+}$  deficiency and growth arrest, which could be rescued by increased levels of  $Mg^{2+}$  in the culture medium. TRPM7 deficient MKs were viable but exhibited reduced  $Mg^{2+}$  contents and impaired proplatelet formation. Similar to TS and HAP1 cells, the changes in MKs were reversed by  $Mg^{2+}$  supplementation. We concluded that the TRPM7 channel controls the cellular  $Mg^{2+}$  uptake necessary for the cell proliferation. To get insights into the cellular role of the native TRPM6 protein, we generated TRPM6 deficient TS cells. We observed that, in contrast to TRPM7 KO TS cells, TRPM6 deficient TS cells were able to proliferate in a medium not fortified by additional  $Mg^{2+}$ . Furthermore, the currents in TRPM6 KO TS cells were reduced and more sensitive to cytosolic Mg-ATP compared to the WT TS cells. These findings are in line with the notion that endogenous TRPM6 functions as a subunit of heteromeric TRPM6/M7 channel complexes, where TRPM6 potentiates  $Mg^{2+}$  currents due to offset of the inhibitory effect of Mg-ATP. Our experiments with the endogenous TRPM6 and TRPM7 channels were further verified

using recombinant TRPM6 and TRPM7 proteins overexpressed in HEK 293 cells. We observed that the recombinant TRPM6 and TRPM7 channels contribute differently to the functional characteristics of the heteromeric TRPM6/M7 channels mimicking the situation with TS cells lacking endogenous TRPM6. Most remarkably, we found that association of TRPM6 with TRPM7 results in large TRPM6/M7 currents insensitive to cytosolic levels of Mg-ATP. Taken together, we conclude that ubiquitously expressed TRPM7 is required for the cellular uptake of Mg<sup>2+</sup> and that this function cannot be compensated by TRPM6. Association of TRPM6 in heteromeric TRPM6/M7 channel complexes allows to maintain a high rate of Mg<sup>2+</sup> uptake in transporting epithelial cells.

---

# Abbreviations

2-APB	2-aminoethyl diphenylborinate
Ab	antibody
APS	ammonium peroxydisulphate
ATP	adenosine triphosphate
BAPTA	1,2-bis(o-aminophenoxy)ethane-N,N,N',N'-tetraacetic acid
bp	base pair
BSA	bovine serum albumin
CC	coiled-coil (domain)
cDNA	complementary DNA
DCT	distal convoluted tubule
DMSO	dimethyl sulfoxide
DNA	deoxyribonucleic acid
dNTP	deoxyribonucleotide triphosphates
DPBS	Dulbecco's phosphate buffered saline
DTT	dithiothreitol
DVF	divalent cation-free solution
ECL	enhanced chemiluminescence
EDTA	ethylenediaminetetraacetic acid
EGFP	enhanced green fluorescent protein
EGTA	ethylene glycol-bis( $\beta$ -aminoethyl ether)-N,N,N',N'-tetraacetic acid
FBS	fetal bovine serum
FGF4	fibroblast growth factor 4
Fwd	forward
GAPDH	glyceraldehyde 3-phosphate dehydrogenase
HAP1 cells	human leukemia haploid cells
HEPES	4-(2-Hydroxyethyl)piperazine-1-ethanesulfonic acid
HEK 293 cells	human embryonic kidney 293 cells
HPR	horseradish peroxidase
HSH	hypomagnesemia with secondary hypocalcemia
IC <sub>50</sub>	half-maximal inhibitory concentration
IgG	immunoglobulin G
IMDM	Iscove's modified Dulbecco's medium
IP	immunoprecipitation
IRES	internal ribosome entry site
ISH	<i>in situ</i> hybridization
I-V	current-voltage relationship

---

KO	knockout
MEM	Eagle's minimum essential medium
MagNum	magnesium nucleotide-regulated metal ion currents
MIC	Mg <sup>2+</sup> -inhibited cation currents
MKs	mekacaryocytes
mRNA	messenger RNA
n.f.	nominally free
NMDG	N-methyl-D-glucamine
NEAA	non-essential amino acids
NeoR	neomycin resistance cassette
NTD	neural tube defect
PCR	polymerase chain reaction
Pf4	platelet factor 4
PIP <sub>2</sub>	phosphatidylinositol 4,5-bisphosphate
PMEF	primary mouse embryonic fibroblasts
Rev	revers
RNA	ribonucleic acid
RPMI	Roswell Park Memorial Institute medium
R <sub>s</sub>	series resistance
RT-PCR	reverse transcription-polymerase chain reaction
SDS	sodium dodecyl sulfate
SDS-PAGE	sodium dodecyl sulfate-polyacrylamide gel electrophoresis
SEM	standard error of the mean
SP	splice acceptor site sequence
TAE	tris-acetate-EDTA
<i>Taq</i>	DNA-polymerase from <i>Thermus aquaticus</i>
TBS	tris-buffered saline
TBST	tris-buffered saline with Tween 20
TGF-β1	transforming growth factor beta 1
TGM	tris-glycine-methanol
TGS	tris-glycine-SDS
Thpo	thrombopoietin
TMs	transmembrane segments
TRP	transient receptor potential channels
TRPM6	transient receptor potential melastatin 6 channel
TRPM7	transient receptor potential melastatin 7 channel
TS cells	trophoblast stem cells
UTR	untranslated region
WT	wild type

# Table of Contents

<b>Eidesstattliche Erklärung</b> .....	<b>i</b>
<b>Abstract</b> .....	<b>ii</b>
<b>Abbreviations</b> .....	<b>iv</b>
<b>Table of Contents</b> .....	<b>vi</b>
<b>1. Introduction</b> .....	<b>1</b>
1.1. TRP channel superfamily .....	1
1.1.1. Phylogenetic groups of TRP channels .....	1
1.1.1.1. Group 1 TRP subfamilies.....	3
1.1.1.2. Group 2 TRP subfamilies.....	5
1.2. Melastatin-related TRP (TRPM) channels .....	5
1.2.1. TRPM6 and TRPM7 kinase-coupled channels.....	7
1.2.1.1. Expression patterns of TRPM6 and TRPM7 .....	7
1.2.1.2. Domain organization of TRPM6 and TRPM7 .....	9
1.2.1.3. Ion permeation profiles of TRPM6 and TRPM7 channels .....	10
1.2.1.4. Regulation of TRPM6 and TRPM7 channels .....	11
1.2.1.5. Modulation of TRPM6 and TRPM7 by small organic drug-like ligands .	12
1.2.1.6. The suggested physiological functions of TRPM7 .....	13
1.2.1.7. Physiological implications of the TRPM6 channel.....	14
1.3. Mg <sup>2+</sup> homeostasis.....	16
1.3.1. Mg <sup>2+</sup> channels and transporters .....	17
1.3.2. Roles of TRPM6 and TRPM7 in organismal Mg <sup>2+</sup> balance .....	19
1.4. Aims of this work .....	23
<b>2. Materials</b> .....	<b>24</b>
2.1. Chemicals, enzymes and commercial kits .....	24
2.2. Cell culture media and supplements.....	26

---

2.3. Antibodies .....	27
2.4. Oligonucleotides.....	28
2.5. cDNA expression constructs.....	29
2.6. Buffers and standard solutions .....	30
2.7. Consumables .....	31
2.8. Equipment.....	32
2.9. Software.....	34
<b>3. Methods.....</b>	<b>35</b>
3.1. Isolation and characterization of <i>Trpm6</i> and <i>Trpm7</i> deficient trophoblast stem (TS) cells.....	35
3.1.1. Mouse strains .....	35
3.1.2. Mouse genotyping.....	36
3.1.3. Housing of mice .....	39
3.1.4. Isolation of TS cells.....	40
3.1.5. Maintaining of TS cell lines .....	40
3.2. Generation of <i>TRPM7</i> deficient HAP1 cells .....	41
3.3. Assessment of primary mouse megakaryocytes.....	42
3.4. Culture and transient transfection of HEK 293 cells.....	43
3.5. Generation of mouse TRPM6 cDNA expression constructs.....	43
3.6. Reverse transcriptase PCR (RT-PCR) analysis.....	43
3.6.1. RT-PCR analysis of <i>Trpm6</i> deficient TS cells.....	44
3.6.2. RT-PCR analysis of <i>Trpm7</i> deficient TS cells.....	45
3.6.3. RT-PCR analysis of <i>TRPM7</i> deficient HAP1 cells .....	46
3.7. Western blot analysis .....	48
3.7.1. Assessment of recombinant TRPM6 and TRPM7 proteins in HEK 293 cells .....	48
3.7.2. Assessment of endogenous TRPM6 and TRPM7 in TS and HAP1 cells....	49
3.8. Patch-clamp assessment of TRPM6 and TRPM7 currents .....	49

---

3.8.1. Examination of the endogenous TRPM7-like currents in TS, HAP1 and MK cells .....	50
3.8.2. Patch-clamp experiments with recombinant TRPM6 and TRPM7 .....	52
3.9. Statistical analysis .....	53
<b>4. Results.....</b>	<b>55</b>
4.1. Elucidating the role of the endogenous TRPM7 currents in cellular Mg <sup>2+</sup> uptake .....	55
4.1.1. Assessment of TRPM7 function in TS cells.....	55
4.1.2. Role of TRPM7 in HAP1 cells .....	60
4.1.3. Assessment of TRPM7 activity in primary megakaryocytes.....	63
4.2. Contribution of TRPM6 to endogenous divalent cation currents .....	64
4.2.1. Functional characterization of <i>Trpm6</i> gene deficient TS cells.....	64
4.2.2. Assessment of native currents in <i>Trpm6</i> gene deficient TS cells.....	67
4.2.3. Effects of cytosolic Mg <sup>2+</sup> and Mg-ATP on currents in WT and <i>Trpm6</i> deficient TS cells.....	69
4.2.4. Assessment of constitutive channel activity in WT and <i>Trpm6</i> deficient TS cells .....	70
4.3. Characterization of recombinant mouse TRPM6 .....	72
4.3.1. Heterologous expression of mouse TRPM6 cDNA in HEK 293 cells.....	72
4.3.2. Patch-clamp analysis of HEK 293 cells expressing mouse TRPM6.....	73
4.3.3. Cation permeability of the mouse TRPM6 channel.....	76
4.3.4. The mouse TRPM6 channel is highly sensitive to intracellular Mg <sup>2+</sup> .....	81
4.3.5. Modulation of TRPM6 and TRPM7 by pharmacological compounds.....	84
4.3.6. Assessment of heteromeric TRPM6/M7 channel complexes.....	88
<b>5. Discussion.....</b>	<b>93</b>
5.1. TRPM7 controls cellular Mg <sup>2+</sup> metabolism .....	93
5.2. TRPM6 cooperates with TRPM7 in TS cells .....	95

5.3. Interplay of TRPM6 and TRPM7 channels determines the sensitivity of TRPM6/M7 channels to cytosolic Mg<sup>2+</sup> and Mg-ATP ..... 98

**6. Conclusions ..... 101**

**References ..... 102**

**Acknowledgments ..... 118**

**Curriculum vitae ..... 120**

# 1. Introduction

## 1.1. TRP channel superfamily

The transient receptor potential (TRP) gene family represents a noteworthy group of ion channels with a high variety in physiological functions, ion selectivity and activation mechanisms [1]. Nevertheless, TRP channels also display common characteristics. All TRP proteins comprise six transmembrane segments and are permeable to cations [1]. A common feature among TRP channels is their importance in sensory physiology. Generally, TRP proteins play essential roles in the organismal responses to a wide range of external stimuli, including temperature, sound, light, touch and chemicals [1]. The mammalian TRP protein family, with its 28 members, is broadly expressed in the nervous system and in non-excitabile cells [2, 3]. TRP proteins exist in a diversity of eukaryotic organisms including humans, mice, zebrafish, fruit flies, worms and yeast [1].

### 1.1.1. Phylogenetic groups of TRP channels

The TRP superfamily includes an increasing number of cation channel proteins characterized by their homology to the *Drosophila* TRP channel, the founding member of this superfamily [1, 4]. On the basis of primary amino acid sequence identity, the superfamily has been divided into two groups (group 1 and 2), which are subdivided into seven subfamilies (Fig. 1.1). Group 1 comprises TRPC (Canonical), TRPV (Vanilloid), TRPM (Melastatin), TRPA (Ankyrin) and TRPN (no mechanoreceptor potential C, NOMPC). Group 2 contains TRPP (Polycystin) and TRPML (Mucolipin) [1, 5]. The eighth subfamily, TRPY, comprises yeast TRP proteins [1].

TRP channels contain six putative transmembrane segments (6 TMs), cytosolic amino- (N-) and carboxy- (C-) termini, and a short hydrophobic stretch located between TM5 and TM6 forming the channel pore [4, 6]. Similar to other 6 TMs channels, TRP channels exist in the form of either homo- or hetero-multimers of four TRP subunits [6-8]. The structure of seven TRP channels (TRPV1, TRPV2, TRPV6, TRPP2, TRPA1, TRPC3, and *Drosophila* NOMPC) has been recently determined by cryo-electron microscopy [9-19]. Overall, these experiments confirmed the initial hypothesis that TRP proteins form tetramers and have a pore-forming segment located between TM5 and TM6.

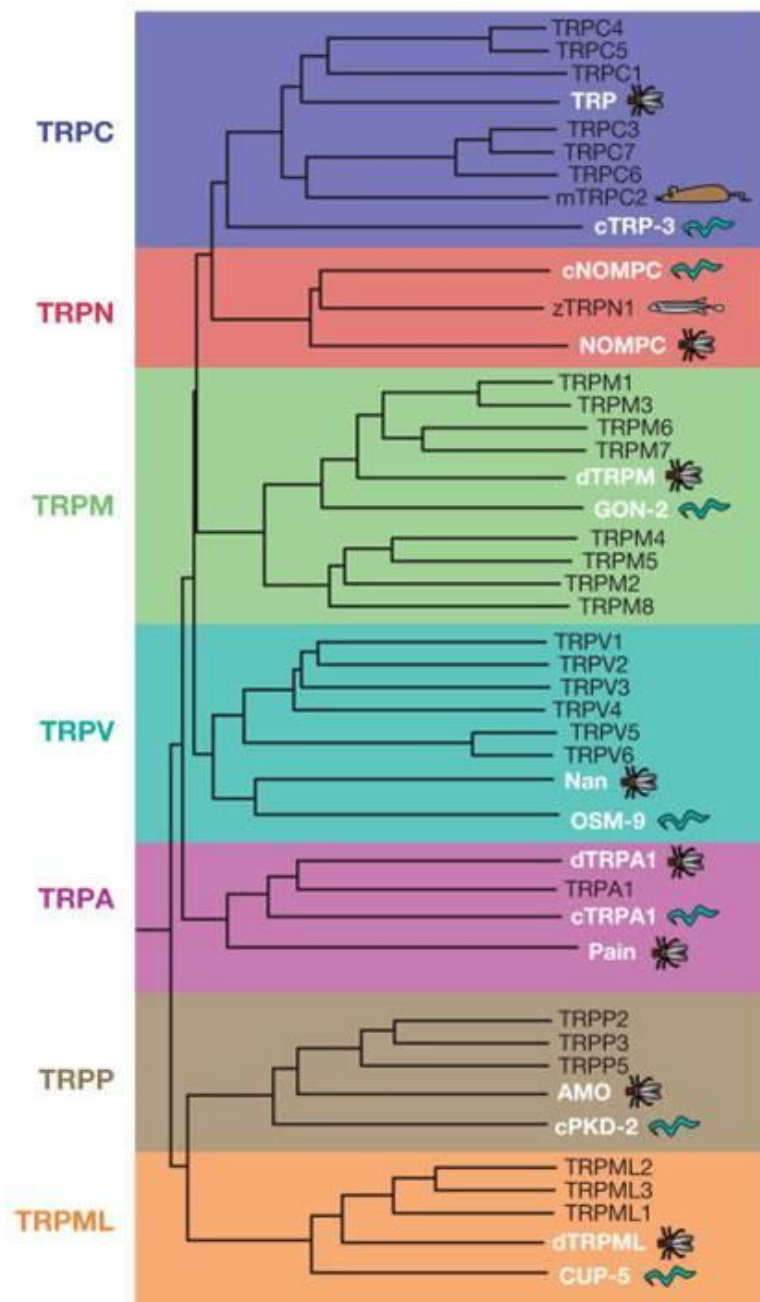


**Figure 1.1. Phylogenetic tree of the TRP gene family.** The dendrogram includes all human TRP subfamilies (black text), mouse TRPC2, and zebrafish TRPN1. Moreover, one *C. elegans* and one *Drosophila* member of each subfamily are shown. Figure taken from [1].

Apart from TRPM channels, TRP proteins in group 1 possess multiple N-terminal ankyrin repeats. Ankyrin repeats are 33-residue domains, which are usually involved in protein-protein interactions [1, 6, 20]. The next highly conserved structural feature of TRPC, TRPM, and TRPN (except for NOMPC) channels is the presence of a TRP domain, which consists of 23-25 residues immediately C-terminal to TM6 [5]. The most

conserved segment of the TRP domain is the TRP box 1 motif composing only 6 amino acids (EWKFAR in TRPC channels) [1, 2, 21]. Another characteristic region present in TRPM and TRPC channels is the so-called coiled-coil (CC) domain, supposed to play a role in channel assembly and trafficking [22-25] (Fig. 1.2).

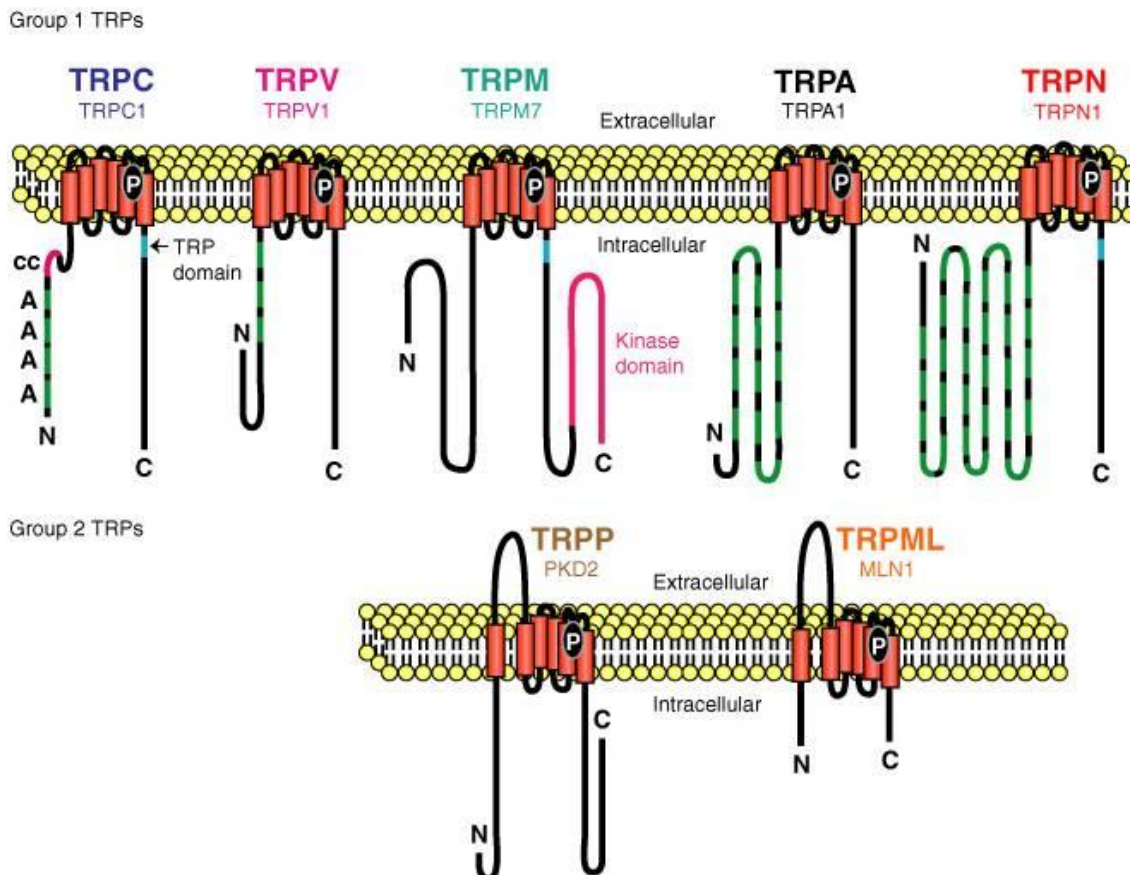


**Figure 1.2. The seven TRP subfamilies.** Representative members from each of the TRP subfamilies are illustrated. Transmembrane segments (red *tubes*), N- and C-termini, and a pore loop (P) located between TM5 and TM6 are commonly present in all TRP proteins. Uncommon domains are also present in some groups: coiled-coil domain (CC), ankyrin repeats (A), TRP domain and protein kinase domain (present only in TRPM6/7). Figure taken from [5].

#### 1.1.1.1. Group 1 TRP subfamilies

**The TRPC subfamily.** The first identified members of TRP channels were named “canonical” or “classical” TRPs and were included in the TRPC subfamily [5]. *Drosophila* TRP, the founding member of this subfamily, was the first discovered TRP channel [26]. Three known *Drosophila* TRP channels are required for maintaining the light responses of photoreceptor cells [26-28]. *trp* gene mutations cause the response to light to be transient associated with a ~10-fold decrease in the level of light-induced

calcium ( $\text{Ca}^{2+}$ ) influx in photoreceptor cells [29]. In mammals, seven TRPC proteins have been identified, distributed into four groups on the basis of amino acid sequence similarity and functional properties: TRPC1, TRPC4/5, TRPC3/6/7 and TRPC2 [2, 30, 31]. These channels display a large amino acid similarity to the *Drosophila* TRP and comprise three to four ankyrin repeats [2]. Mammalian TRPC proteins form non-selective cation channels [2].

**The TRPV subfamily.** TRPV1, the archetypal mammalian TRPV member, was found during an expression cloning experiment aimed to produce a channel activated by vanilloid compounds, such as capsaicin [32]. On the basis of their amino acid sequence homology, ion selectivity and mechanisms of activation, mammalian TRPV proteins are subdivided into two groups: TRPV1–V4 and TRPV5/V6 [3]. TRPV1–V4 are called thermo-TRP channels, as they are activated by heat [3]. TRPV proteins contain three to six ankyrin repeats, lack a TRP box and display ~25% amino acid similarity with TRPC proteins [6].

**The TRPM subfamily.** The melastatin-related subfamily consists of eight proteins (TRPM1-8) in mammals, which were denominated after the first discovered member, melastatin or TRPM1 [1, 3, 25]. Members of this subfamily, TRPM6 and TRPM7, are the subject of this study, and will be described in greater details in section 1.2.

**The TRPA subfamily.** The human TRPA1, the first discovered member of this subfamily, was found by screening for the identification of genes down-regulated after oncogenic transformation of human fibroblasts [1, 33]. Mammals contain only one gene of the subfamily, TRPA1. TRPA1 is a non-selective  $\text{Ca}^{2+}$ -permeable channel and is chemically activated by several pungent compounds present in mustard oils, the psychoactive compound of marijuana (tetra-hydrocannabinol or THC) and bradykinin [34, 35]. A particular feature of TRPA proteins is the presence of high numbers of N-terminal ankyrin repeats [5].

**The TRPN subfamily.** Several TRPN genes exist in invertebrate species (such as flies, worms) and non-mammalian vertebrates (fish, amphibians) [1]. *Drosophila* NOMPC (no mechanoreceptor potential C), the founding member of the subfamily, is involved in mechanosensory transduction [5, 36]. TRPN members contain 29 ankyrin repeats N-terminal to TM6 and exhibit ~20% amino acid sequence similarity with TRPC proteins [1].

### 1.1.1.2. Group 2 TRP subfamilies

TRP proteins from the group 2 display a relatively high homology to each other, but a low primary amino acid sequence identity to the group 1 TRP channels [5]. Unlike other TRP channels, the group 2 proteins contain an extensive extracellular loop between TM1 and TM2 [5]. Nevertheless, the members of the group 2 contain a channel segment comprising six TMs [5].

**The TRPP subfamily.** The archetypal TRPP channel is TRPP2 (polycystin-2 or PKD2) [1]. Mutations in the human PKD2 underline the autosomal dominant polycystic kidney disease (ADPKD) [37]. Additionally to PKD2, this subfamily contains two other mammalian channels, named TRPP3 (PKD2L1, polycystin-L, PCL) [38, 39] and TRPP5 (PKD2L2) [40, 41]. TRPP proteins are  $\text{Ca}^{2+}$ -permeable ion channels, which display ~25% amino acid sequence similarity with TRPC proteins [5]. TRPP2 proteins lack ankyrin repeats and the TRP domain [2].

**The TRPML subfamily.** The TRPML subfamily was found by a discovery of the human TRPML1 channel (mucolipidin1; ML1) [5]. Mutations in the human TRPML1 gene are associated with a lysosomal storage disorder (mucopolipidosis type IV) [42-44]. Besides TRPML1, two other closely related subfamily members, TRPML2 and TRPML3, exist in mammals [5]. The mammalian TRPML proteins show a very limited sequence homology to TRPC proteins [5].

## 1.2. Melastatin-related TRP (TRPM) channels

The mammalian members from the TRPM subfamily exhibit ~20% primary amino acid sequence similarity with TRPC proteins and, similar to TRPCs, they possess a TRP domain placed C-terminal to TM6 [1, 2]. Sequence comparison of the channel pore-forming segment (TM5-TM6) reveals that the pore-forming sequence is highly conserved among all proteins of the TRPM subfamily [4]. TRPM proteins are devoid of ankyrin repeats and their N-terminal domain is substantially longer than the analogous region in TRPV and TRPC channels [2]. The TRPM subfamily contains eight members subdivided into five groups: TRPM1/3, TRPM4/5, and TRPM6/7; TRPM2 and TRPM8 display a very low amino acid sequence identity and thus represent independent groups [3]. TRPM2, TRPM6, and TRPM7 possess the particular feature to contain enzymatically active proteins fused to their ion channel segments (therefore entitled as chanzymes) [1, 3].

The first mammalian member of the TRPM subfamily, TRPM1 (or melastatin), was identified as a putative melanoma marker [1]. Duncan *et al.* demonstrated an inverse correlation between the expression levels of this protein and the metastatic potential in human melanoma cell lines [45]. Besides the full-length clone (TRPM1-L), a short isoform of TRPM1 (TRPM1-S) lacking predicted transmembrane segments was cloned [1]. TRPM1-S was shown to interact and inhibit TRPM1-L trafficking to the plasma membrane [46]. Functional properties of the TRPM1 channel remain poorly understood. Its closest relative protein, TRPM3, is mainly expressed in human kidney and brain where it functions as a constitutively active  $\text{Ca}^{2+}$ -permeable cation channel [47]. Currents mediated by TRPM3 are activated by heat, cell swelling and steroids like pregnenolone sulphate (PS) [47-50]. It has been found that various splice variants of TRPM3 can affect ion selectivity of the channel [51]. TRPM3 functions as a thermosensitive nociceptor channel implicated in the noxious heat detection [48, 50]. Recent reports showed that the TRPM3 channel is inhibited by agonists of G protein-coupled receptors like  $\mu$ -opioid, GABA-B and neuropeptide Y receptors [52-55]. This inhibition occurs through direct binding of the  $\text{G}\beta\gamma$  subunits to the TRPM3 channel [52-55].

TRPM4 [56] and TRPM5 [57] are uncommon TRP channels as they are  $\text{Ca}^{2+}$ -activated, voltage-modulated and monovalent cation-selective channels. At physiological conditions, these channels are activated by G protein-coupled receptors linked to phospholipase C (PLC) induced  $\text{Ca}^{2+}$  raises [56, 57]. TRPM4 has two splice variants, one of which (TRPM4a) displays very low (if any) channel activity, whereas the second (TRPM4b) is a highly active splice variant [56]. TRPM5 is expressed in chemosensory cells, such as the taste receptor cells [58], where it is required for bitter, sweet, and umami taste sensations [59].

TRPM2 is a chanzyme containing a C-terminal ADP-ribose pyrophosphatase domain [60, 61]. This protein functions as a  $\text{Ca}^{2+}$ -permeable cation channel, and is activated by intracellular pyrimidine nucleotides, ADP-ribose and nicotinamide adenine dinucleotide (NAD) [60, 61]. TRPM2 acts as cellular redox sensor: it is activated by hydrogen peroxide and other reactive oxygen/nitrogen species [62, 63].

TRPM8 is a non-selective cation “thermoTRP” channel, which is activated by cold temperatures (8-28°C) and by ‘cooling’ compounds, such as eucalyptol, menthol, and icilin [64, 65]. TRPM8 is specifically expressed in sensory neurons functioning as cold sensors [64, 65].

### 1.2.1. TRPM6 and TRPM7 kinase-coupled channels

Among known ion channels, TRPM6 and TRPM7 are unique since they contain C-terminal functional kinase domains [66, 67]. TRPM6 and TRPM7 are highly homologous channels with a global primary amino acid sequence similarity of 52%, which rises to >80% in the pore-forming region between TM5 and TM6 [68]. Both proteins were found to be linked to the regulation of cellular magnesium ( $Mg^{2+}$ ) homeostasis. Chicken DT40 B lymphocytes with a targeted gene deletion of TRPM7 developed  $Mg^{2+}$  deficiency and underwent growth arrest [67, 69], whereas loss-of-function mutations in the human *TRPM6* gene cause an autosomal recessive disorder, named hypomagnesemia with secondary hypocalcemia (HSH) [70, 71]. TRPM6 is highly expressed in the kidney and intestine [68, 70, 71], whereas TRPM7 shows a ubiquitous expression profile [66, 67]. TRPM6 and TRPM7 form divalent cation-selective channels, conducting a wide range of divalent cations including  $Ca^{2+}$  and  $Mg^{2+}$  [72]. TRPM6 and TRPM7 channels are regulated by intracellular  $Mg^{2+}$  and Mg-ATP [67, 68], and phosphatidylinositol 4,5-bisphosphate ( $PIP_2$ ) levels [73, 74].

TRPM7 was cloned independently by three groups. In a first group, TRPM7 was discovered in the effort to identify phospholipase C (PLC)-interacting proteins with similarity to eukaryotic elongation factor 2 kinase (eEF-2 kinase) and *Dictyostelium* myosin heavy chain kinase B (MHCK B) [66]. In a second group, TRPM7 was identified by screening for homologues of human eEF-2 kinase [75]. Finally, a third group cloned mouse and human TRPM7 aiming at identifying novel  $Ca^{2+}$ /cation channels expressed in haematopoietic cells [67]. Accordingly, this protein was named TRP-PLIK (TRP-Phospholipase C Interacting Kinase) [66], LTRPC7 (Long TRP Channel 7) [67] or ChaK1 (Channel-Kinase 1) [76].

TRPM6 was originally discovered by Ryazanova *et al.* in screening experiments to identify homologues of human eEF-2 kinase [75]. In follow-up efforts, two other groups showed independently that TRPM6 mutations are linked to HSH [70, 71]. TRPM6 was also known as TRP-PLIK2, LTRPC6 or Chak2.

#### 1.2.1.1. Expression patterns of TRPM6 and TRPM7

The human *TRPM7* gene is located on chromosome 15q21.2 (NCBI Gene ID 54822) and encodes a protein of 1,865 amino acids (~220 kDa). TRPM7 orthologs have been found in mouse (*Mus musculus*), chimpanzee (*Pan troglodytes*), rat (*Rattus norvegicus*), dog (*Canis familiaris*) and cow (*Bos taurus*) (GeneCards). TRPM7 was

also identified in non-mammalian genetically tractable organisms, in particular, in Zebrafish (*Danio rerio*) and *Xenopus laevis* [25].

In *Homo sapiens*, the *TRPM6* gene is located on chromosome 9q21.13 (NCBI Gene ID 140803) and the full-length isoform encodes a protein of 2,022 amino acids (~230 kDa) [71, 77, 78] (Fig. 1.3A). TRPM6 orthologs were identified in all vertebrate species, including *Rattus norvegicus*, *Mus musculus* and *Danio rerio* (GeneCards) [78].

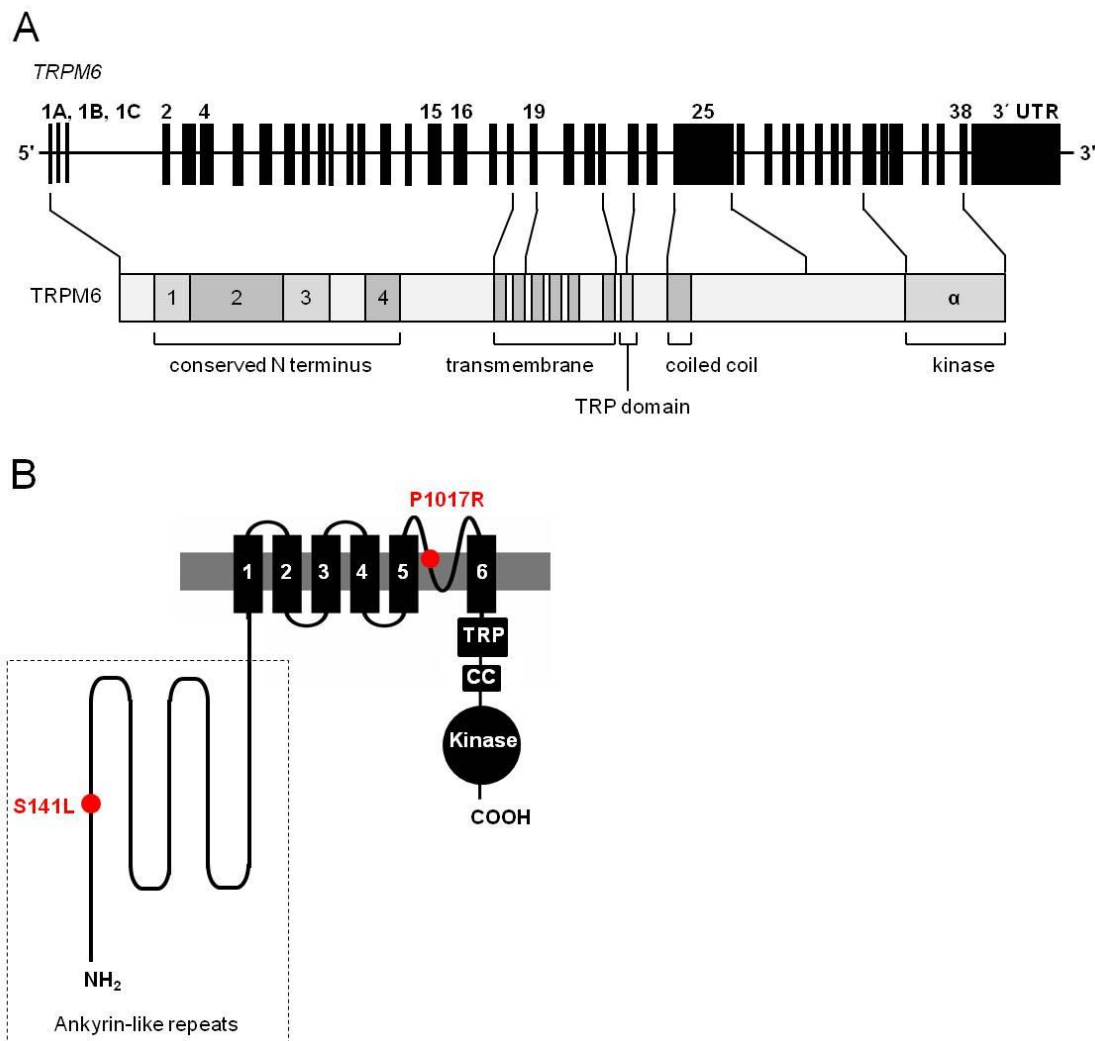


**Figure 1.3. Gene structure and domain organization of the human TRPM6 protein. (A)** Structure of the human *Trpm6* gene and mRNA. The gene includes 39 exons (numbered 1-39, black boxes), including three alternative first exons (1A, 1B, 1C), the 3' untranslated region (UTR) and the 5'UTR. Figure modified from [71, 77, 78]. **(B)** Domain topology of TRPM6. The six transmembrane helices form the channel segment of TRPM6, with a pore-forming loop between TM5 and TM6. The intracellular C-terminal of TRPM6 contains the kinase domain. The TRP and coiled-coil (CC) domains are also illustrated. The position of two missense mutations found in HSH patients [77, 79] are represented with red dots. Figure modified from [78].

Initial analyses of multiple mouse tissues (brain, heart, lung, spleen, liver, kidney, muscle and testis) by Northern blot [66] and electrophysiological investigations of several cell lines (HEK 293, RBL-2H3 and Jurkat T-lymphocytes) [67] revealed that TRPM7 is widely expressed. An extensive analysis by quantitative real-time PCR (qRT-PCR) of human [80] and mouse [81] tissues showed a ubiquitous expression of TRPM7. In humans, the highest expression of TRPM7 was found in the heart, pituitary, bone and adipose tissue [80]. The mouse TRPM7 channel is highly expressed in the intestine, kidney, lung and brain [81].

Different studies documented the expression of TRPM6 in various tissues. RT-PCR analysis of rat tissues detected TRPM6 in the kidney and intestine [71]. Additional analysis on microdissected rat nephrons showed high expression levels of TRPM6 in the distal convoluted tubule (DCT), the major site of active transcellular  $Mg^{2+}$  reabsorption of the nephron [71]. In addition, TRPM6 was found to be weakly expressed in proximal tubule and collecting duct [71]. *In situ* hybridization (ISH) in different human tissues revealed TRPM6 transcripts in the duodenum, jejunum, ileum and colon as well as in DCT segments of the kidney [71]. By Northern blot analysis, TRPM6 expression was detected in the human kidney, colon, and lung and testis [70]. Thus, TRPM6 seems to be mostly expressed in transporting epithelia of the intestine and kidney, but TRPM6 mRNA was also found in other tissues.

#### **1.2.1.2. Domain organization of TRPM6 and TRPM7**

In analogy to other members of the TRP superfamily, both TRPM6 and TRPM7 include six transmembrane helices with a putative pore-forming loop located between TM5 and TM6 [1, 3, 6] (Fig. 1.3B). Like other TRP channels, TRPM6 and TRPM7 are thought to form tetrameric channel complexes [4]. It has been proposed that TRPM6 and TRPM7 can function as homo- as well as hetero-tetramers [6-8]. In particular, TRPM6 assembles with TRPM7. Such interaction seems to promote the translocation of TRPM6 from an intracellular membrane compartment to the cell membrane [77, 82]. The TRP domain, located downstream of TM6 of TRPM6 and TRPM7, contains the conserved TRP box sequence WKYNRY in TRPM6 and WKYQRY in TRPM7 [1, 3]. The TRP domain is followed by the cytoplasmic CC domain, which appears to be involved in homo- and heterotetrameric associations of TRPM6 and TRPM7 [22, 23, 83]. TRPM6 and TRPM7 comprise an active serine/threonine kinase domain at their C-ends, which belongs to the atypical family of eukaryotic  $\alpha$ -kinases [66, 67, 76, 84].

Several  $\alpha$ -kinases are known in mammals, including TRPM6 and TRPM7.  $\alpha$ -Kinases show no obvious sequence identity to conventional eukaryotic protein kinases [76, 85]. Contrary to conventional protein kinases phosphorylating amino acids located within loops, the  $\alpha$ -kinases phosphorylate amino acids within  $\alpha$ -helices [84, 85]. The kinase domain of TRPM7 autophosphorylates its own residues [86]. Various TRPM7 kinase substrates were identified, including annexin I [87], myosin II (also phosphorylated by TRPM6 kinase) [88], eEF-2 kinase [89], and phospholipase C gamma 2 (PLC $\gamma$ 2) [90]. The physiological significance of channel kinase activity remains poorly understood.

### 1.2.1.3. Ion permeation profiles of TRPM6 and TRPM7 channels

Initially, TRPM7 was functionally characterized in heterologous expression systems where it functions as a constitutively active cation channel, which is highly permeable to Mg<sup>2+</sup> and Ca<sup>2+</sup> [66, 67, 69]. Subsequent studies demonstrated that at physiological membrane potentials (–80 - –40 mV), the channel is also able to conduct a wide range of physiological divalent cations, including Zn<sup>2+</sup>, Co<sup>2+</sup>, Mn<sup>2+</sup> as well as nonphysiological cations such as Sr<sup>2+</sup>, Ba<sup>2+</sup>, Ni<sup>2+</sup>, and Cd<sup>2+</sup> with the following permeability sequence of Zn<sup>2+</sup>  $\approx$  Ni<sup>2+</sup>  $\gg$  Ba<sup>2+</sup> > Co<sup>2+</sup> > Mg<sup>2+</sup>  $\geq$  Mn<sup>2+</sup>  $\geq$  Sr<sup>2+</sup>  $\geq$  Cd<sup>2+</sup>  $\geq$  Ca<sup>2+</sup> [72]. However, in divalent cation-free intracellular solutions TRPM7 conducts monovalent cations quite well [66, 67].

The biophysical characteristics of recombinant TRPM6 remain controversial. Two independent studies demonstrated that the human TRPM6 is not able to constitute functional homomeric channel complexes in the cell membrane when overexpressed in *Xenopus* oocytes and HEK 293 cells, but it needs TRPM7 to be co-targeted to the cell surface [77, 82]. In addition, heteromultimeric TRPM6/M7 channels seem to display different biophysical properties as compared to homomultimeric TRPM7 channel complexes [77, 79, 82, 91]. Oppositely, Voets *et al.* detected functional human TRPM6 currents when the channel was heterologously expressed in HEK 293 cells [68] exhibiting high permeability to Zn<sup>2+</sup>, Mg<sup>2+</sup>, Ca<sup>2+</sup>, Ba<sup>2+</sup>, Mn<sup>2+</sup>, Sr<sup>2+</sup>, Cd<sup>2+</sup> and Ni<sup>2+</sup> [68, 82]. Recently, it was reported that the recombinant human TRPM6 cDNA can be functionally expressed only if it is inserted into pCINeo-IRES-GFP vector but not in other expression constructs [92].

#### 1.2.1.4. Regulation of TRPM6 and TRPM7 channels

TRPM6 and TRPM7 channels are regulated by several mechanisms. It is commonly accepted that one of the most important negative regulatory factors is intracellular content of free  $Mg^{2+}$  [67-69], ranging in most mammalian cells between 0.5 and 1 mM [93, 94].  $IC_{50}$  values of 720 and 569  $\mu M$  free  $Mg^{2+}$  for recombinant [95] and native [92] TRPM7 channels, respectively, have been determined. Kozak and Cahalan [96] revealed that internal  $Mg^{2+}$  is not exclusive in its ability to inhibit TRPM7 currents, as  $Ba^{2+}$ ,  $Sr^{2+}$ ,  $Zn^{2+}$  and  $Mn^{2+}$  could also elicit inhibitory effect on TRPM7 currents. Experiments with recombinant human TRPM6 produced conflicting results regarding the sensitivity to intracellular  $Mg^{2+}$ . One study concluded that human TRPM6 is suppressed by internal  $Mg^{2+}$  with  $IC_{50}$  values of 510  $\mu M$  [68]. In other second study, human TRPM6 was found to be inhibited by very low  $Mg^{2+}$  levels with an  $IC_{50}$  of 29  $\mu M$  [92].

Another physiologically relevant regulatory factor of the channel activity is intracellular free Mg-ATP (estimated in 3-7 mM in mammalian cells [93, 94]). Mg-ATP elicited its inhibitory effect on TRPM7 with an  $IC_{50}$  of 2 mM when internal  $Mg^{2+}$  was buffered to physiological levels ( $\sim 800 \mu M$ ) [67, 95]. Because of the high sensitivity of TRPM7 to  $Mg^{2+}$  and Mg-ATP, TRPM7 currents are often named as Mg<sup>2+</sup>-inhibited cation (MIC) currents [97, 98] or magnesium nucleotide-regulated metal ion (MagNum) currents [67, 99]. Mg-ATP could suppress human TRPM6 currents with  $IC_{50}$  of 1.3 mM in one study [100], but it was unable to inhibit human TRPM6 in other study [92]. Hence, regulatory properties of TRPM6 await further clarifications.

Low external pH ( $\sim 4.0$ ) significantly enlarges TRPM6 and TRPM7 inward currents, by increasing the monovalent cation permeability of the channel, i.e., by removing the divalent cation block of the channel pore by divalent currents [101, 102]. On the other hand, TRPM7/MIC currents can be activated by elevated internal pH ( $\sim 9.0$ ) [103]. The physiological relevance of these regulatory mechanisms remains unknown.

TRPM6 and TRPM7 are positively regulated by phosphatidylinositol 4,5-bisphosphate ( $PIP_2$ ) [73, 74]. It was shown that G protein-coupled receptors-mediated activation of phospholipase C (PLC) lead to  $PIP_2$  hydrolysis, with consequent inactivation of TRPM6 and TRPM7, suggesting that both channels require  $PIP_2$  for its function [73, 74].

Recently, it has been reported that TRPM7 can function as a channel in intracellular membrane compartments [104]. Thus, the majority of TRPM7 was found to be localized in intracellular vesicles, referred to as M7Vs, containing high levels of

glutathione [104]. M7Vs are distinct from other organelles or vesicles as endosomes or lysosomes [104]. These vesicles are capable to accumulate  $Zn^{2+}$  when its cytosolic levels are elevated [104]. Reactive oxygen species (ROS) were able to trigger the release of  $Zn^{2+}$  from M7Vs into the cytosol via TRPM7 channel [104]. In addition, reduced levels of glutathione prevented TRPM7-dependent cytosolic  $Zn^{2+}$  raises [104]. The authors concluded that intracellular TRPM7 senses oxidative stress to release  $Zn^{2+}$  from M7Vs [104].

The role of the kinase domain in the regulation of the channel activity is not well understood. A currently prevailing view is that TRPM7 kinase is not necessary for channel activity [86]. However, some groups suggested that the TRPM7 kinase domain moderately regulates TRPM7 channel sensitivity to intracellular  $Mg^{2+}$  and  $Mg\cdot ATP$  [69, 95]. It has been shown that the function of TRPM7 kinase domain can be separated from the channel moiety. Thus, it was found that the caspase-dependent cleavage of TRPM7 resulted in a release of the kinase domain into the cytosol [105]. The cleaved channel unit was found to be crucial for the potentiation of Fas-induced apoptosis by TRPM7 in T cells [105]. The released kinase domain was able to translocate to the nucleus, where it can phosphorylate specific histones, resulting in epigenetic chromatin modification [106].

In contrast to the TRPM7  $\alpha$ -kinase domain, little is known about a role of the TRPM6 kinase. One work suggested that the TRPM6 kinase is involved in an inhibitory action of ATP on the TRPM6 channel [100]. Similar to TRPM7, the C-terminal kinase domain of TRPM6 was recently found to be cleaved from the channel domain [107]. The cleaved TRPM6 kinase was able to translocate to the nucleus and interact with arginine methyltransferase 5 (PRMT5) molecular complex [107]. This interaction permitted TRPM6 kinase domain to phosphorylate serine and threonine residues of histones near arginines methylated by PRMT5 [107]. Histone phosphorylation by TRPM6 kinase domain resulted in decreased methylation of the arginine residues and large-scale alterations in gene expression profiles [107].

#### **1.2.1.5. Modulation of TRPM6 and TRPM7 by small organic drug-like ligands**

Several small organic compounds enable to inhibit or activate TRPM6 and TRPM7 currents. 2-Aminoethyl diphenylborinate (2-APB) elicits an inhibitory effect on endogenous [108] and recombinant TRPM7 channels [91]. Surprisingly, TRPM6 currents could be enhanced by 2-APB [91, 92].

Waixenicin A, a compound extracted from the soft coral *Sarcothelia edmondsoni* [109], was found as a potent inhibitor of TRPM7, which blocked the channel irreversibly in a  $Mg^{2+}$ -dependent manner. Thus, in the presence of physiologically relevant 700  $\mu M$  cytosolic  $Mg^{2+}$ , the  $IC_{50}$  was 16 nM. However, removing of  $Mg^{2+}$  resulted in  $IC_{50}$  of 7  $\mu M$  [109]. Importantly, waixenicin A does not affect TRPM6 [109].

Our laboratory identified a set of other potent TRPM7 inhibitors [110]. Among them, NS8593 was studied in details. NS8593 has an  $IC_{50}$  of 1.6  $\mu M$  under free  $Mg^{2+}$  internal conditions [110]. Similarly to waixenicin A, NS8593 acts on TRPM7 in a  $Mg^{2+}$ -dependent manner. The inhibitory effect of NS8593 on TRPM7 was fully reversible [110].

More recently, our laboratory identified a subset of TRPM7 activators, like naltriben [111] and mibefradil [112]. Naltriben activated TRPM7 currents without prior depletion of intracellular  $Mg^{2+}$  and exhibited an half-maximal effective concentration ( $EC_{50}$ ) of 20  $\mu M$  [111]. The effect of naltriben was fully reversible and interfered with the inhibitory action of NS8593 [111]. Mibefradil activated TRPM7 currents with an  $EC_{50}$  of 53  $\mu M$  [112]. In contrast to naltriben, mibefradil stimulated TRPM7 currents only at physiological internal  $Mg^{2+}$  levels, and its activating effect was abolished by high intracellular  $Mg^{2+}$  concentrations [112].

#### **1.2.1.6. The suggested physiological functions of TRPM7**

It has been demonstrated that chicken DT40 B lymphocytes with a targeted deletion of the *Trpm7* gene developed  $Mg^{2+}$  deficiency and consequently growth arrest [67, 69]. The proliferation defect of these mutant cells were rescued by increasing  $Mg^{2+}$  (but not  $Ca^{2+}$ ,  $Zn^{2+}$  or  $Mn^{2+}$ ) in the culture medium [69]. Since the TRPM7 channel pore is permeable to  $Mg^{2+}$  ions, these observations led to the concept that the TRPM7 channel regulates cellular  $Mg^{2+}$  homeostasis in DT40 cells [69, 113, 114]. Endogenous TRPM7-like currents have been observed in all cell types examined so far [110], indicating that TRPM7 plays a similar role in all vertebrate cells. In addition, several studies have suggested a plethora of other (patho)physiological processes regulated by the TRPM7 channel, including cell motility [88, 115, 116], cell cycle [67, 69, 109, 114], mechanosensitivity [116-118], exocytosis [119], anoxic neuronal death [120], hypertension [121], neurodegenerative disorders [122, 123], cardiac fibrosis [124], and cancer [108, 125-127].

A global disruption of TRPM7 in mice leads to early embryonic lethality prior day 7.5 of embryogenesis (e7.5) for unknown reasons [128]. The epiblast-specific inactivation of TRPM7 fails to produce viable KO mice, indicating that TRPM7 is required for embryonic development [128]. Furthermore, tissue- and organ-specific inactivation of *Trpm7* in mouse embryos affected the normal development and function of internal organs, highlighting an essential role of TRPM7 in organogenesis [128, 129]. Thus, conditional inactivation of TRPM7 in the T-cell lineage disrupts thymopoiesis, without altering  $Mg^{2+}$  homeostasis [128]. Moreover, it has been shown that TRPM7 is indispensable for proper kidney development [129]. The role of TRPM7 has been also shown in cardiogenesis using mutant mice with specific ablation of *Trpm7* in the embryonic heart [130, 131]. Early loss of cardiac TRPM7 causes heart failure and death, suggesting that TRPM7 is indispensable for myocardial morphogenesis [130]. In addition, TRPM7 has been shown to be essential for maintaining cardiac automaticity in adult mice [131].

It has been shown that mice with a complete deletion of the TRPM7 kinase domain die at e7.5 for unknown reasons [113]. Heterozygous mice lacking TRPM7 kinase domain exhibited an altered  $Mg^{2+}$  homeostasis, since they have lower  $Mg^{2+}$  concentrations in urine, plasma and bones [113]. In contrast, TRPM7 kinase-dead mutant mice containing a substitution of a key lysine involved in Mg-ATP binding had a normal development and unchanged serum  $Mg^{2+}$  levels [132]. In addition, TRPM7 kinase-dead mice were found to be more resistant to dietary  $Mg^{2+}$  deprivation [133]. Using the same mouse line with inactivation in the TRPM7 kinase domain, Zierler *et al.* showed that this domain is involved in mast cell degranulation and release of histamine [134]. Finally, it has been recently demonstrated that TRPM7 kinase plays a role in hypertension [135].

#### **1.2.1.7. Physiological implications of the TRPM6 channel**

In 2002, two groups independently identified a loss-of-function mutation in the human *TRPM6* gene leading to an autosomal recessive hypomagnesemia with secondary hypocalcemia (HSH) [70, 71]. This disorder, characterized by very low  $Mg^{2+}$  and  $Ca^{2+}$  serum levels, manifests shortly after birth with neurologic symptoms, including muscle spasms and seizures [70, 71]. Untreated, HSH may be fatal or may result in neurological damage; however, all the symptoms can be relieved by oral  $Mg^{2+}$  supplementation [70, 71]. The pathophysiological mechanisms of HSH are not well understood. For example, it remains unclear whether the disease is mainly caused by a

defect in the intestinal  $Mg^{2+}$  absorption or due to an abnormal renal loss of  $Mg^{2+}$  [70, 71]. A considerable number of HSH mutations in the *TRPM6* gene introduces stop and frame-shift mutations and affects exon splicing, causing a complete lack of protein production [70, 71, 77, 79, 136-141]. In addition, several point mutations in *TRPM6* have been identified [78]. Mutations characterized by our group are depicted on Fig. 1.3B. One mutation, *TRPM6*<sup>S141L</sup>, is located in the N-terminal of the channel, implying a fundamental role of this domain for the channel activity [77]. Interestingly, the *TRPM6*<sup>S141L</sup> mutant fails to associate with TRPM7 [77]. P1017R, another missense mutation, is located in the *TRPM6* putative pore-forming region [79]. *TRPM6*<sup>P1017R</sup> showed a dominant negative effect when it was co-expressed with TRPM7 [79].

Until now, only two groups studied mice strains lacking TRPM6. Walder *et al.* [142] revealed that *Trpm6*<sup>-/-</sup> mice almost never survived to weaning. Most mutant individuals died prior e12.5 [142]. The few survived mice beyond this stage showed massive neural tube defects (NTD) [142]. Feeding parents high  $Mg^{2+}$  diet did not improve the embryonic survival of the mutants [142]. Hence, the authors suggested that TRPM6 plays a critical role in embryonic development and in neural tube closure. However, the specific molecular mechanisms underlying NTD in *Trpm6* deficient mice are still unclear [142]. Employing another *Trpm6* deficient mutant line (*Trpm6* <sup>$\beta$ geo</sup>), Woudenberg-Vrenken *et al.* [143] confirmed that homozygous null TRPM6 mutation leads to the embryonic death. However, mice heterozygous for *Trpm6* deletion are viable and develop a mild hypomagnesemia [143]. A  $Mg^{2+}$ -enriched diet neither rescued the embryos nor improved hypomagnesemia induced by *Trpm6* <sup>$\beta$ geo</sup> [143]. Thus, the targeted deletion of the mouse *Trpm6* gene caused an unexpected phenotype in mice which differs from symptoms observed in HSH patients.

Very recently, our group has confirmed that mice lacking *Trpm6* (*Trpm6* <sup>$\beta$ geo/ $\beta$ geo</sup> mice) are not viable [144]. KO embryos died at a mid-gestational stage (e12.5) exhibiting a smaller size compared to *Trpm6*<sup>+/+</sup> embryos and NTD [144] (Fig. 1.4). Furthermore, the KO embryos were  $Mg^{2+}$  deficient [144]. Since diverse mouse lines develop NTD due to mutations in genes, which are active in the neural tube epithelium [145], e8.5 embryos were examined for TRPM6 expression using *in situ* hybridization (ISH). Surprisingly, *Trpm6* was not detectable in embryos, but specifically expressed in the yolk sac and placental labyrinth [144] (a more detailed expression of *Trpm6* in the placenta is explained in section 1.3.2).

Consequently, a conditional *Trpm6* mutation was used for a specific inactivation of *Trpm6* allele in the epiblast cells of the early embryo, but not in extraembryonic tissues

[144]. This approach produced vital offspring deficient in TRPM6, supporting an idea that TRPM6 activity in extraembryonic cells is required for prenatal development of mice. In follow-up experiments, it was found that adult TRPM6 deficient mice developed a severe organismal  $Mg^{2+}$  deficiency, shorter lifespan compared to WT mice and an accelerated aging-like phenotype [144]. All these phenotypes were fully reversed by dietary  $Mg^{2+}$  supplementation of mice [144]. Taken together, experiments with gene-modified mice have established a critical role of TRPM6 in systemic homeostasis of prenatal and adult mice.

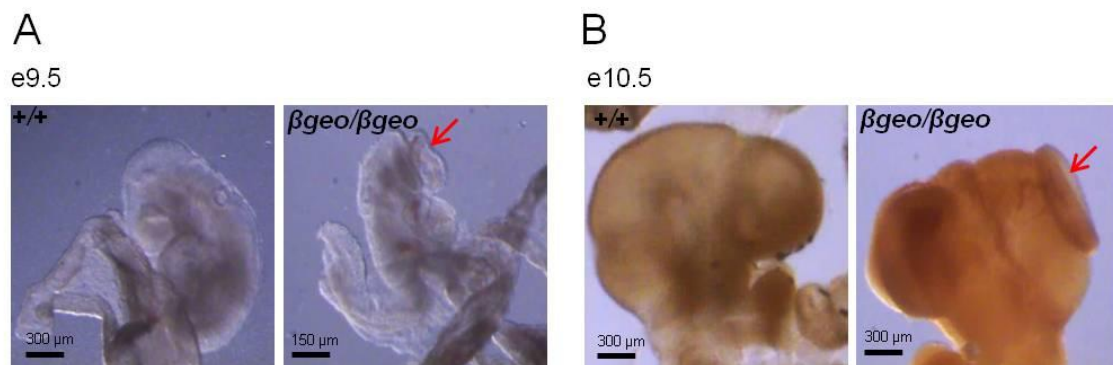


**Figure 1.4. Comparison between *Trpm6*<sup>+/+</sup> and *Trpm6*<sup>βgeo/βgeo</sup> embryos. (A)** At e9.5, the mutant embryo is smaller in size, not turned (S-shaped) and growth retarded compared with the control. The arrow shows the open neural tube of the mutant embryo. **(B)** At e10.5, the mutant embryo exhibits NTD. The unclosed neural tube in the head region is shown by an arrow. Figure modified from [144].

### 1.3. $Mg^{2+}$ homeostasis

Magnesium is the second most abundant intracellular cation playing a key role in the regulation of many cellular processes [93]. This essential element is a cofactor in over 300 enzymatic reactions.  $Mg^{2+}$  controls the activity of enzymes by (i) binding to the active site of the enzyme, (ii) interaction with substrates such as ATP, (iii) causing a conformational changes of the enzyme leading to modulation of the catalytic reaction, or (iv) promoting the assembly of multi-enzyme complexes [93, 146, 147].  $Mg^{2+}$  is also an essential structural factor of many proteins, nucleic acids, and a regulatory ligand of membrane transporter and channels [94, 147, 148]. Furthermore,  $Mg^{2+}$  is involved in many other vital processes such as nucleic acid and protein synthesis, cellular energy metabolism, mitochondrial and cytoskeletal integrity [94, 147]. Finally,  $Mg^{2+}$  operates as a  $Ca^{2+}$  channel antagonist; it alters processes regulated by intracellular  $Ca^{2+}$  and, thus, is critical for normal neurological and muscular functions [146, 147].

The total cellular  $Mg^{2+}$  concentration ranges between 5 and 10 mM in the majority of mammalian cell types examined, and it can be up to 20 mM in some cells. Most ionized  $Mg^{2+}$  is bound to ATP and other nucleotides, sequestered in mitochondria, and endo-(sarco)-plasmic reticulum [94, 149]. Accumulation of  $Mg^{2+}$  in these organelles is due to the ability of  $Mg^{2+}$  to bind to proteins, phospholipids, nucleic acids, nucleotides and chromatin [94, 149]. In the cytosol,  $Mg^{2+}$  forms complexes with adenosine trisphosphate (ATP) and other phosphometabolites [93, 94]. Free  $Mg^{2+}$  concentrations in the cytosol have been estimated to range between 0.5 and 1 mM (~10% of total cellular  $Mg^{2+}$ ) in the majority of cell types examined [93, 94].

### 1.3.1. $Mg^{2+}$ channels and transporters

The maintenance of the intracellular  $Mg^{2+}$  concentrations is regulated by a dynamic balance of  $Mg^{2+}$  uptake, intracellular  $Mg^{2+}$  storage, and  $Mg^{2+}$  efflux. Thus, similarly to other cations,  $Mg^{2+}$  is transported across the plasma membrane or the membrane of cellular organelles through channels ( $Mg^{2+}$  uptake into the cells) and exchanger mechanisms ( $Mg^{2+}$  extrusion from the cells) [94, 150]. Diverse channels transporting  $Mg^{2+}$  into the cell have been described in mammals. Some of these channels exhibit higher specificity for  $Mg^{2+}$ , whereas other can conduct several other divalent cations.  $Mg^{2+}$  channels are located in the plasma membrane, in the mitochondrial membranes, ER or in Golgi [94, 150]. Known mammalian  $Mg^{2+}$  transporters are described below.

**Claudins.** The first  $Mg^{2+}$  transporter found in mammals was paracellin-1 (PCLN-1) or claudin-16 [151]. This protein, encoded by *Paracellin-1 (PCLN-1)* gene, was identified in a genetic screening of patients affected by familial hypomagnesemia with hypercalciuria and nephrocalcinosis (FHHNC, OMIM 248250), a severe disorder characterized by fast and chronic renal failure due to massive renal  $Ca^{2+}$  and  $Mg^{2+}$  wasting [151]. PCLN-1 is a member of the claudin gene family, a group of tight junction proteins characterized by 4 TMs and cytoplasmic C- and N-termini [94]. Claudin-16 is a renal tight junction protein required for paracellular  $Mg^{2+}$  and  $Ca^{2+}$  fluxes across the nephron epithelial layers [151]. However, the mechanisms underlying these fluxes remain to be elucidated. A recent study has demonstrated that another claudin, claudin-19, is involved in the renal  $Mg^{2+}$  and  $Ca^{2+}$  reabsorption [152].

**MagT1.** MagT1, identified by Goytain and Quamme in human epithelial cells, was suggested as a  $Mg^{2+}$ -selective plasma membrane transporter [153]. The murine

orthologue of MagT1 is expressed in many tissues, including the heart, kidney, liver and colon [153]. Transport of  $Mg^{2+}$  by MagT1 is likely voltage-dependent [153].

**SLC41 proteins.** The three members (A1, A2, and A3) of this gene family are remotely related to prokaryotic MgtE transporter [154]. The first member to be identified was SLC41A1 [155]. This protein is characterized by the presence of 10 TMs [155]. Functional expression of murine SLC41A1 in *Xenopus laevis* oocyte reveals that this transporter conducts  $Mg^{2+}$  but also  $Zn^{2+}$ ,  $Cu^{2+}$ ,  $Fe^{2+}$ ,  $Ba^{2+}$  and  $Co^{2+}$  [156]. SLC41A2 was identified in humans and mice and, similar to SLC41A1, is able to transport  $Mg^{2+}$  and other divalent cations [157, 158]. Recent work indicates that SLC41A3 plays a role in organismal  $Mg^{2+}$  homeostasis since its expression was specifically detected in DCT and intestine, and because SLC41A3 KO mice developed hypomagnesemia [159]. It has been demonstrated that SLC41A3 is present in the inner mitochondrial membrane and functions as a mitochondrial  $Mg^{2+}/Na^+$  exchanger [160].

**ACDP proteins.** Wang *et al.* identified four different genes, ACDP1– 4, belonging to the human ACDP gene family [161]. ACDP proteins are conserved and also exist in prokaryotes [162]. They show a moderate sequence similarity to CorC transporter of *Salmonella typhimurium* involved in  $Mg^{2+}$  efflux [163]. Mammalian ACDP2 mediated the fluxes of  $Mg^{2+}$  and other divalent cations when heterologously expressed in *Xenopus* oocytes [164].

**NIPA proteins.** This family comprises four NIPA (NIPA 1-4) genes called after a non-imprinted in Prader-Willi/Angelman syndrome, a genetic disorder characterized by complex symptoms [165, 166]. NIPA1 is expressed in many tissues, but is particularly abundant in the brain. NIPA1 functions as a  $Mg^{2+}$  transporter, but can conduct other divalent cations [167]. NIPA2 protein is a transporter that mediates selective  $Mg^{2+}$  flux. NIPA2 is widely expressed, but was found to be more abundant in the kidney [168]. Similarly to NIPA1, NIPA3 and NIPA4 mediate  $Mg^{2+}$  uptake [168].

**MMgTs proteins.** This gene family comprises two proteins named MMgT1 and MMgT2 (Membrane M $g^{2+}$  Transporter 1 and 2) [169]. When exogenously expressed in *Xenopus laevis* oocytes, MMgT1 and MMgT2 transport  $Mg^{2+}$ , but they can also conduct other divalent cations [169]. MMgT transcripts were detected many tissues. MMgT proteins are presumably located in the Golgi complex and post-Golgi vesicles [169].

**Mrs2.** The mitochondrial RNA splicing2 (Mrs2) protein is located in the inner mitochondrial membrane. Mrs2 was identified in a screening of genes involved in splicing of mitochondrial RNA in yeast [170, 171]. Structurally, human Mrs2 is distantly

related to bacterial *CorA* and yeast *Alr* genes, which are both located in the plasma membrane of prokaryotic cells [171, 172]. Heterologously expression of yeast Mrs2 enhanced  $Mg^{2+}$  uptake, whereas the lack of this channel nearly abolished  $Mg^{2+}$  influx, implying that Mrs2 plays a crucial role in the regulation of mitochondrial  $Mg^{2+}$  balance [173].

### 1.3.2. Roles of TRPM6 and TRPM7 in organismal $Mg^{2+}$ balance

The healthy adult human body contains 22-26 g of  $Mg^{2+}$  [147].  $Mg^{2+}$  is predominantly stored in bones (~85%) and skeletal muscle (~10%); less than 1% of body  $Mg^{2+}$  is present in the plasma [146, 147, 174].

$Mg^{2+}$  homeostasis in humans is controlled by the intestinal  $Mg^{2+}$  absorption and renal  $Mg^{2+}$  excretion [147, 174, 175].  $Mg^{2+}$  absorption occurs in the small and large intestine (colon) via two different mechanisms: an active transcellular and a passive paracellular transport pathway. At low intraluminal concentrations,  $Mg^{2+}$  is absorbed mainly via the transcellular pathway, which is driven by the active  $Mg^{2+}$  uptake in the apical cell surface of epithelial cells. The paracellular route becomes relevant when luminal  $Mg^{2+}$  concentration rises, and is underlined by passive  $Mg^{2+}$  transport via tight junctions formed by the epithelial cells [174-176]. The composition of the intestinal tight junctions involved in the  $Mg^{2+}$  transport is still controversial [176].  $Mg^{2+}$  absorption in the small intestine is supposed to be mediated entirely by passive paracellular mechanism driven by electrochemical gradient. In the large intestine,  $Mg^{2+}$  is thought to be transported solely via the transcellular pathway [176] (Fig. 1.5). TRPM6 is highly expressed in epithelial cells of the colon [71, 144]. Recently, our group demonstrated that the  $Mg^{2+}$  uptake mediated by TRPM6 is principally important in the intestine since the gut-specific ablation of TRPM6 in mice leads to hypomagnesemia, indicating that the WT kidney is not able to compensate the deletion of *Trpm6* in the intestine [144].

In the kidney, approximately 80% of total serum  $Mg^{2+}$  is filtered in the glomeruli, with >95% being reabsorbed along the nephron back into the blood. Only 3–5% of the filtered  $Mg^{2+}$  is excreted with the urine at physiological conditions. Around 10–15% of filtered  $Mg^{2+}$  is re-absorbed in the proximal convoluted tubules, while 60–70% is passively re-absorbed in the thick ascending loop of Henle [147, 174-176]. This paracellular transport is mediated by claudin-16 and claudin-19 forming the epithelial tight junctions [152]. Only 5–10% of the filtered  $Mg^{2+}$  is reabsorbed via transcellular transport in the distal convoluted tubule (DCT). As there is no significant reabsorption

of  $Mg^{2+}$  in the distal tubule and collecting duct, DCT defines the final urinary  $Mg^{2+}$  excretion levels. TRPM6 is specifically expressed in DCT and thought to be responsible for a final regulation of urinary excretion of  $Mg^{2+}$  [147, 174-176] (Fig. 1.5). However, our experiments with mutant mice containing a specific inactivation of *Trpm6* in the kidney exhibited normal plasma  $Mg^{2+}$  levels [144]. This finding challenges the idea that TRPM6 plays an essential role in DCT segment of the kidney.

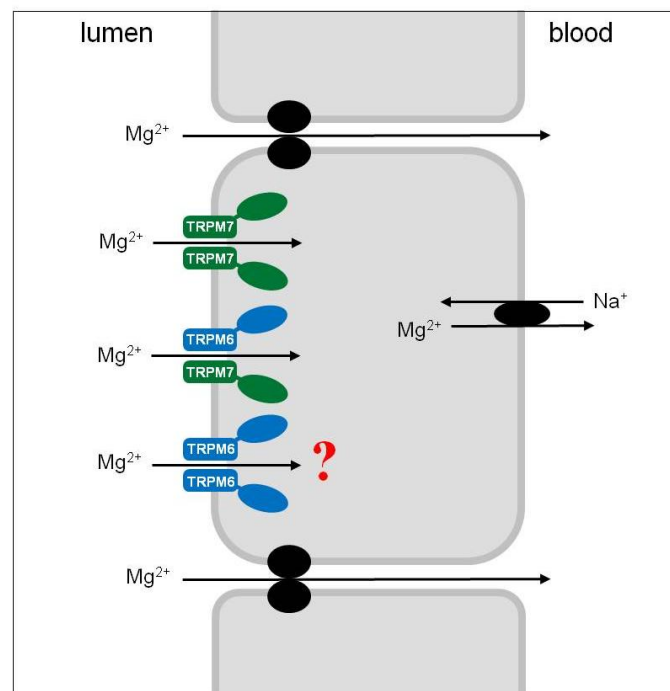


**Figure 1.5. A proposed model of transcellular  $Mg^{2+}$  transport in intestine, kidney and placenta mediated by TRPM6/M7 channel complexes.** TRPM6 and TRPM7 channels transport  $Mg^{2+}$  via transcellular pathway. The paracellular  $Mg^{2+}$  transport occurring through the small spaces between the epithelial cells and the  $Na^+$ -dependent  $Mg^{2+}$  extrusion are also represented. Figure modified from [177].

Placental  $Mg^{2+}$  supply for the embryo is poorly understood. The fully developed mouse placenta is organized into two main zones, called junctional and labyrinth zones [178] (Fig. 1.6A). The junctional zone contains mainly spongiotrophoblasts and glycogen-containing cells releasing endocrine factors [178]. The labyrinth zone is involved in the materno-fetal transport of minerals (and likely  $Mg^{2+}$ ), nutrients and waste metabolites, and gas exchange. This zone consists of maternal blood spaces (sinusoids) and fetal capillaries organized in a labyrinth-like structure, separated by three layers of fetal trophoblasts. The first layer lining the maternal blood spaces is composed by large mononuclear trophoblasts followed by two layers of syncytiotrophoblasts forming

syncytiotrophoblasts layer I (SynT-I) and syncytiotrophoblasts layer II (SynT-II) [178, 179].

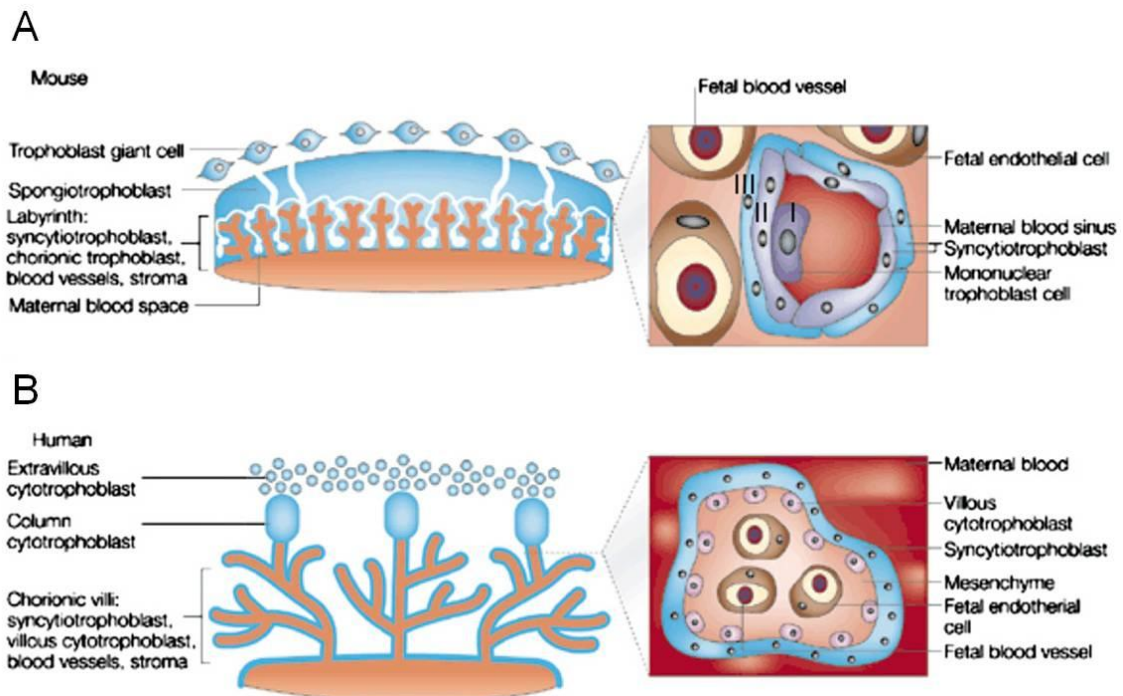


**Figure 1.6. The structure of placenta in mouse and human. (A)** The mouse placenta is organized in the junctional (formed by spongiosotrophoblasts) and labyrinth zones. The labyrinth represents the maternal-fetal interface and contains three trophoblast layers, layer I (mononuclear trophoblasts), layers II (syncytiotrophoblasts layer I, SynT-I) and III (syncytiotrophoblasts layer II, SynT-II). **(B)** The human placenta comprises chorionic villi, trophoblast-derived structures (blue) and mesoderm-derived tissues (orange). Figure modified from [178].

As mentioned in section 1.2.1.7, *Trpm6* was found to be highly expressed in the endoderm layer of the yolk sac and in placental trophoblasts [144]. In particular, in the early phases of the morphogenesis of the labyrinth (e8.5), when SynT-I and SynT-II are still two distinguishable layers, *Trpm6* expression was found in cells expressing *SynA* (marker of SynT-I cells), but not in cells positive for *Gcm1* (marker of SynT-II cells) [144]. In the fully developed labyrinth (e14.5), *Trpm6* was localized in the syncytiotrophoblasts as well [144]. It has been supposed that  $Mg^{2+}$  and other nutrients are exchanged via SynT-I/SynT-II layers via the transcellular pathway [144]. In addition, the endoderm cells of the yolk sac appear to play an essential role in  $Mg^{2+}$  transport of early embryo prior formation of the placental labyrinth [144]. Thus, experiments with gene-modified mice revealed that *Trpm6* underlines  $Mg^{2+}$  transporters by the placental and yolk sac in mammals [144].

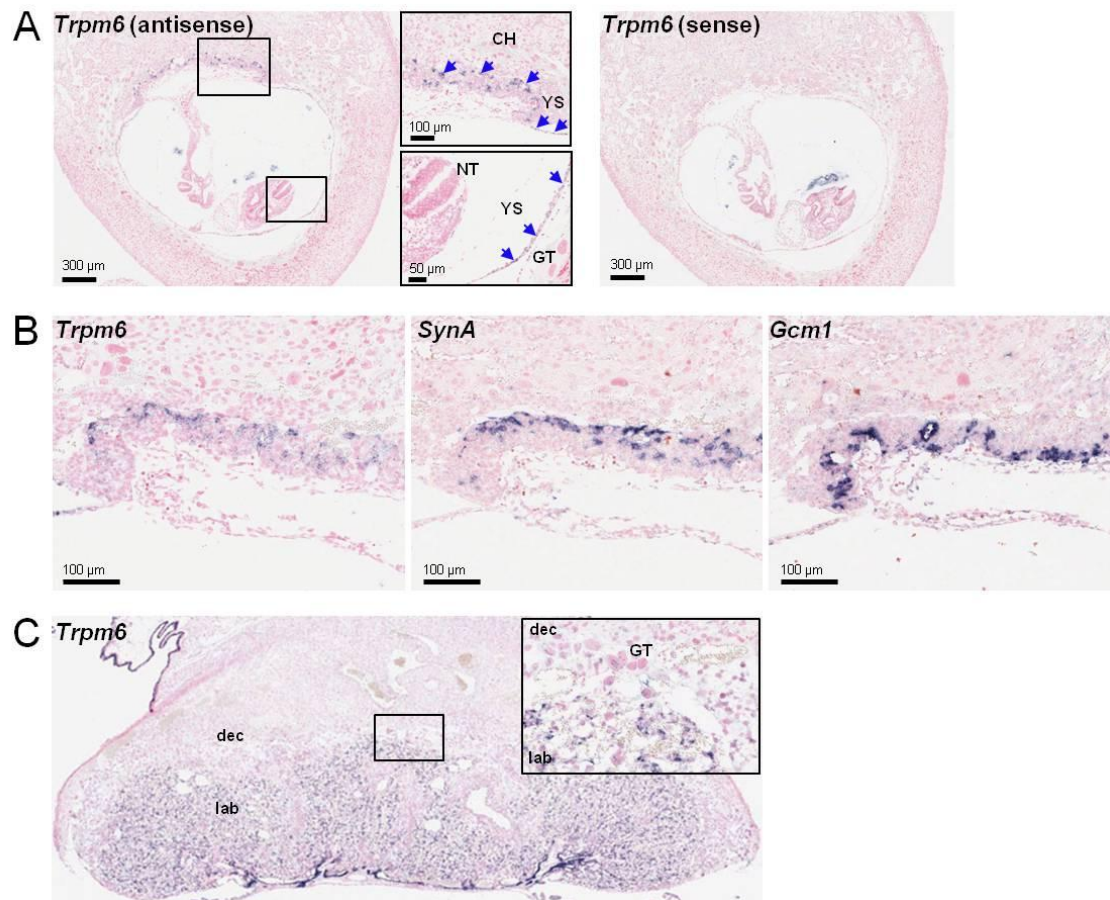


**Figure 1.7. ISH of fetal/placental samples. (A)** ISH on serial paraffin sections derived from e8.5 *Trpm6*<sup>+/+</sup> fetus. Specific antisense (left) and sense (right) DIG-labeled probes for *Trpm6* were used. The two boxes represent magnified regions of the chorion (CH) and yolk sac (YS), respectively, located in the middle. *Trpm6* is detectable in the developing labyrinth (chorion) and in the endoderm layer of the yolk sac. NT = neural tube; GT = giant trophoblast. **(B)** ISH on serial paraffin sections derived from e8.5 *Trpm6*<sup>+/+</sup> placenta employing DIG-labeled probes for *Trpm6* (left), *SynA* (middle) and *Gcm1* (right), respectively. *Trpm6* is located in cells expressing *SynA* (the marker of SynT-I), but absent in cells positive for *Gcm1* (the marker of SynT-II). **(C)** ISH on serial paraffin sections derived from e14.5 *Trpm6*<sup>+/+</sup> placenta using antisense *Trpm6* probe. The box indicates positions of the magnified images. *Trpm6* signal is limited to the labyrinth (*lab*) and not detectable in the decidua (*dec*) and trophoblast giant cells (GT). Figure modified from [144].

Taken together, emerging evidence indicates TRPM6 is a master regulator of systemic Mg<sup>2+</sup> balance during the prenatal development and in adult organism due to its activity primarily in the placental trophoblastic and intestinal epithelial cells. However, a specific cellular function of TRPM6 remains poorly understood and is discussed controversially in the scientific literature.

## **1.4. Aims of this work**

Emerging evidence indicates that TRPM6 and TRPM7 channels are critically involved in the regulation of  $Mg^{2+}$  homeostasis. However, the exact molecular functions of TRPM6 and TRPM7 remain incompletely understood.

In the first part of this work, we aimed at elucidating the cellular role of TRPM7 using different cell lines deficient in TRPM7 protein.

In the second part of this study, we were aimed to uncover the mechanisms underlying the TRPM6-dependent transport of  $Mg^{2+}$  in epithelial cells using trophoblast stem (TS) cells derived from TRPM6 deficient mice.

The main findings with TS cells were further evaluated using recombinant TRPM6 protein overexpressed in HEK 293 cells. Overall, our study revealed specific functional characteristics of TRPM6 and TRPM7, which appear to be central for the physiological role of these remarkable proteins.

## 2. Materials

### 2.1. Chemicals, enzymes and commercial kits

1,2-Bis(o-aminophenoxy)ethane-N,N,N',N'-tetraacetic acid (BAPTA)	Biotium, # 50001
10X PCR buffer for PCR with MgCl <sub>2</sub>	Sigma-Aldrich, # P2192
2-Aminoethyl diphenylborinate (2-APB)	Sigma-Aldrich, # D9754
2-Mercaptoethanol	Carl Roth, # 4227
4-(2-Hydroxyethyl)piperazine-1-ethanesulfonic acid (HEPES)	Sigma-Aldrich, # H3375
Adenosine 5'-triphosphate magnesium salt (Mg-ATP)	Sigma-Aldrich, # A9187
Agarose	Carl Roth, # 3810
Ammonium peroxydisulphate (APS)	Carl Roth, # 9592
Bovine serum albumin (BSA)	Sigma-Aldrich, # A2153
Bromophenol blue sodium salt	Carl Roth, # A512
Calcium chloride dihydrate (CaCl <sub>2</sub> )	Carl Roth, # HN04
Cesium hydroxide solution (CsOH)	Sigma-Aldrich, # 232068
D-(+)-Glucose	Sigma-Aldrich, # G8270
D-Mannitol	Sigma-Aldrich, # 63559
dNTP mix (10 mM each)	Thermo Fisher Scientific, # R0192
Ethylene glycol-bis(β-aminoethyl ether)-N,N,N',N'-tetraacetic acid (EGTA)	Carl Roth, # 3054
Ethylenediaminetetraacetic acid (EDTA)	Sigma-Aldrich, # E6758
Expand high fidelity	Roche, # 11732641001
GeneJET gel extraction kit	Thermo Fisher Scientific, # K0691
GenElute mammalian genomic DNA miniprep kit	Sigma-Aldrich, # G1N350
GenElute mammalian total RNA miniprep kit	Sigma-Aldrich, # RTN70

---

GeneRuler 100 bp DNA ladder	Thermo Fisher Scientific, # SM0241
Glycerol	Carl Roth, # 3783
Glycine	Carl Roth, # 3908
Hydrochloric acid 37%	Merck Millipore, # 100317
Hydrogen peroxide solution	Sigma-Aldrich, # 16911
L-Glutamic acid	Sigma-Aldrich, # G1251
Luminol	Sigma-Aldrich, # 123072
Magnesium chloride hexahydrate (MgCl <sub>2</sub> )	Carl Roth, # 2189
Methanol	Carl Roth, # 4627
Naltriben mesylate	Tocris, # 0892
Neon transfection system 10 µl Kit	Thermo Fisher Scientific, # MPK1025
N-Methyl-D-glucamine (NMDG)	Sigma-Aldrich, # M2004
NS8593 hydrochloride	Tocris, # 4597
p-Coumaric acid	Sigma-Aldrich, # C9008
Phosphatase inhibitor cocktail (tubes A and B)	Biotool, # B15001
Pierce classic IP kit	Thermo Fisher Scientific, # 26146
Poly-D-lysine hydrobromide	Sigma-Aldrich, # P7280
Potassium chloride (KCl)	Carl Roth, # 6781
Powdered milk	Carl Roth, # T145
Protease inhibitor cocktail	Biotool, # B14001
Protein quantification kit-rapid	Sigma-Aldrich, # 51254
QuikChange site-directed mutagenesis kit	Agilent Technologies, # 200518
REDTaq genomic DNA polymerase (1 U/µl)	Sigma-Aldrich, # D0688
RevertAid H minus first strand cDNA synthesis kit	Thermo Fisher Scientific, # K1632
Roti-GelStain	Carl Roth, # 3865
Rotiphorese gel 30 (37,5:1)	Carl Roth, # 3029

---

SDS ultra pure	Carl Roth, # 2326
SIGMAFAST protease inhibitor tablets	Sigma-Aldrich, # S8820
Sodium chloride (NaCl)	Carl Roth, # 3957
Sodium hydroxide (NaOH)	Carl Roth, # 6771
Spectra multicolor broad range protein ladder	Thermo Fisher Scientific, # 26634
Spectra multicolor high range protein ladder	Thermo Fisher Scientific, # 26625
Tetramethylethylenediamine (TEMED)	Carl Roth, # 2367
Tris(hydroxymethyl)-aminomethane (TRIS)	Carl Roth, # 4855
TWEEN 20 (Polyethylene glycol sorbitan monolaurate)	Sigma-Aldrich, # P1379
Zinc chloride (ZnCl <sub>2</sub> )	Carl Roth, # T887

## 2.2. Cell culture media and supplements

2-Mercaptoethanol for cell culture	Sigma-Aldrich, # M7522
Dimethyl sulfoxide (DMSO)	Sigma-Aldrich, # D4540
Dulbecco's phosphate buffered saline (DPBS)	Sigma-Aldrich, # D8537
Eagle's minimum essential medium (MEM)	Sigma-Aldrich, # M4655
Fetal bovine serum (FBS)	Thermo Fisher Scientific, # 10270
Fetal bovine serum, embryonic stem cell-qualified	Thermo Fisher Scientific, # 16141
Heparin sodium salt from porcine intestinal mucosa	Sigma-Aldrich, # H3149
Hirudin	Providing by Attila Brown's laboratory [180]
Iscove's modified Dulbecco's medium (IMDM)	Thermo Fisher Scientific, # 12440053
Lipofectamine 2000 transfection reagent	Thermo Fisher Scientific, # 11668
MEM non-essential amino acids solution (100X)	Thermo Fisher Scientific, # 11140
Penicillin-Streptomycin	Sigma-Aldrich, # P4333

Primary mouse embryo fibroblasts (PMEF)	Millipore, # PMEF-CF
Recombinant human fibroblast growth factor-4 (FGF-4)	R&D Systems, # 235-F4
Recombinant human transforming growth factor beta 1 (TGF- $\beta$ 1)	R&D Systems, # 240-B
Recombinant human/mouse/rat activin A	R&D Systems, # 338-AC
RPMI-1640 medium	Sigma-Aldrich, # R8758
Sodium pyruvate solution	Sigma-Aldrich, # S8636
Thrombopoietin (Thpo)	Providing by Attila Brown's laboratory [180]
Trypsin-EDTA solution	Sigma-Aldrich, # T3924

## 2.3. Antibodies

**Table 2.1.** Primary antibodies used in this study.

Name	Specificity	Epitope sequence	Supplier
Anti-TRPM7 [S74-25]	Mouse monoclonal Ab against human and mouse TRPM7	LKLPDLKRND YTPDKIIFPQ DESSDLNLQS GNSTKESEAT NSVRLML	Abcam, # ab85016
Anti-TRPM7 [EPR4582]	Rabbit monoclonal Ab against human and mouse TRPM7	Not available	Abcam, # ab109438
Anti-TRPM6 Ab 75	Rabbit polyclonal Ab against mouse TRPM6	CERDKNRSSLEDHTRL	Eurogentec (custom made)
Anti-TRPM6	Guinea pig polyclonal Ab against mouse TRPM6	GCERDKNRSSLERHTRL	Abcam, # ab47017
Anti-(p)T1730 TRPM6	Rabbit polyclonal Ab against mouse (p)TRPM6	RLSQ(p)TIPFTPIQC	Eurogentec (custom made)
Anti- $\beta$ -Actin Peroxidase	Mouse monoclonal Ab against $\beta$ -actin	DDDIAALVIDNGSGK	Sigma-Aldrich, # A3854

**Table 2.2.** Secondary antibodies used in this study.

Name	Specificity	Epitope sequence	Supplier
Anti-rabbit IgG HRP-linked (H+L chain)	Goat Ab against rabbit Ig-G	Not available	Cell Signaling, # 7074
Anti-guinea pig IgG HRP-linked (H+L chain)	Rabbit Ab against guinea pig Ig-G	Not available	Acris, # R1322HRP

## 2.4. Oligonucleotides

All oligonucleotides were produced in Metabion (Planegg-Martinsried) except for GAPDH primers, which were included in the RevertAid H Minus First Strand cDNA Synthesis Kit.

**Table 2.3.** Oligonucleotides used in this study.

Primer name	Sequence (5' → 3')	Amplicon (bp)	Annealing temperature (°C)
Trpm6 <sup>βgeo</sup> -Fwd	GCGTTGGCTACCCGTGAT	367	55
Trpm6 <sup>βgeo</sup> -Rev	CTGATAAGGAAGGCTGCTCTAAG		
Trpm6 <sup>+</sup> -Fwd	ATGGAAAGTAAATGATGCGTGAA	464	52
Trpm6 <sup>+</sup> -Rev	GGAAACTGACAGATGCCTTACTC		
Trpm7 <sup>Δ17</sup> -Fwd	TTATGGTTGCTGGGAATC	340	51
Trpm7 <sup>Δ17</sup> -Rev	CACAATGACAATACTGAAAGAACT		
Trpm7 <sup>+</sup> -Fwd	GGATACATTCACTCAGCACTAACT	530	52
Trpm7 <sup>+</sup> -Rev	CACTTATGAACTCAAAAAGTGA		
Trpm6RTa-Fwd	GCTGCCAAATCTGCCACAAT	651	50
Trpm6RTa-Rev	TGCCACAGTCCCATCATCACA		

**Table 2.3.** Oligonucleotides used in this study (continued).

Primer name	Sequence (5' → 3')	Amplicon (bp)	Annealing temperature (°C)
Trpm6RTb-Fwd	CCAGCTCAAAGACCCTCACAGATGC	586	56
Trpm6RTb-Rev	CACACCACATCTTTTCCGACCAG		
Trpm7RTa-Fwd	TCCCCCAGAATTACGACAGAGACGAC	365	54
Trpm7RTa-Rev	CATTCACTATATCCAGCAGCACCCACAT		
Trpm7RTb-Fwd	AGTAATTCAACCTGCCTCAA	287	50
Trpm7RTb-Rev	ATGGGTATCTCTTCTGTTATGTT		
hTrpm6RT-Fwd	TGCCCTCCTGGTTCTTTTCTTACT	421	57
hTrpm6RT-Rev	TTTCTGATGTCACTCGGATTCGTT		
hTrpm7RT-Fwd	GGAGTCCGCCCCGTGAGG	802	63
hTrpm7RT-Rev	TGACTTCCGCCCCATACTTTCCAACAG		
GAPDH-Fwd	CAAGGTCATCCATGACAACCTTTG	496	58
GAPDH-Rev	GTCCACCACCCTGTTGCTGTAG		

## 2.5. cDNA expression constructs

**Table 2.4.** cDNA expression constructs used in the present study.

Plasmid name	Vector backbone	Protein expressed	Reference
mTRPM6	pIRES	WT mouse TRPM6 protein	[181]
mTRPM6	pcDNA3.1 TOPO-TA	WT mouse TRPM6 protein	[181]
mTRPM6 <sup>K1810R</sup>	pIRES	'Kinase-dead' variant of mouse TRPM6	[181]
mTRPM6 <sup>T1730A</sup>	pIRES	'Kinase-dead' variant of mouse TRPM6	[181]
mTRPM7	pIRES	WT mouse TRPM7 protein	[110]

## 2.6. Buffers and standard solutions

**Tris-acetate-EDTA (TAE):** 40 mM Tris, 1 mM EDTA, 20 mM acetic acid

### **Solutions used for Western blot analysis:**

**Loading buffer (2X Laemmli buffer):** 250 mM TrisHCl pH 6.8, 40% Glycerin, 8% SDS, 0.04% Bromophenol blue, 1%  $\beta$ -mercaptoethanol

**Running gel:** 6% acrylamide/bisacrylamide, 375 mM TrisHCl pH 8.8, 0.1% SDS, 0.1% APS, TEMED (1:1000)

**Stacking gel:** 3% acrylamide/bisacrylamide, 125 mM TrisHCl pH 6.8, 0.1% SDS, 0.1% APS, TEMED (1:1000)

**Running buffer (Tris-Glycine-SDS (TGS)):** 25 mM Tris, 190 mM glycine, 0,1% SDS

**Transfer buffer (Tris-Glycine-methanol (TGM)):** 25 mM Tris, 190 mM glycine, 20% methanol

**Tris-buffered saline with Tween 20 (TBST):** 20 mM Tris, 137 mM NaCl, 0,1% Tween 20

**Blocking solution:** 5% non-fat milk in TBST

**Stripping solution:** 60 mM TrisHCl pH 6.8, 2% SDS, 0.7%  $\beta$ -mercaptoethanol

### **Enhanced chemiluminescence (ECL) solution:**

Solution 1: 100 mM TrisHCl pH 8.5, 2.5 mM luminol, 0.4 mM p-coumaric acid

Solution 2: 100 mM TrisHCl pH 8.5, 0.06%  $H_2O_2$

(Solution 1 and 2 were mixed 1:1 and used immediately for WB imaging)

## 2.7. Consumables

Biosphere filter tip 20	Sarstedt, # 70.1116.210
Biosphere filter tip 100	Sarstedt, # 70.760.212
Biosphere filter tip 1000	Sarstedt, # 70.762.211
Borosilicate glass with firepolished ends with filament	Science Products, # GB150TF-8P
Center-well organ cell culture dish, 60mm	BD, # 353037
Corning Costar cell culture plates (12-well)	Sigma-Aldrich, # CLS3513
Filtropur S 0.2	Sarstedt, # 83.1826.001
Filtropur S 0.45	Sarstedt, # 83.1826
Glass coverslips ø 12 mm	Carl Roth, # P231.1
HOLDERS for standard retransfer & handling pipettes	BioMedical Instruments
Injekt-F Solo syringe 2 ml	B Braun; # 4606027 V
Injekt Solo syringe 20 ml	B Braun; # 4606205 V
Micropipettes MicroFil 28 g, 97 mm	WPI; # MF28G-5
Micro tube 0.5 ml, PP	Sarstedt, # 72.699
Micro tube 1.5 ml, PP	Sarstedt, # 72.690.001
Multiply-Pro cup 0.2 ml, PP	Sarstedt, # 72.737.002
Multiply-µStrip Pro 8-strip (PCR reaction tubes)	Sarstedt, # 72.991.002
Nitrocellulose membrane Amersham Protran 0.45 µM	GE Healthcare Life Sciences, # 10600002
Norm-Ject syringe 10 ml	Henke Sass Wolf, # 4100.000V0
Parafilm M	Pechiney Plastic Packaging; # PM992
Pasteur pipettes	Carl Roth, # 4522
Pipette tip 20µl	Sarstedt, # 70.1116
Pipette tip 200µl	Sarstedt, # 70.760.002
Pipette tip 1000µl	Sarstedt, # 70.762

SafeSeal micro tube 2 ml, PP	Sarstedt, # 72.695.500
Serological pipette 2 ml	Sarstedt, # 86.1252.001
Serological pipette 5 ml	Sarstedt, # 86.1253.001
Serological pipette 10 ml	Sarstedt, # 86.1254.001
Serological pipette 25 ml	Sarstedt, # 86.1685.001
Standard retransfer & handling pipettes	BioMedical Instruments
Sterican needles ø 0,40 x 20 mm, 27 G X ¼	B Braun; # 4657705
TC dish 100, standard	Sarstedt, # 83.3902
TC dish 35, standard	Sarstedt, # 83.1800
TC flask T25, standard, ventilation cap	Sarstedt, # 83.3910.002
TC flask T75, standard, ventilation cap	Sarstedt, # 83.3911.002
TC plate 6-Well, standard, F	Sarstedt, # 83.3920
Tube 15 ml, 120x17 mm, PP	Sarstedt, # 62.554.502
Tube 50 ml, 114x28 mm, PP	Sarstedt, # 62.547.254

## 2.8. Equipment

**Table 2.5.** Equipment employed in the present study.

Instrument	Model	Supplier
Air pressure control	MPCU-3	Lorenz Meßgerätebau
Cell culture hood	HERAsafe	Thermo Fisher Scientific
Centrifuges	Heraeus Labofuge 400	Thermo Fisher Scientific
	Heraeus Pico 17	Thermo Fisher Scientific
Counting chambers	Neubauer, 0640110	Marienfeld Superior
Electroporator	Neon Transfection System	Thermo Fisher Scientific
Gel imaging systems	Chemi-Smart-5100	PeqLab
	Infinity-3026WL/26MX	PeqLab

**Table 2.5.** Equipment employed in the present study (continued).

<b>Instrument</b>	<b>Model</b>	<b>Supplier</b>
Horizontal gel electrophoresis	Compact M	Biometra
Incubator with CO <sub>2</sub>	HERAcell 240	Thermo Fisher Scientific
Microelectrode Puller	DMZ-UNIVERSAL-PULLER	Zeitz Instruments
Micromanipulator	ACCi UC	Scientifica
Microscopes	Axiovert 40 CFL	ZEISS
	Axio Vert.A1 equipped with Power supply 12V 100W and COLIBRI.2 Controller	ZEISS
	SteREO Discovery.V8 equipped with Cold Light Source KL 2500 LCD	ZEISS
Microwave	Microwave & Grill	Severin
Osmometer	VAPRO Vapor Pressure 5600	Wescor Inc
Patch Clamp Amplifier	EPC 10 USB	HEKA
pH Meter	Lab 850	Schott Instruments
Pipettes	P10, P20, P200, P1000, P100	PeqLab
Power supply	PowerPac HC	Bio-rad
	EV231	PeqLab
Precision balance	572	Kern
	ALT 220-5DAM	Kern
Rotator	LD79	Labinco
Shaker	Mini Rocker MR-1	PeqLab
Spectrophotometer	BioPhotometer plus	Eppendorf
Thermocycler	TProfessional TRIO	Analytik Jena
Thermo shaker	TS-100	PeqLab

**Table 2.5.** Equipment employed in the present study (continued).

<b>Instrument</b>	<b>Model</b>	<b>Supplier</b>
Vertical gel electrophoresis	Mini-PROTEAN Tetra Cell	Bio-rad
Vortexer	TOP-MIX 94500	Bioblock Scientific

## 2.9. Software

**Table 2.6.** Software used in this project.

<b>Software</b>	<b>Version</b>	<b>Supplier</b>
Chemi-Capt 5000	v15.02	Vilber
FitMaster	v2x53	HEKA
Igor Pro	v.6.2.2.2	Wavemetrics
Infinity-Capt	v14.2	Vilber
IrfanView	v4.36	Irfan Skiljan
PatchMaster	v2x69	HEKA
WEBMAXC STANDARD	12/31/03	maxchelator.stanford.edu
ZEN 2 Pro	V2.0.0.0	ZEISS Microscopy

## 3. Methods

### 3.1. Isolation and characterization of *Trpm6* and *Trpm7* deficient trophoblast stem (TS) cells

#### 3.1.1. Mouse strains

For this study, we employed two different mutant mouse lines. The first line with a null mutation in *Trpm6* (129S5/SvEvBrd-C57BL/6) was obtained from the Texas Institute for Genomic Medicine as previously reported [143]. These *Trpm6* deficient mice were generated by a 'gene-trap' approach using a targeting vector containing a  $\beta$ geo reporter sequence ( $\beta$ geo), designed to replace the exons 2 and 3 of *Trpm6* (Fig. 3.1). The  $\beta$ geo sequence contained a splice acceptor site sequence (SP), a bacterial  $\beta$ -galactosidase marker sequence (*LacZ*), an internal ribosome entry site (*IRES*) and a neomycin resistance cassette (*NeoR*) (Fig. 3.1). In the mutant allele (*Trpm6* <sup>$\beta$ geo</sup>), the endogenous *Trpm6* promoter drove the expression of an aberrant transcript encoding only exon 1 of *Trpm6* spliced to *LacZ* sequence, instead of WT mRNA, resulting in a loss-of-function mutation of TRPM6. *Trpm6* <sup>$\beta$ geo</sup> mice were crossed with C57BL/6J mice for six generations.

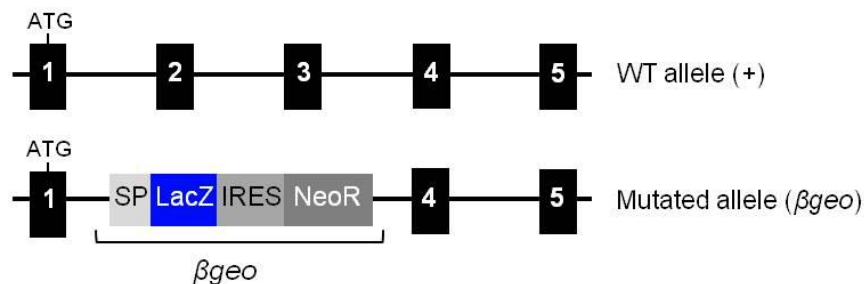


**Figure 3.1. Targeting strategy used for the generation of *Trpm6* <sup>$\beta$ geo</sup> allele.** The mutant locus contains a  $\beta$ geo cassette ( $\beta$ geo) instead of the genomic sequence encompassing exons 2 and 3 of *Trpm6*. Consequently, the *Trpm6* promoter drives the expression of the mutant transcript encoding bacterial  $\beta$ -galactosidase (*LacZ*) and neomycin resistance protein (Neo). SP = splice acceptor site; IRES = internal ribosome entry site.

The second mouse line with a conditional mutation in *Trpm7* (*Trpm7*<sup>*fl/fl*</sup> mice, 129S6/SvEvTac) was provided by David Clapham from Harvard Medical School, Boston, USA [128]. *Trpm7*<sup>*fl/fl*</sup> allele was produced using a targeting vector with two intronic LoxP sites flanking exon 17 of the *Trpm7* gene (*Trpm7*<sup>*fl*</sup> allele) (Fig. 3.2A). We

crossed  $Trpm7^{fl/fl}$  females and  $Sox2-Cre$  transgenic males (expressing a  $Cre$  recombinase controlled by  $Sox-2$  promoter [182]) to induce a deletion of exon 17 ( $Trpm7^{\Delta 17}$  allele) in early embryo (Fig. 3.2B). The generated  $Trpm7^{\Delta 17/+}$  line was maintained by intercross of  $Trpm7^{\Delta 17/+}$  parents. In line with the original work [128],  $Trpm7^{\Delta 17/\Delta 17}$  offspring was never obtained, suggesting that  $Trpm7^{\Delta 17}$  allele is a true null mutation.

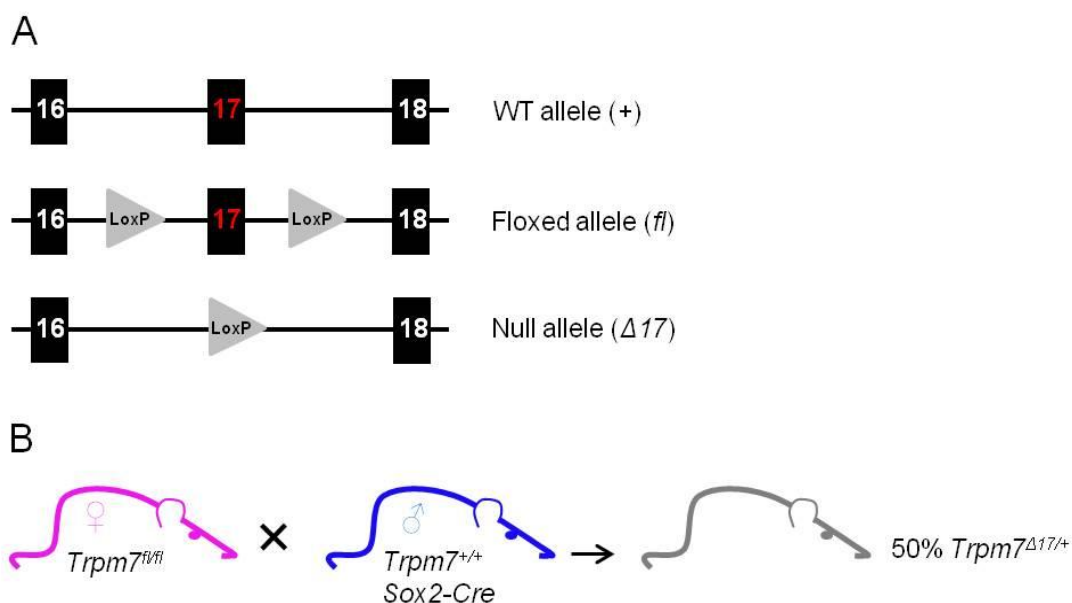


**Figure 3.2. Generation of  $Trpm7^{\Delta 17/+}$  mice (A)** A null mutation of  $Trpm7$  ( $\Delta 17$ ) was generated by a  $Sox2-Cre$  mediated deletion of the floxed exon 17. **(B)** Breeding strategy for the generation of  $Trpm7^{\Delta 17/+}$  mice.  $Trpm7^{fl/fl}$  females were crossed with  $Sox2-Cre$  males to obtain mice heterozygous for  $Trpm7^{\Delta 17}$  allele.

### 3.1.2. Mouse genotyping

The mice were genotyped using PCR analysis of DNA isolated from tail fragments. The extraction of DNA was performed using GenElute mammalian genomic DNA miniprep kit (Sigma-Aldrich) according to the manufacturer's instructions. PCR reaction contained 0.5  $\mu$ l extracted DNA, 0.2 mM each dNTPs (Thermo Fisher Scientific), 1X REDTaq PCR buffer with  $MgCl_2$  included (Sigma-Aldrich), 0.4  $\mu$ M oligonucleotides mixture (Metabion), 1 U REDTaq DNA polymerase (Sigma-Aldrich) to reach a final volume of 25  $\mu$ l as outlined in Table 3.1.

**Table 3.1.** Master mix for PCR reaction.

Reagent	Initial concentration	Final concentration	Volume ( $\mu$ l)
DNA extract			0.5
REDTaq Buffer	10X	1X	2.5
dNTPs	10 mM (each)	0.2 mM	0.5
Forward Primer	100 $\mu$ M	0.4 $\mu$ M	0.1
Reverse Primer	100 $\mu$ M	0.4 $\mu$ M	0.1
REDTaq Genomic DNA Polymerase	1 U/ $\mu$ l	1 U	1
Water			20.3
		<b>Total</b>	<b>25</b>

*Trpm6* <sup>$\beta$ geo</sup> allele was assessed using the following oligonucleotides: *Trpm6* <sup>$\beta$ geo</sup>-Forward 5'-GCG TTG GCT ACC CGT GAT-3' and *Trpm6* <sup>$\beta$ geo</sup>-Reverse 5'-CTG ATA AGG AAG GCT GCT CTA AG-3'. 367 bp amplicon was produced with the following PCR settings:

Hot start	95°C	5 min	
Denaturation	95°C	30 sec	10 cycles ( $-1^{\circ}$ C per cycle)
Annealing	65°C	30 sec	
Elongation	72°C	60 sec	
Denaturation	95°C	30 sec	35 cycles
Annealing	55°C	30 sec	
Elongation	72°C	60 sec	
Final elongation	72°C	5 min	

*Trpm6*<sup>+</sup> allele was analyzed using the following oligonucleotides: *Trpm6*<sup>+</sup>-Forward 5'-ATG GAA AGT AAA TGA TGC GTG AA-3' and *Trpm6*<sup>+</sup>-Reverse 5'-GGA AAC TGA CAG ATG CCT TAC TC-3'. 464 bp amplicon was produced as follows:

Hot start	95°C	5 min	
Denaturation	95°C	30 sec	10 cycles (−1°C per cycle)
Annealing	62°C	30 sec	
Elongation	72°C	60 sec	
Denaturation	95°C	30 sec	35 cycles
Annealing	52°C	30 sec	
Elongation	72°C	60 sec	
Final elongation	72°C	5 min	

The following primer pair were used to detect the *Trpm7*<sup>Δ17</sup> allele: *Trpm7*<sup>Δ17</sup>-Forward 5'-TTA TGG TTG CTG GGA ATC-3' and *Trpm7*<sup>Δ17</sup>-Reverse 5'-CAC AAT GAC AAT ACT GAA AGA ACT-3'. The amplified PCR product was 340 bp. We used the following PCR conditions:

Hot start	94°C	5 min	
Denaturation	94°C	30 sec	10 cycles (−1°C per cycle)
Annealing	61°C	30 sec	
Elongation	72°C	60 sec	
Denaturation	95°C	30 sec	40 cycles
Annealing	51°C	30 sec	
Elongation	72°C	60 sec	
Final elongation	72°C	5 min	

To assess of *Trpm7*<sup>+</sup> allele, we used the following oligonucleotides: *Trpm7*<sup>+</sup>-Forward 5'-GGA TAC ATT CAC TCA GCA CTA ACT-3' and *Trpm7*<sup>+</sup>-Reverse 5'-CAC TTA TGA ACT CAA AAA CTG GA-3'. 530 bp amplicon was generated using the following program:

Hot start	94°C	5 min	
Denaturation	94°C	30 sec	10 cycles (−1°C per cycle)
Annealing	62°C	30 sec	
Elongation	72°C	60 sec	
Denaturation	95°C	30 sec	35 cycles
Annealing	52°C	30 sec	
Elongation	72°C	60 sec	
Final elongation	72°C	5 min	

PCR reactions were carried out with TProfessional TRIO thermocycler (Analytik Jena). PCR products were separated by electrophoresis using 1% agarose gel in 1X Tris-acetate-EDTA (TAE) buffer and stained with Roti-GelStain (Carl Roth). Gels were imaged using Infinity-3026WL/26MX (PeqLab).

### 3.1.3. Housing of mice

Animals were housed in individually ventilated polycarbonate cages (IVC System, Tecniplast, Germany) in the animal facility of WSI, LMU Munich. Cages were changed weekly. Mice were kept under a 12:12h light-dark cycle with artificial lighting. Temperature and relative humidity were 22+/-1°C and 50+/-5%, respectively. Breeding mice had free access to multigrain chow ssniff M-Z (#V1125, ssniff Spezialdiäten GmbH) and drinking water (*ad libitum*). Litters were weaned at three weeks of age, genotyped and maintained as described above except that a 'maintenance' chow ssniff R/M-H (#V1535, ssniff Spezialdiäten GmbH) was used.

### 3.1.4. Isolation of TS cells

Trophoblast stem cells were isolated as described earlier [183] with minor modifications [184, 185]. To produce WT (control) and *Trpm6* deficient TS cells, we used *Trpm6*<sup>geo/+</sup> parents. 3.5 days post-coitum blastocysts were isolated from sacrificed pregnant mice. Individual blastocysts were cultured in 12-well plates (Sigma-Aldrich) containing 8x10<sup>4</sup>/well irradiated primary mouse embryonic fibroblasts (PMEFs) (Millipore) in RPMI-1640 medium (Sigma-Aldrich), 20% fetal bovine serum (FBS) (ES type, Thermo Fisher Scientific), 1 mM sodium pyruvate (cell culture type, Sigma-Aldrich), 100 µM β-mercaptoethanol (cell culture tested, Sigma-Aldrich), 50 U/ml penicillin and 50 µg/ml streptomycin (Sigma-Aldrich), 1 µg/ml heparin (cell culture type, Sigma-Aldrich), 25 ng/ml human recombinant FGF4, 5 ng/ml human recombinant TGF-β1, 10 ng/ml human/mouse/rat recombinant Activin A (all growth factors from R&D Systems) and additional 10 mM MgCl<sub>2</sub> (Carl Roth). The 12-well plates containing the blastocysts were incubated in a humidified cell culture incubator (HERAcell 240, Thermo Fisher Scientific) at 37°C and 5% CO<sub>2</sub>. During the following 3 days, the blastocysts were monitored for hatching from the zona pellucida and attachment to the MEFs. The attached blastocysts were disaggregated using 0.05% trypsin-EDTA (Sigma-Aldrich) and further cultured as described above. Tight epithelial-like TS colonies were appeared after 3-7 days. The obtained TS clones were propagated in MEF-free conditions, genotyped and further cultured without additional Mg<sup>2+</sup> in the medium.

*Trpm7* gene deficient and the relative control TS cells were obtained from mice heterozygous for *Trpm7*<sup>A17/+</sup> allele as described above and maintained using the culture medium supplemented with 10 mM MgCl<sub>2</sub>.

### 3.1.5. Maintaining of TS cell lines

TS cells were cultured in MEF-free conditions at 37°C, 5% CO<sub>2</sub> in T25 flasks (Sarstedt) using the TS medium described above. Additional 10 mM MgCl<sub>2</sub> were included only to the cell culture medium of *Trpm7* gene deficient cells. The cells were passaged every 3-4 days. The cell culture medium was aspirated, the cells were washed with Dulbecco's phosphate-buffered saline (DPBS) (Sigma-Aldrich) and 0.05% trypsin-EDTA was added, followed by 3 minutes incubation at 37°C. The trypsin reaction was terminated by adding the TS medium and the cells were gently disaggregated by pipetting. After centrifugation (1.200 g, 2 min, RT), the cell pellet was resuspended in fresh medium and transferred to a new flask. For long-term storage, aliquots of TS cells

were kept in liquid nitrogen. For cryopreservation, TS cells were trypsinated, pelleted and resuspended in TS medium containing 50% FBS, 30% TS medium and 20% DMSO (Sigma-Aldrich). TS cells were placed in Mr. Frosty freezing container (Thermo Fisher Scientific) and incubated at  $-80^{\circ}\text{C}$  overnight. The next day, TS cells were passed to a tank with liquid nitrogen.

To determine whether *Trpm6* and *Trpm7* deficient TS cells were able to proliferate in a regular medium without  $\text{Mg}^{2+}$  supplementation, TS cells were seeded in 6-well plates ( $1 \times 10^5$  cells/well) in a medium supplemented with 10 mM  $\text{Mg}^{2+}$  (day 0). After 24 h (day 1), the cells were washed twice with PBS and a fresh culture medium with or without  $\text{Mg}^{2+}$  (10 mM) was added. Cell density was examined 24 (day 2), 48 (day 3) and 72 h (day 4) using a Neubauer chamber (Marienfeld Superior). To calculate growth rates, cell density at day 1 was considered as 100% (mean $\pm$ SEM). The experiment was repeated 3 times. Two-tailed *t*-test was applied for comparison of growth rates of *Trpm6* or *Trpm7* deficient vs corresponding control cells.

Genotype of TS clones were determined by PCR analysis of extracted genomic DNA, using the same reagents and conditions reported above for the mouse genotyping.

TS cells were electroporated using Neon Transfection System (Invitrogen).  $1 \times 10^5$  cell suspension containing 2  $\mu\text{g}$  cDNA pcDNA-IRES-TRPM6 expression plasmid were electroporated with the following program: pulse voltage 1000 v, pulse width 30 ms and pulse number 2. The cells were examined 24 h after electroporation.

### 3.2. Generation of *TRPM7* deficient HAP1 cells

Human near-haploid (HAP1) cells was derived from the male chronic myeloid leukemia (CML) cell line KBM-7 [186-189]. *TRPM7* deficient (KO) HAP1 cells (clone 10940-04) were engineered from parental HAP1 cell line (clone C631) using CRISPR/Cas9 system in Horizon Genomics (Vienna, Austria) [144].

HAP1 clones were cultured in Iscove's modified Dulbecco's medium (IMDM) (Thermo Fisher Scientific) supplemented with 10% fetal bovine serum (FBS) (Thermo Fisher Scientific) and 100 U/ml penicillin and 100  $\mu\text{g}/\text{ml}$  streptomycin (Sigma-Aldrich). The KO clone was cultured in the presence of additional 10 mM  $\text{MgCl}_2$  (Carl Roth). Cells were maintained in a humidified cell culture incubator (HERAcell 240, Thermo Fisher Scientific) at  $37^{\circ}\text{C}$  and 5%  $\text{CO}_2$ . HAP1 cells were passaged twice a week in T75 flask

(Sarstedt). For electrophysiological experiments, the cells were passaged and seeded directly on glass coverslips (Carl Roth).

To study whether *TRPM7* deficient and control HAP1 cells were able to proliferate in a regular medium without  $Mg^{2+}$  supplementation, we performed experiments similarly to studies described for TS cells (see section 3.1.5).

For the long-term storage in liquid nitrogen, the cells were pelleted by centrifugation and resuspended in IMDM medium with 20% FBS. Next, an equal amount of IMDM medium containing 20% FBS and 20% DMSO (Sigma-Aldrich) was added to the cellular suspension, placed in Mr. Frosty freezing container (Thermo Fisher Scientific) and incubated at  $-80^{\circ}C$  overnight. The next day, cells were passed to a tank with liquid nitrogen.

### 3.3. Assessment of primary mouse megakaryocytes

The primary megakaryocytes (MKs) were isolated from the bone marrow of either *Trpm7<sup>fl/fl</sup>* mice or mice with a conditional megakaryocytes-specific *Trpm7* mutation (*Trpm7<sup>fl/fl</sup>;Pf4cre* mice) using a negative depletion strategy as described in [180]. *Trpm7<sup>fl/fl</sup>;Pf4cre* mice were generated by intercrossing *Trpm7<sup>fl/fl</sup>* mice (Fig. 3.2A) with mice carrying the *Cre* recombinase under a control of the platelet factor 4 (*Pf4*) promoter [190]. The obtained cells were cultured in MK-medium containing IMDM (Thermo Fisher Scientific), 10% FBS (Thermo Fisher Scientific), 1% non-essential amino acids (NEAA) (Thermo Fisher Scientific), 100 U/ml penicillin and 100  $\mu$ g/ml streptomycin (Sigma-Aldrich), 0.5% thrombopoietin (Thpo) and 50  $\mu$ g/ml recombinant hirudin (both reagents are provided by Dr. Attila Braun's laboratory) at  $37^{\circ}C$  and 5%  $CO_2$  for 3 days.

MK fraction was enriched immediately prior patch-clamp experiments as follows. The cells were centrifuged (200 g, 5 min, RT) and resuspended in 1.5 ml MK medium. The bovine serum albumin (BSA) gradient was produced in a 15 ml tube with 1.5 ml volume using two buffers containing 1.5% and 3% BSA. MKs were placed on the top of BSA gradient, allowed to sediment during 30 min at RT. The obtained cell pellet was resuspended in 3 ml MK medium, centrifuged (200 g, 5 min, RT) and resuspended in 2 ml MK medium. The cell suspension was transferred onto glass coverslips (Carl Roth) for patch-clamp experiments (see 3.8).

### 3.4. Culture and transient transfection of HEK 293 cells

Human embryonic kidney (HEK) 293 cells were cultured in Eagle's minimum essential medium (MEM) (Sigma Aldrich) supplemented with 10% FBS (Thermo Fisher Scientific) and 100 U/ml penicillin and 100 µg/ml streptomycin (Sigma-Aldrich). Cells were maintained in a humidified cell culture incubator (HERAcell 240, Thermo Fisher Scientific) at 37°C and 5% CO<sub>2</sub>. For electrophysiological experiments, the cells were seeded in 6-well plates (Sarstedt) (~10<sup>5</sup> cells/well). The next day, the cells were transiently transfected with various cDNA plasmids (1 or 2 µg/well as indicated in the text) using Lipofectamine 2000 reagent (Thermo Fisher Scientific) according to the manufacturer's instructions. We performed experiments 24h after transfection.

### 3.5. Generation of mouse TRPM6 cDNA expression constructs

cDNA encoding mouse TRPM6 (NCBI accession KX375810) was cloned in pIRES2-EGFP (Clontech) expression vectors as reported before [181]. K1810R and T1730A point mutations in mouse TRPM6 were introduced by site-directed mutagenesis (QuikChange kit, Agilent Technologies) and confirmed by sequencing. The mouse TRPM7 expression constructs in pIRES2-EGFP vector was reported previously [191]. 3D predictions of the TRPM6 kinase domain structure were generated as reported previously [79, 191] using MODELLER ([modbase.compbio.ucsf.edu/modweb](http://modbase.compbio.ucsf.edu/modweb)) and UCSF Chimera ([www.cgl.ucsf.edu/chimera](http://www.cgl.ucsf.edu/chimera)).

### 3.6. Reverse transcriptase PCR (RT-PCR) analysis

Total RNA was extracted from cell pellets using the GenElute mammalian total RNA miniprep kit (Sigma-Aldrich). RNA content was determined using a spectrophotometer (BioPhotometer plus, Eppendorf). RNA was converted into a complementary DNA (cDNA) by the RevertAid H Minus M-MuLV reverse transcriptase (Thermo Fisher Scientific). 1 µg total RNA were processed using 0.2 µg random hexamer primers mix, 1 mM dNTPs mix, reaction buffer (containing 250 mM Tris-HCl pH 8.3, 250 mM KCl, 20 mM MgCl<sub>2</sub>, 50 mM DTT), 20 U RiboLock RNase inhibitor and 200 U RevertAid H Minus M-MuLV reverse transcriptase as outlined in Table 3.2. The reverse-transcription reaction was performed for 5 min at 25°C, followed by 60 min incubation at 42°C and heat-terminated for 5 min at 72°C.

**Table 3.2.** Master mix for reverse-transcriptase reaction.

Reagent	Initial concentration	Final concentration	Volume ( $\mu$ l)
Total RNA			1 $\mu$ g
Random Hexamer Primer	100 $\mu$ M (0.2 $\mu$ g/ $\mu$ L)	5 $\mu$ M (0.2 $\mu$ g)	1
dNTPs Mix	10 mM	1 mM	2
Reaction Buffer	5X	1X	4
RiboLock RNase Inhibitor	20 U/ $\mu$ l	20 U	1
RevertAid H Minus M-MuLV Reverse Transcriptase	200 U/ $\mu$ l	200 U	1
Water			to 20 $\mu$ l
		<b>Total</b>	<b>20</b>

### 3.6.1. RT-PCR analysis of *Trpm6* deficient TS cells

The obtained cDNA was used for PCR analysis using REDTaq DNA polymerase. To detect *Trpm6* transcripts in *Trpm6* deficient TS cells, we used two different primer pairs. *Trpm6*RTa-Forward 5'-GCT GCC AAA TCT GCC ACA AT-3' and *Trpm6*RTa-Reverse 5'-TGC CCA CAG TCC CAT CAT CAC A-3' primers were used to generate 651 bp amplicon:

Hot start	94°C	5 min	
Denaturation	94°C	30 sec	10 cycles (–1°C per cycle)
Annealing	60°C	30 sec	
Elongation	72°C	60 sec	
Denaturation	94°C	30 sec	30 cycles
Annealing	50°C	30 sec	
Elongation	72°C	60 sec	
Final elongation	72°C	5 min	

The second PCR reaction (586 bp amplicon) was performed using Trpm6RTb-Forward 5'-CCA GCT CAA AAG ACC CTC ACA GAT GC-3' and Trpm6RTb-Reverse 5'-CAC ACC ACA TCT TTT CCG ACC AG-3' primers with the following PCR settings:

Hot start	94°C	5 min	
Denaturation	94°C	30 sec	10 cycles (–1°C per cycle)
Annealing	66°C	30 sec	
Elongation	72°C	60 sec	
Denaturation	94°C	30 sec	35 cycles
Annealing	56°C	30 sec	
Elongation	72°C	60 sec	
Final elongation	72°C	5 min	

Expression of *Trpm7* in TS cells was study using Trpm7RTa-Forward 5'-TCC CCC AGA ATT ACG ACA GAG ACG AC-3' and Trpm7RTa-Reverse 5'- CAT TCA CTA TAT CCA GCA GCA CCC ACA T-3' primers (365 bp amplicon) and the following PCR conditions:

Hot start	94°C	3 min	
Denaturation	94°C	30 sec	25 cycles
Annealing	54°C	30 sec	
Elongation	72°C	60 sec	
Final elongation	72°C	5 min	

### 3.6.2. RT-PCR analysis of *Trpm7* deficient TS cells

We employed Trpm7RTb-Forward 5'-AGT AAT TCA ACC TGC CTC AA-3' and Trpm7RTb-Reverse 5'-ATG GGT ATC TCT TCT GTT ATG TT-3' primers to detect *Trpm7* transcripts (287 bp product) with the following conditions:

Hot start	94°C	5 min	
Denaturation	94°C	30 sec	10 cycles (–1°C per cycle)
Annealing	60°C	30 sec	
Elongation	72°C	60 sec	
Denaturation	94°C	30 sec	
Annealing	50°C	30 sec	35 cycles
Elongation	72°C	60 sec	
Final elongation	72°C	5 min	

To study *Trpm6* transcripts, we used primers (Trpm6RTb) described for *Trpm6* deficient TS cells (see 3.6.1).

### 3.6.3. RT-PCR analysis of *TRPM7* deficient HAP1 cells

For the detection of *TRPM6* and *TRPM7* transcripts in HAP1 cells, we used another set of primers since these cells have a human origin. The primers hTrpm6RT-Forward 5'-TGC CCT CCT GGT TCT TTT CTT ACT-3' and hTrpm6RT-Reverse 5'-TTT CTG ATG TCA CTC GGA TTC GTT-3' were used to probe *TRPM6* expression (421 bp) with the following conditions:

Hot start	95°C	5 min	
Denaturation	95°C	30 sec	10 cycles (–1°C per cycle)
Annealing	67°C	30 sec	
Elongation	72°C	60 sec	
Denaturation	95°C	30 sec	
Annealing	57°C	30 sec	40 cycles
Elongation	72°C	60 sec	
Final elongation	72°C	5 min	

The primers hTrpm7RT-Forward 5'-GGA GTC CGC CCC GTG AGG -3' and hTrpm7RT-Reverse 5'-TGA CTT CCG CCC CAT ACT TTC CAA CAG-3' were used to detect *TRPM7* (802 bp) with the following conditions:

Hot start	95°C	5 min	
Denaturation	95°C	30 sec	10 cycles (−1°C per cycle)
Annealing	73°C	30 sec	
Elongation	72°C	90 sec	
Denaturation	95°C	30 sec	35 cycles
Annealing	63°C	30 sec	
Elongation	72°C	90 sec	
Final elongation	72°C	5 min	

Expression levels of glyceraldehyde 3-phosphate dehydrogenase (*GAPDH*) were assessed using the primer pair GAPDH-Forward 5'-CAA GGT CAT CCA TGA CAA CTT TG-3' and GAPDH-Reverse 5'-GTC CAC CAC CCT GTT GCT GTA G-3' and the following conditions (496 bp amplicon):

Hot start	94°C	5 min	
Denaturation	94°C	30 sec	10 cycles (−1°C per cycle)
Annealing	68°C	30 sec	
Elongation	72°C	30 sec	
Denaturation	94°C	30 sec	35 cycles
Annealing	58°C	30 sec	
Elongation	72°C	30 sec	
Final elongation	72°C	5 min	

PCR reactions were carried out in TProfessional TRIO thermocycler (Analytik Jena). Amplified PCR products were stained with Roti-GelStain (Carl Roth) and visualised by electrophoresis using 1% agarose gel in 1X TAE buffer. The gels were examined using Infinity-3026WL/26MX gel imaging system (PeqLab).

### 3.7. Western blot analysis

#### 3.7.1. Assessment of recombinant TRPM6 and TRPM7 proteins in HEK 293 cells

HEK 293 cells cultured in 6-well plates (~50% confluence) were transfected with WT or mutant variants of mouse TRPM6 cDNAs using Lipofectamine2000 reagent (see 3.4). 24 h after transfection, the cells were lysed using 300 µl/well Pierce IP lysis buffer (Thermo Fisher Scientific) supplemented with 3 µl protease inhibitor cocktail (Biotool) and 6 µl phosphatase inhibitor cocktail solution (Biotool). After centrifugation (13.000 g, 1 min, 4°C), the supernatant was collected in a fresh 1.5 ml tube. Next, the cell lysates were diluted 1:1 with 2X Laemmli buffer (supplemented with 1% β-mercaptoethanol) followed by heating at 70°C for 10 minutes, aliquoted (20 µl) and stored at -80 °C.

20 µl of the cell lysates were subjected to a sodium dodecyl sulfate-polyacrylamide gel electrophoresis (SDS-PAGE) at +120 mV in Mini-PROTEAN Tetra Cell unit (Bio-rad). 6% polyacrylamide gel (Rotiphorese gel 30, Carl Roth) was used. Separated proteins were transferred from the gel to a nitrocellulose membrane (GE Healthcare Life Sciences) using Mini-PROTEAN Tetra Cell transfer unit for ~12h at 150 mA. Next, the membrane was incubated in Tris-buffered saline (TBS)/0.1% Tween (TBST) supplemented with 5% non-fat dry milk (Carl Roth) for 1 hour at RT. The membranes were incubated for ~12h at 4°C with primary antibodies diluted in TBST and 5% BSA (Sigma-Aldrich). A guinea pig anti-TRPM6 polyclonal antibodies (Abcam, ab47017) were used to detect TRPM6 (1:4000 dilution), whereas a rabbit monoclonal anti-TRPM7 [EPR4582] antibody (Abcam, ab109438) (1:2000) was used to detect TRPM7. To assesses autophosphorylation of TRPM6, 1 µg/ml anti-(p)T1730 mouse TRPM6 polyclonal antibodies (Eurogentec) was used. Next, the membranes were washed (x3) with TBST and incubated for 1 hour at RT with corresponding horseradish peroxidase (HPR) labeled antibodies diluted 1:1000 in TBST and 5% BSA. The secondary antibodies were either goat anti-rabbit IgG (Cell Signaling, 7074) or rabbit anti-guinea pig IgG (Acris, R1322HRP). After washing with TBST (x3), the membranes were examined using an enhanced chemiluminescence (ECL) reagent and Chemi-Smart-

5100 (PepLab). As a loading control,  $\beta$ -actin was detected in the same cell lysates using mouse anti- $\beta$ -Actin-HPR (1:50000) (Sigma-Aldrich, A3854) as described above.

### **3.7.2. Assessment of endogenous TRPM6 and TRPM7 in TS and HAP1 cells**

To detect native TRPM6 and TRPM7 proteins, we performed immunoprecipitation (IP) of TRPM6 and TRPM7 followed by Western blot analysis. IP was conducted with Pierce Classic IP kit (Thermo Fisher Scientific) according to the manufacturer's instructions. Briefly, TS or HAP1 cells grew at ~80% confluence in 100 mm dish. Cell lysates were obtained by treatment of the cells by ice-cold 800  $\mu$ l lysis buffer provided by the kit supplemented with 1.5 mg/ml SIGMAFAST Protease Inhibitor mix (Sigma-Aldrich). The cell lysates were assessed for protein contents (Protein Quantification Kit-Rapid, Sigma-Aldrich) and their volumes were adjusted to obtain an equal concentration of total proteins in control vs KO samples. Next, 500  $\mu$ l of the cell lysates were incubated with 10  $\mu$ g of either anti-TRPM6 or anti-TRPM7 antibodies for 1 h at 4°C using a rotation setup (Labinco). The rabbit anti-TRPM6 Ab 75 polyclonal antibodies (Eurogentec) were used for TRPM6 IP, whereas the mouse anti-TRPM7 [S74-25] monoclonal antibody (Abcam, ab85016) was employed for TRPM7 IP. Next, 20  $\mu$ l suspension of A/G proteins immobilized on agarose beads were added to the cell lysates and the tubes were incubated for ~12 h at 4°C at the rotation. The beads were precipitated by centrifugation (1.000 g, 1 min) and washed 3x with 200  $\mu$ l of the lysis/wash buffer. Finally, 50  $\mu$ l 2X Laemmli buffer containing 1%  $\beta$ -mercaptoethanol was added to the individual IP samples and immune complexes were dissociated by incubation of the beads at 70°C for 10 minutes. Lastly, the obtained IP samples were loaded to 6% SDS-PAGE and Western blot analysis was performed as described above.

### **3.8. Patch-clamp assessment of TRPM6 and TRPM7 currents**

~1 h before performing electrophysiological experiments, the cells were dissociated by trypsin and placed on 12 mm glass coverslips (Carl Roth) covered with poly-D-lysine (0.1 mg/ml) (Sigma-Aldrich). The cells were allowed to adhere by incubating for ~1 h in a humidified cell culture incubator (HERAcell 240, Thermo Fisher Scientific) at 37°C and 5% CO<sub>2</sub> in the corresponding cell culture medium. Next, the culture medium was

replaced by different physiological saline (see 3.8.1 and 3.8.2) and the cells were studied at RT (22-25°C) during 1 h.

We used a tight-seal whole-cell configuration. Currents were recorded using an EPC10 patch-clamp amplifier (HEKA) controlled by PatchMaster software (v2x69, HEKA). Data were analysed using FitMaster (v2x53, HEKA) and Igor Pro (v.6.2.2.2, Wavemetrics) software. Patch pipettes were made of borosilicate glass with fire-polished ends with filament (Science Products) and had resistances between 2.6 to 3.4 M $\Omega$  after filling with the Cs-glutamate based standard internal solution. All voltages were corrected for a liquid junction potential of +10 mV between external and internal solutions when internal solutions contained glutamate. Currents were elicited by 50 ms ramps from -100 to +100 mV (0.5 Hz) with 0 mV holding potential. Inward and outward current amplitudes were acquired at -80 mV and +80 mV, normalized to the cell size (pA/pF) and plotted versus time. Capacitive currents and series resistance ( $R_s$ ) were determined and corrected before each ramp using the automatic capacitance compensation of the software. Series resistance compensation of 80% was used to reduce voltage errors in all experiments.

To determine IC<sub>50</sub> values, data were fitted with the Hill equation:

$$E(c) = E_{\max} \times (c^h / (IC_{50}^h + c^h))$$

with E being the effect/current at a given concentration c of activator/inhibitor,  $E_{\max}$  the maximally achievable effect, IC<sub>50</sub> the half-maximal concentration and h the Hill factor.

### **3.8.1. Examination of the endogenous TRPM7-like currents in TS, HAP1 and MK cells**

As described above (3.8), the cells were grown on glass coverslips. The coverslips were transferred to 35 mm cell culture dishes containing a standard external solution comprising (mM): 140 NaCl, 3 CaCl<sub>2</sub>, 2.8 KCl, 10 HEPES-NaOH and 11 glucose (Sigma-Aldrich or Carl Roth as outlined in section 2.1). For some experiments (indicated in the text), an external solution contained 1 mM CaCl<sub>2</sub> and 2 mM MgCl<sub>2</sub> instead of 3 mM CaCl<sub>2</sub>. The divalent cation-free (DVF) extracellular solution contained (in mM): 140 NaCl, 2.8 KCl, 5 Na-EDTA, 10 HEPES-NaOH and 11 glucose. Unless stated otherwise, the divalent cation-free intracellular solution contained (in mM): 120 Cs-glutamate, 8 NaCl, 5 Cs-EDTA, 10 Cs-EGTA and 10 HEPES-CsOH (Carl Roth and Sigma-Aldrich, as outlined in 2.1).

To obtain  $Mg^{2+}$  concentration-response datasets, the intracellular pipette solution comprised (in mM): 120 Cs-glutamate, 8 NaCl, 10 Cs-BAPTA (Biotium), 10 HEPES-CsOH and different amount of  $MgCl_2$  and Cs-EDTA as outlined in Table 3.3. To access the Mg-ATP concentration-response, the intracellular solution contained (in mM): 120 or 140 Cs-glutamate, 8 NaCl, 2.7 Cs-EDTA, 10 HEPES-CsOH, and different amount of Mg-ATP (Sigma-Aldrich) and  $MgCl_2$  as indicated in Table 3.4. Concentrations of either free  $Mg^{2+}$  or Mg-ATP were calculated by WebMaxC ([maxchelator.stanford.edu](http://maxchelator.stanford.edu)) using the following settings: 25 °C, pH 7.2 and 0.16 empirical ionic equivalents. All the solutions were adjusted to pH 7.2 with Lab 820 pH-meter (Schott Instruments) using either CsOH (for internal solutions) or NaOH (for external solutions). Osmolarity of the internal solutions was adjusted to 285-295 mOsm using Vapro® Vapor Pressure Osmometer model 5600 (Wescor Inc.).

**Table 3.3.** Internal solution used for examining of  $Mg^{2+}$  concentration-response of native currents in TS cells.

free [ $Mg^{2+}$ ] <sub>i</sub> ( $\mu$ M)	Cs-glutamate (mM)	NaCl (mM)	Cs-HEPES (mM)	Cs-BAPTA (mM)	Cs-EDTA (mM)	$MgCl_2$ (mM)
0	120	8	10	10	5	0
0	120	8	10	10	0	0
30	120	8	10	10	0.1	0.13
88	120	8	10	10	0.1	0.21
233	120	8	10	10	0	0.3
390	120	8	10	10	0	0.5
782	120	8	10	10	0	1
1176	120	8	10	10	0	1.5
2370	120	8	10	10	0	3
4799	120	8	10	10	0	6

**Table 3.4.** Internal solution used to determine Mg-ATP concentration-response of endogenous currents in TS cells.

[Mg-ATP] <sub>i</sub> (mM)	free [Mg <sup>2+</sup> ] <sub>i</sub> (μM)	Cs- glutamate (mM)	NaCl (mM)	Cs- HEPES (mM)	Cs- EDTA (mM)	Mg-ATP (mM)	MgCl <sub>2</sub> (mM)
0.25	250	140	8	10	2.7	0.36	2.81
0.5	250	140	8	10	2.7	0.8	2.68
1	250	140	8	10	2.7	1.44	2.5
1.5	250	140	8	10	2.7	2.2	2.27
2	250	140	8	10	2.7	2.9	2.07
2.75	250	140	8	10	2.7	3.9	1.77
3.5	250	140	8	10	2.7	5	1.45
5	250	120	8	10	2.7	7.1	0.83
6	250	120	8	10	2.7	8.5	0.42
7	250	120	8	10	2.7	10	0
8	260	120	8	10	2.7	11	0

### 3.8.2. Patch-clamp experiments with recombinant TRPM6 and TRPM7

The transfected HEK 293 cells were seeded on the glass coverslips as indicated above (3.8). During patch-clamp recordings the cells were exposed to an extracellular solution containing (in mM): 140 NaCl, 1 CaCl<sub>2</sub>, 2 MgCl<sub>2</sub>, 2.8 KCl, 10 HEPES-NaOH and 11 glucose pH 7.2. In some experiments, we used DVF extracellular solution described previously (3.8.1). For assessment of cation permeation profiles of TRPM6 and TRPM7, the external solutions contained 10 mM HEPES-NaOH, 260 mM mannitol and 10 mM of individual divalent cations (ZnCl<sub>2</sub>, MgCl<sub>2</sub>, or CaCl<sub>2</sub>). The divalent-based solutions were adjusted to pH 7.0 (to prevent the precipitation of ZnCl<sub>2</sub>) using N-methyl-D-glucamine (NMDG).

The standard Mg<sup>2+</sup>-free intracellular pipette solution was identical to experiments with TS cells (3.8.2). A nominally Mg<sup>2+</sup>-free intracellular solution contained (in mM) 140 Cs-glutamate, 8 NaCl and 10 HEPES-CsOH. A pipette solution with 1 μM free [Mg<sup>2+</sup>]<sub>i</sub> comprised (in mM): 140 Cs-glutamate, 8 NaCl, 0.0016 MgCl<sub>2</sub>, 10 Cs-EGTA and 10

HEPES-CsOH. A pipette solution with 2 mM free  $[Mg^{2+}]_i$  contained (in mM): 120 Cs-glutamate, 8 NaCl, 2 Cs-EDTA, 10 HEPES-CsOH and 4 mM  $MgCl_2$ . A pipette solution with 210  $\mu M$   $[Mg\cdot ATP]_i$  and 10  $\mu M$  free  $[Mg^{2+}]_i$  contained (in mM): 140 Cs-glutamate, 8 NaCl, 3 Cs-EDTA, 10 HEPES-CsOH and 2.5 mM  $Mg\cdot ATP$ .

For the assessment of  $Mg^{2+}$  concentration-response of recombinant TRPM6 and TRPM7, the intracellular pipette solution contained of (in mM): 120 (or 140) Cs-glutamate, 8 NaCl, 10 Cs-EGTA, 10 HEPES-CsOH and different amount of  $MgCl_2$  (Table 3.5). To study  $Mg\cdot ATP$  concentration-response, we used the following intracellular solution (in mM): 120 (or 140) Cs-glutamate, 8 NaCl, 10 Cs-EGTA, 3 Cs-EDTA, 10 HEPES-CsOH, and different amount of  $Mg\cdot ATP$  and  $MgCl_2$  as outlined in Table 3.6. The internal solutions were adjusted to pH 7.2 and 290 mOsm.

**Table 3.5.** Internal solution used to study  $Mg^{2+}$  concentration-response of TRPM6 currents.

free $[Mg^{2+}]_i$ (mM)	Cs-glutamate (mM)	NaCl (mM)	Cs-HEPES (mM)	Cs-EGTA (mM)	$MgCl_2$ (mM)
0.1	140	8	10	10	0.16
0.25	140	8	10	10	0.38
0.55	140	8	10	10	0.83
1	140	8	10	10	1.5
2.3	120	8	10	10	3.4
5	120	8	10	10	7.1

### 3.9. Statistical analysis

Statistical analysis was performed using either Igor Pro or Microsoft Excel. The data are shown as means  $\pm$  standard error of the mean (SEM). We used a two-tailed Student's *t*-test and statistical significance was accepted at  $p \leq 0.05$ .

**Table 3.6.** Internal solution used to determine Mg-ATP concentration-response of TRPM6 currents.

<b>[Mg-ATP]<sub>i</sub> (mM)</b>	<b>free [Mg<sup>2+</sup>]<sub>i</sub> (μM)</b>	<b>Cs- glutam. (mM)</b>	<b>NaCl (mM)</b>	<b>Cs- HEPES (mM)</b>	<b>Cs- EGTA (mM)</b>	<b>Cs- EDTA (mM)</b>	<b>Mg-ATP (mM)</b>	<b>MgCl<sub>2</sub> (mM)</b>
0	250	140	8	10	10	3	0	0.38
1.5	250	120	8	10	10	3	2.15	2.71
3	250	120	8	10	10	3	4.3	2.1
6	250	120	8	10	10	3	8.55	0.85
9	250	120	8	10	10	3	12.4	0

## 4. Results

### 4.1. Elucidating the role of the endogenous TRPM7 currents in cellular Mg<sup>2+</sup> uptake

It has been previously reported by Schmitz *et al.* [69] and Ryazanova *et al.* [113] that TRPM7 deficient chicken DT40 lymphocytes and mouse embryonic stem cells displayed a growth arrest when cultured in a cell culture medium. However, a Mg<sup>2+</sup>-supplemented medium rescued the proliferation defect of TRPM7 deficient cells, indicating that the TRPM7 channel plays a key role in the cellular Mg<sup>2+</sup> homeostasis [67, 69, 77, 113, 114, 180]. In contrast, other laboratories suggested that TRPM7 is involved in different Ca<sup>2+</sup> signaling processes regulating cell motility [88, 115, 116], cell proliferation/differentiation/death [67, 69, 109, 114] and mechanosensitivity [116-118]. Furthermore, experiments with mouse strains carrying tissue-specific null mutations in *Trpm7* failed to confirm that TRPM7 is important for Mg<sup>2+</sup> homeostasis in the targeted tissues [128, 130]. To this end, the cellular function of TRPM7 requires further clarification. In the present work, we made use of newly generated experimental models, such as mouse trophoblast stem (TS) cells, human haploid leukemia (HAP1) cells and primary mouse megakaryocytes (MKs) to elucidate whether the endogenous TRPM7 channel is required for Mg<sup>2+</sup> metabolism in mammalian cells.

#### 4.1.1. Assessment of TRPM7 function in TS cells

Placental trophoblasts are extra-embryonic cells playing an indispensable role in the prenatal development of mammals. Placental trophoblasts release hormones and growth factors regulating the patterning and growth of the embryo. In addition, placental trophoblasts directly participate in the transport of nutrients and minerals to the fetal blood [192].

Recently, our group has shown that TRPM6 activity in placental trophoblasts underlines an essential role of *Trpm6* in the prenatal development of mice [144]. To this end, we reasoned that placental trophoblasts, such as trophoblast stem (TS) cells, can be an instrumental model for addressing the cellular functions of the kinase-coupled TRPM6 and TRPM7 channels. TS cells can be isolated from mouse blastocysts. These cells have the capability to proliferate indefinitely in the presence of specific growth factors in the culture medium. TS cells are able to differentiate *in vitro* into the various

placental trophoblasts forming the fetal portion of the placenta [183, 184]. Finally, TS cells are well suited for examining the transport functions of placental trophoblasts [179, 183].

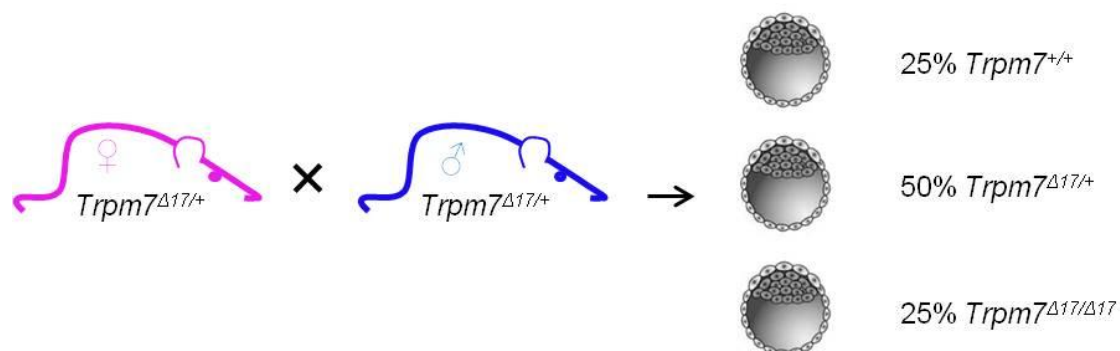


**Figure 4.1. Breeding strategy used to generate  $Trpm7^{\Delta17/\Delta17}$  and WT ( $Trpm7^{+/+}$ ) e3.5 blastocysts.**  $Trpm7^{\Delta17/+}$  mice were expected to produce 25%  $Trpm7^{+/+}$ , 50%  $Trpm7^{\Delta17/+}$  and 25%  $Trpm7^{\Delta17/\Delta17}$  blastocysts.

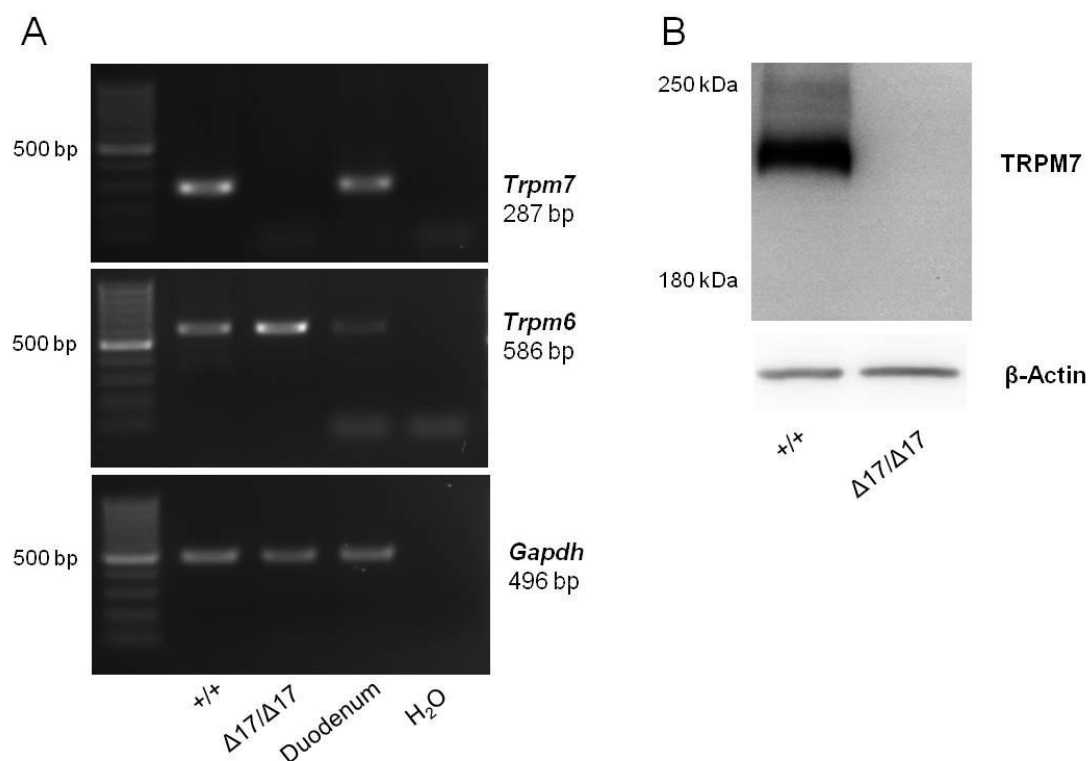


**Figure 4.2. Analysis of  $Trpm7^{+/+}$  ( $+/+$ ) and  $Trpm7^{\Delta17/\Delta17}$  ( $\Delta17/\Delta17$ ) TS cells.** (A)  $Trpm6$  and  $Trpm7$  mRNA expression was assessed by RT-PCR approach. RNA extracted from the duodenum was employed as a positive control, whereas  $H_2O$  was used as a negative control.  $GAPDH$  was probed to show an equal quality of cDNA samples. GeneRuler 100 bp DNA ladder was used to estimate the indicated size of PCR products. (B) Western blot analysis of native TRPM7 in TS cells.  $\beta$ -Actin was used as a loading control. Spectra multicolor high range protein ladder was used to estimate the size of TRPM7 signal.

To produce WT and *Trpm7* gene deficient TS cells, we isolated embryonic day 3.5 (e3.5) blastocysts derived from *Trpm7*<sup>A17/+</sup> parents as outlined in Fig. 4.1. The generated TS clones were propagated and analyzed by PCR of genomic DNA. The identified WT and KO clones were subjected to further RT-PCR analysis. These experiments confirmed that TS cells co-expressed *Trpm6* and *Trpm7* transcripts in *Trpm7*<sup>+/+</sup> clone, and that *Trpm7*<sup>A17/Δ17</sup> cells expressed only *Trpm6* transcripts (Fig. 4.2A). Because of a very low expression level of native TRPM7 protein in mammalian cells, the presence of endogenous TRPM7 protein in *Trpm7*<sup>+/+</sup> and *Trpm7*<sup>A17/Δ17</sup> TS cells was studied by immunoprecipitation (IP) step with TRPM7-specific antibody followed by Western blot analysis of the precipitate using an alternative TRPM7-specific antibody. These experiments revealed TRPM7 protein (~212 kDa) in WT cells (Fig. 4.2B). As expected, *Trpm7*<sup>A17/Δ17</sup> TS cells showed no detectable TRPM7 signal (Fig. 4.2B). Hence, WT TS cells express TRPM6 and TRPM7 and *Trpm7*<sup>A17/Δ17</sup> cells are deficient in TRPM7.

During isolation and initial propagation, we maintained all TS clones in the cell culture medium supplemented with 10 mM Mg<sup>2+</sup>, since *Trpm7* deficient cells may require additional Mg<sup>2+</sup> to proliferate [67, 69]. In these conditions, *Trpm7*<sup>+/+</sup> and *Trpm7*<sup>A17/Δ17</sup> TS clones displayed the characteristic morphology of TS cells [183]. They formed tight colonies with an epithelial sheets-like appearance (Fig. 4.3A). *Trpm7*<sup>+/+</sup> and *Trpm7*<sup>A17/Δ17</sup> TS cells showed no obvious morphological changes. The clones of both genotypes could self-renew during >20 passages. In line with previous studies [183], a small fraction of solitary spontaneously differentiated cells were also observed.

To evaluate whether the growth rate of *Trpm7*<sup>A17/Δ17</sup> TS cells is dependent on additional Mg<sup>2+</sup>, we performed the following experiments. Equal amounts of WT and KO TS cells were seeded in the medium supplemented with 10 mM MgCl<sub>2</sub>. After 24 h (day 1), the medium was replaced with either the standard medium (containing ~2 mM Mg<sup>2+</sup>) or the Mg<sup>2+</sup>-supplemented medium (containing additional 10 mM MgCl<sub>2</sub>). The cells were examined after 24, 48 and 72 h (days 2-4). We found that unlike WT cells, *Trpm7*<sup>A17/Δ17</sup> TS cells could not proliferate in the presence of the control medium (Fig. 4.3). However, the application of 10 mM Mg<sup>2+</sup> rescued the growth defect of *Trpm7* deficient cells (Fig. 4.3) suggesting that the genetic inactivation of TRPM7 leads to Mg<sup>2+</sup> depletion and proliferation block of TS cells.

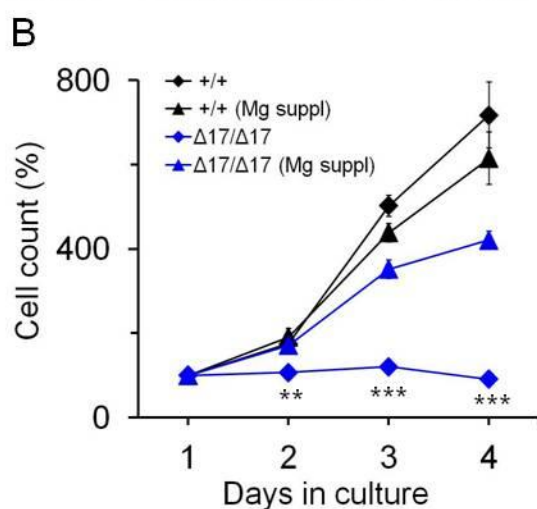
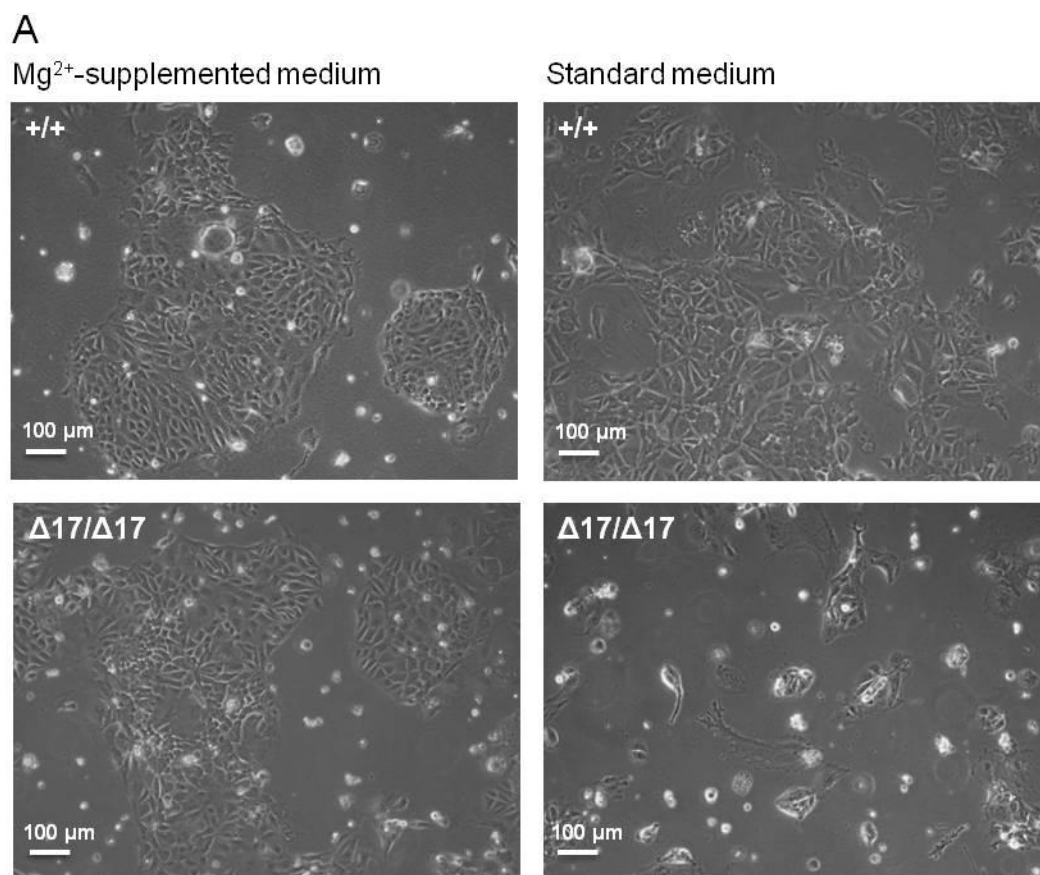


**Figure 4.3. Proliferation rates of *Trpm7*<sup>+/+</sup> (+/+) and *Trpm7*<sup>Δ17/Δ17</sup> (Δ17/Δ17) TS cells.** 1x10<sup>5</sup> cells/well of WT and KO TS cells were seeded in 6-well plates in TS medium supplemented by 10 mM Mg<sup>2+</sup>. After 24 h (day 1), the culture medium was replaced either with the regular or Mg<sup>2+</sup>-supplemented media. **(A)** Phase-contrast images taken at day 3 of the cell culture. **(B)** Growth curves of TS cells. Cell density at day 1 was taken as 100%. Data represent the mean±SEM from three independent experiments. *t*-Test was applied for comparison of growth rates of *Trpm7*<sup>+/+</sup> versus *Trpm7*<sup>Δ17/Δ17</sup> cells in the regular medium (\*\* *p* ≤ 0.01; \*\*\* *p* ≤ 0.001).

So far, no data have been published regarding functional characteristics of the native TRPM6 channel. Therefore, we wondered whether it would be possible to detect TRPM7-like divalent cation-selective currents in *Trpm7* deficient TS cells expressing only *Trpm6* (Fig. 4.2A). To address this question, we employed patch-clamp technique and measured whole-cell currents induced by a Mg<sup>2+</sup>-free intracellular solution. Specifically, WT and KO TS cells were incubated in a physiological extracellular

solution containing 3 mM  $\text{Ca}^{2+}$  and perfused with a  $\text{Mg}^{2+}$ -free  $\text{Cs}^+$ -based intracellular solution containing  $\text{Mg}^{2+}$  chelants, 5 mM EDTA and 10 mM EGTA. These conditions are commonly used to activate the native TRPM7 channels as well as to induce the recombinant TRPM7 channels in heterologous expression systems [67]. In these experiments, *Trpm7*<sup>+/+</sup> TS cells were maintained in culture either in the regular or  $\text{Mg}^{2+}$ -supplemented media since supplementary  $\text{Mg}^{2+}$  could potentially reduce expression levels of TRPM7. As shown on Fig. 4.4, WT cells grown in the  $\text{Mg}^{2+}$ -supplemented medium were capable to develop TRPM7-like divalent cation-selective currents by removal of intracellular  $\text{Mg}^{2+}$ , exhibiting a characteristic current-voltage (I-V) relationship of TRPM7 such as a steep rectification, large outward currents and relatively small inward currents [67]. Interestingly, WT cells grown in regular medium showed significantly increased current amplitudes as compared to cells grown in the  $\text{Mg}^{2+}$ -supplemented medium likely due to down-regulation of TRPM7 expression (Fig. 4.4). In contrast, KO TS cells completely lacked such TRPM7-like currents (Fig. 4.4), suggesting that TRPM6 activity is not measurable in the absence of TRPM7.

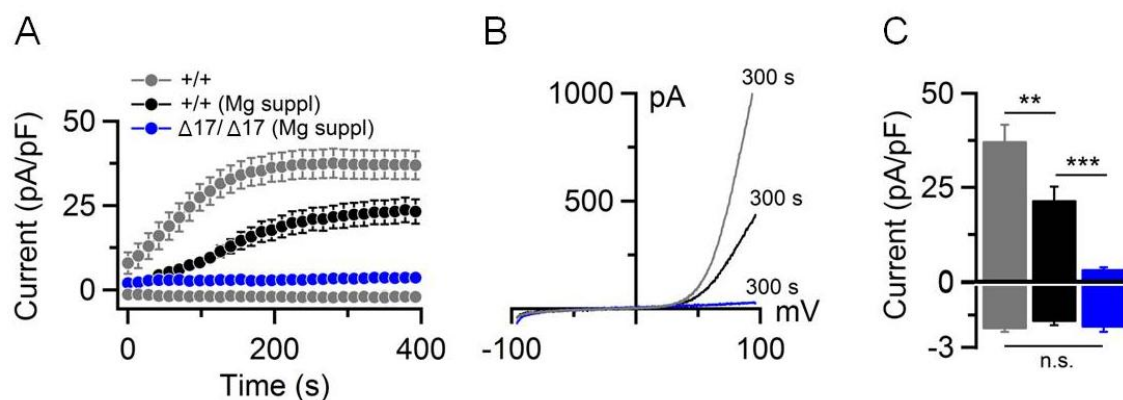


**Figure 4.4. Divalent cation-selective currents in *Trpm7*<sup>+/+</sup> (+/+) and *Trpm7*<sup>Δ17/Δ17</sup> (Δ17/Δ17) TS cells induced by  $\text{Mg}^{2+}$ -free intracellular solution. (A)** Whole-cell currents (mean  $\pm$  SEM) recorded in WT with (n=10) and without (n=15)  $\text{Mg}^{2+}$  supplementation in the culture medium and KO (n=10) TS cells. The currents were extracted at  $-80$  and  $+80$  mV, normalized to cell size and plotted versus time of the experiment. **(B)** Representative current-voltage (I-V) relationships extracted from individual ramps at 300 s. **(C)** Bar graphs of averaged outward ( $+80$  mV, upper panel) and inward ( $-80$  mV, lower panel) currents (mean  $\pm$  SEM) obtained at 300 s (n.s., not significant; \*\*  $p \leq 0.01$ ; \*\*\*  $p \leq 0.001$ ). n, number of cells measured.

Taken together, our findings suggest that TRPM7 plays an indispensable role in  $\text{Mg}^{2+}$  uptake in TS cells and that its genetic inactivation is associated with  $\text{Mg}^{2+}$ -dependent proliferation defect. This cellular function of TRPM7 in TS cells cannot be maintained by TRPM6 alone. Our results indicate only that the endogenous TRPM6 channel is not measurable in the absence of TRPM7.

#### 4.1.2. Role of TRPM7 in HAP1 cells

To further verify our findings with TS cells, we investigated a role of TRPM7 in an alternative experimental model, human leukemia haploid (HAP1) cells [186-189]. HAP1 is a near-haploid human cell line that displays a fibroblast-like morphology. This line was originally derived from a 39-year-old man with chronic myeloid leukemia (CML) in blast crisis. HAP1 cells are positive for the Philadelphia chromosome and express the BCR-ABL oncogenic fusion protein. As HAP1 cells only have one copy of each gene, CRISPR/Cas9 system allows a quick introduction of loss-of-function mutations in these cells. *TRPM7* gene deficient HAP1 cells are commercially available (clone 10940-04, Horizon genomics, <https://www.horizondiscovery.com/>). Specifically, CRISPR/Cas9 was used to introduce a 17-bp deletion in exon 4 of the human *TRPM7* gene. Accordingly, we studied whether this new experimental model could be instrumental for addressing a role of the endogenous TRPM7 in hematopoietic cells.

To confirm that the KO clone carries a loss-of-function mutation in *TRPM7*, we conducted RT-PCR followed by sequencing of the obtained PCR product. We used PCR primers flanking exon 4 of the gene. In WT HAP1 cells, we obtained a single PCR product at expected molecular weight, whereas in KO cells we could amplify two products as illustrated in Fig. 4.5A. The sequencing of these amplicons demonstrated that KO cells express two alternatively spliced *TRPM7* transcripts with frame-shift mutations. Notably, further RT-PCR analysis revealed that WT and KO HAP1 cells expressed *TRPM6* (Fig. 4.5A). Finally, using Western blot analysis we could show that TRPM7 protein was not detectable in KO clone in contrast to WT cells (Fig. 4.5B).

To examine WT and KO cells functionally, we performed patch-clamp measurements of endogenous TRPM7-like currents analogously to experiments conducted with TS cells. During recordings, WT and KO HAP1 cells were incubated in a standard extracellular solution containing 1 mM  $\text{Ca}^{2+}$  and 2 mM  $\text{Mg}^{2+}$  and perfused with a  $\text{Mg}^{2+}$ -free  $\text{Cs}^+$ -based intracellular solution. As expected, WT cells developed TRPM7-like currents (Fig. 4.6). In contrast, KO cells exhibited no detectable TRPM7-like currents (Fig. 4.6). We concluded that the 17-bp deletion in exon 4 of the human *TRPM7* gene results in the loss-of-function mutation.

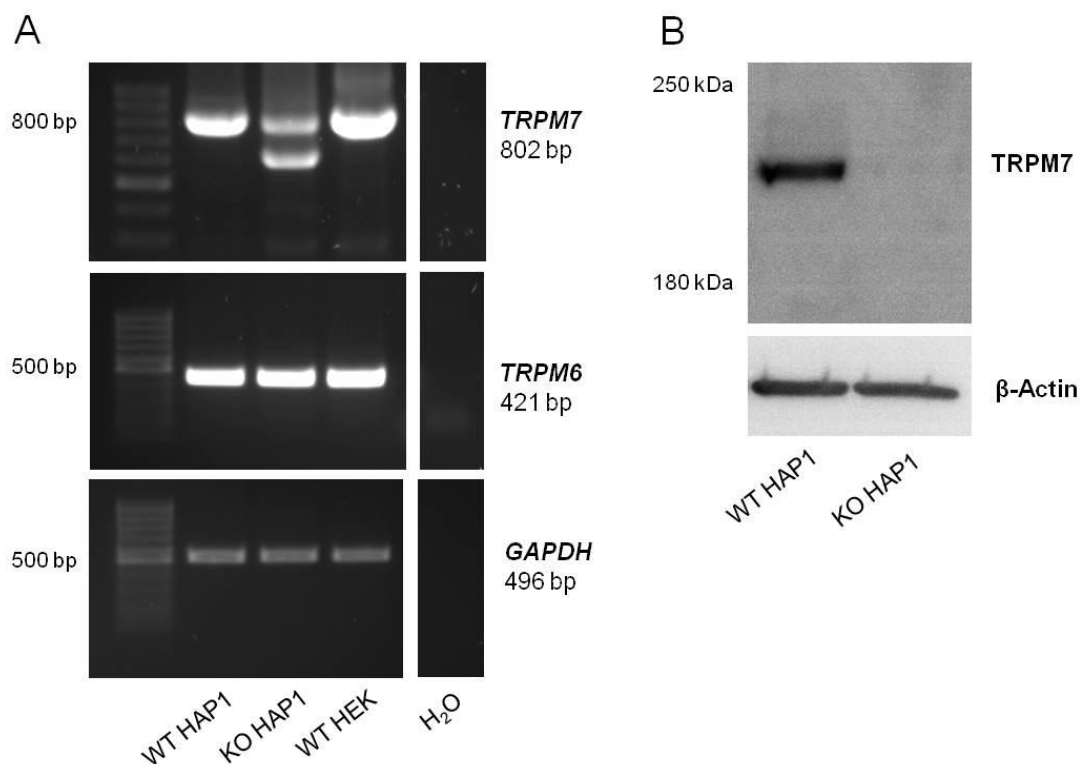


**Figure 4.5. Assessment of TRPM7 and TRPM6 expression levels in control (WT) and KO HAP1 cells.** (A) RT-PCR analysis of mRNA for expression of *TRPM6* and *TRPM7*. RNA extracted from HEK 293 cells were used as a positive control and H<sub>2</sub>O as negative control. *GAPDH* was used to assess RNA quality. GeneRuler 100 bp DNA ladder was used. (B) Western blot analysis of native TRPM7 in HAP1 cells. β-Actin was used as a loading control. Spectra multicolor high range protein ladder was used.

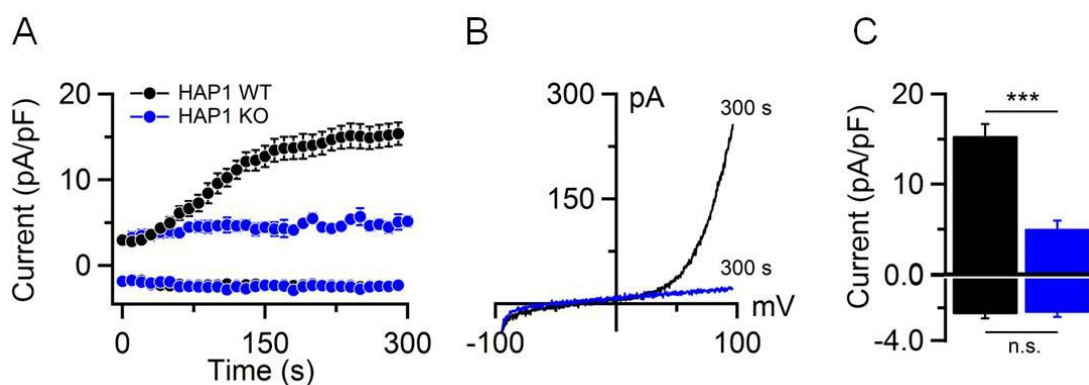


**Figure 4.6. Examination of endogenous TRPM7-like currents in control (WT) and KO HAP1 cells.** (A) Whole-cell currents (mean ± SEM) recorded in WT (n=9) and KO (n=4) HAP1 cells. The currents were extracted at -80 and +80 mV, normalized to cell size and plotted versus time of the experiment. (B) Representative I-V relationships extracted from individual ramps at 300 s. (C) Bar graphs of averaged outward (+80 mV, upper panel) and inward (-80 mV, lower panel) currents (mean ± SEM) obtained at 300 s (n.s., not significant; \*\*\*  $p \leq 0.001$ ). n, number of cells measured.

Next, we evaluated  $Mg^{2+}$  requirements for proliferation of KO HAP1 cells. These experiments were performed similarly to studies with TS cells illustrated in Fig. 4.3. WT and KO HAP1 cells displayed comparable growth rates in a  $Mg^{2+}$ -enriched cell culture medium (Fig. 4.7). However, unlike WT cells, KO cells showed a proliferation defect in a regular cell culture medium (Fig. 4.7), recapitulating the situation with *Trpm7* deficient TS cells (Fig. 4.3).

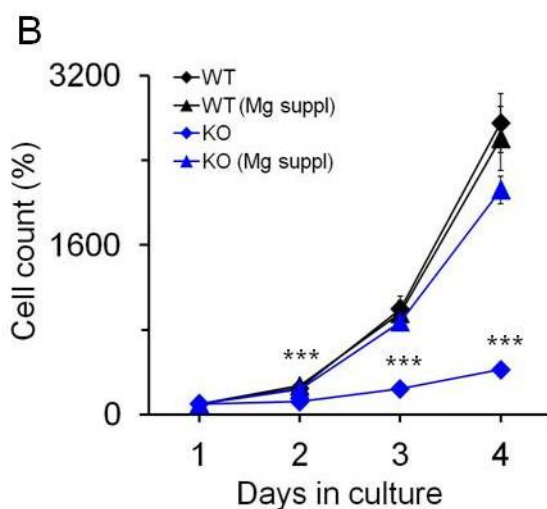
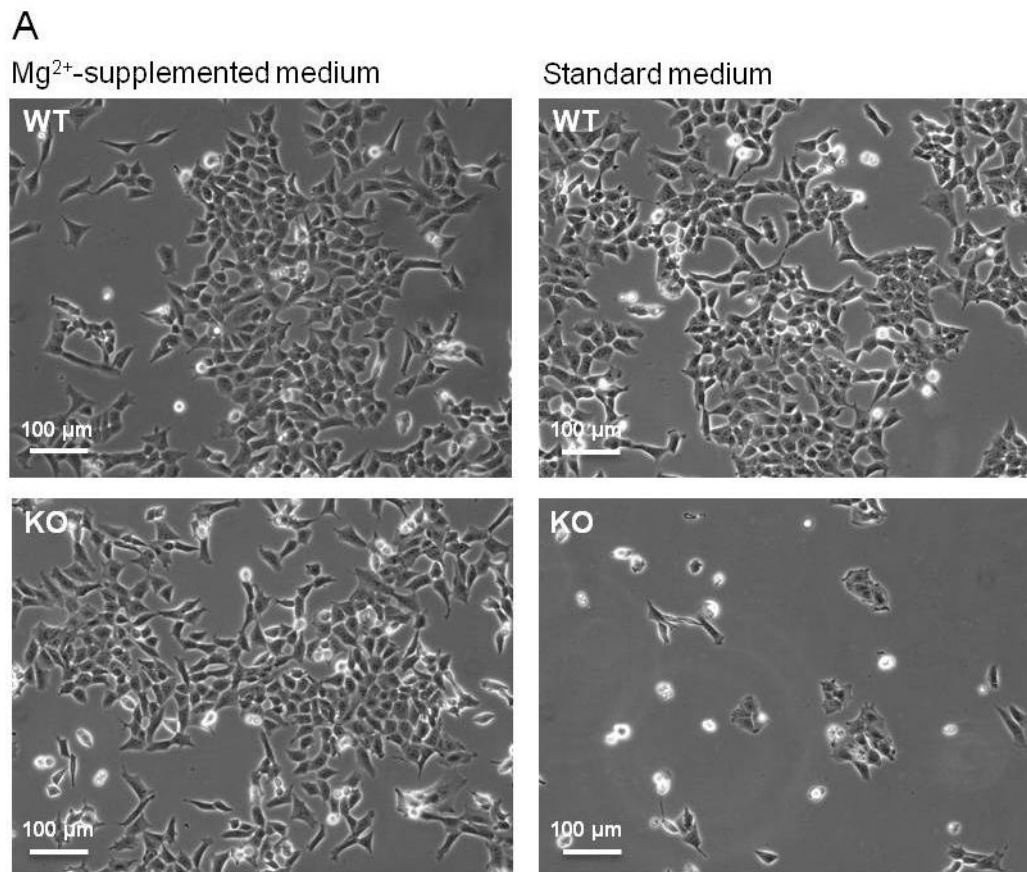


**Figure 4.7. Proliferation rates of control (WT) and KO HAP1 cells.**  $1 \times 10^5$  cells/well of WT and KO HAP1 cells were seeded in 6-well plates in medium supplemented by 10 mM  $Mg^{2+}$ . After 24 h (day 1), the culture medium was replaced either with the regular or  $Mg^{2+}$ -supplemented media. **(A)** Images of living WT and KO HAP1 cells cultured for 3 days. **(B)** Growth rates of WT and KO HAP1 cells. Cell density at day 1 was accounted as 100%. Data represent the mean  $\pm$  SEM from three independent experiments. *t*-Test was applied for comparison of growth rates of WT versus KO cells in the regular medium (\*\*\*)  $p \leq 0.001$ .

Taken together, we concluded that the phenotype of *TRPM7* deficient HAP1 cells resembles the alterations displayed by *Trpm7* KO TS cells, supporting the idea that TRPM7 is required for the cellular  $Mg^{2+}$  metabolism. We also noted that, similar to TS cells, TRPM6 activity is not detectable in HAP1 cells lacking *TRPM7*.

#### 4.1.3. Assessment of TRPM7 activity in primary megakaryocytes

In the next set of experiments, we asked whether our findings with cultured cell lines could be replicated in primary cells. To address this question, we exploited megakaryocytes (MKs) isolated from a mouse strain with a conditional mutation disrupting *Trpm7* specifically in MK progenitors. MKs are large bone marrow cells responsible for the generation of thrombocytes (platelets) in bone marrow sinusoids [180]. Firstly, we generated conditional MK-specific *Trpm7* deficient mice by intercrossing of *Trpm7<sup>fl/fl</sup>* mice with mice carrying the *Cre* recombinase under the platelet factor 4 promoter (*Pf4Cre*) [180]. Primary MKs were isolated from *Trpm7<sup>fl/fl</sup>* (control) and *Trpm7<sup>fl/fl</sup>;Pf4cre* (MK-specific *Trpm7* KO) mice. Remarkably, MK-specific *Trpm7* KO mice developed macrothrombocytopenia associated with cytoskeletal alterations and reduced intracellular  $Mg^{2+}$  concentrations [180]. Also, it was demonstrated that the impaired proplatelets formation could be rescued by  $Mg^{2+}$  supplementation [180], indicating that deregulated  $Mg^{2+}$  homeostasis may account for the impaired proplatelets formation in *Trpm7* KO platelets.

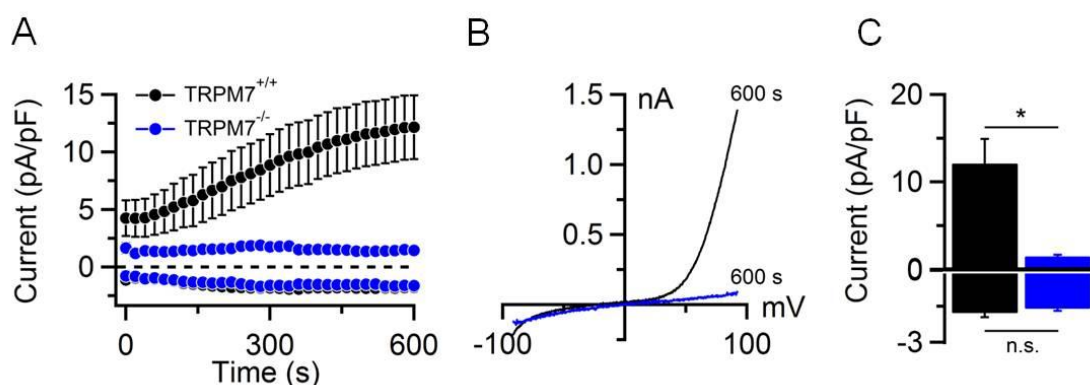


**Figure 4.8. Measurements of native TRPM7-like currents in *Trpm7<sup>+/+</sup>* (+/+) and *Trpm7<sup>-/-</sup>* (-/-) MKs. (A)** Whole-cell currents (mean  $\pm$  SEM) recorded in WT (n=13) and KO (n=11) MKs. The currents were extracted at  $-80$  and  $+80$  mV, normalized to cell size and plotted versus time of the experiment. **(B)** Representative I-V relationships extracted from individual ramps at 600 s. **(C)** Bar graphs of averaged outward ( $+80$  mV, upper panel) and inward ( $-80$  mV, lower panel) current (mean  $\pm$  SEM) amplitudes obtained at 600 s (n.s., not significant; \*  $p \leq 0.05$ ). n, number of cells measured.

To get a better insight into a mechanistic role of TRPM7 in MKs, we performed patch-clamp measurements of control and KO MKs using a standard extracellular solution containing 3 mM  $\text{Ca}^{2+}$  and a  $\text{Mg}^{2+}$ -free  $\text{Cs}^+$ -based intracellular solution. We observed characteristic TRPM7-like currents in control cells but not in KO MKs. Hence, similarly to other cell types, the native TRPM7 channel in primary MKs maintains the endogenous divalent cation-selective currents controlling  $\text{Mg}^{2+}$  metabolism in the cell.

## 4.2. Contribution of TRPM6 to endogenous divalent cation currents

TRPM6 has been shown to be involved in the regulation of systemic  $\text{Mg}^{2+}$  homeostasis since loss-of-function mutation of TRPM6 in humans and mice are associated with  $\text{Mg}^{2+}$  deficiency [68, 70, 71, 77, 79, 142, 144]. However, a functional analysis of the recombinant TRPM6 channel resulted in controversial results [68, 77, 92]. Furthermore, biophysical characteristics of the native TRPM6 channels have remained unknown so far. Hence, in this study we investigated the role of the native TRPM6 channels using TS cells.

### 4.2.1. Functional characterization of *Trpm6* gene deficient TS cells

Because of the high expression of *Trpm6* in trophoblasts in the placenta [144], we asked whether TS cells could be used to address a role of endogenous TRPM6. As shown above (Fig. 4.2A), WT TS cells express both TRPM6 and TRPM7 proteins. *Trpm7* KO cells expressed only TRPM6 but showed no detectable TRPM7-like currents (Fig. 4.4). Accordingly, we thought to generate *Trpm6* gene deficient TS cells and compare a phenotype of these cells with that of *Trpm7* deficient cells. To produce WT and *Trpm6* gene deficient TS cells, we isolated e3.5 blastocysts from pregnant *Trpm6* <sup>$\beta$ geo/+</sup> females crossed with *Trpm6* <sup>$\beta$ geo/+</sup> males (Fig. 4.9). Genotypes of obtained TS clones were determined by PCR approach and only *Trpm6*<sup>+/+</sup> and *Trpm6* <sup>$\beta$ geo/ $\beta$ geo</sup> TS cells were propagated in the  $\text{Mg}^{2+}$ -supplemented cell culture medium and further examined. First, *Trpm6*<sup>+/+</sup> and *Trpm6* <sup>$\beta$ geo/ $\beta$ geo</sup> TS cells were analyzed using RT-PCR. *Trpm6* transcripts were detected using two independent primer pairs. As expected, WT TS cells showed expression of *Trpm6* and *Trpm7* transcripts (Fig. 4.10A). Moreover, RT-PCR confirmed that the mutant cells were devoid of *Trpm6* transcripts, while *Trpm7* was expressed in WT and mutant cells (Fig. 4.10A). Second, using Western blot

analysis, we could detect the TRPM6 protein (~232 kDa) in *Trpm6*<sup>+/+</sup> TS cells, but not in *Trpm6*<sup>βgeo/βgeo</sup> TS cells (Fig. 4.10B).

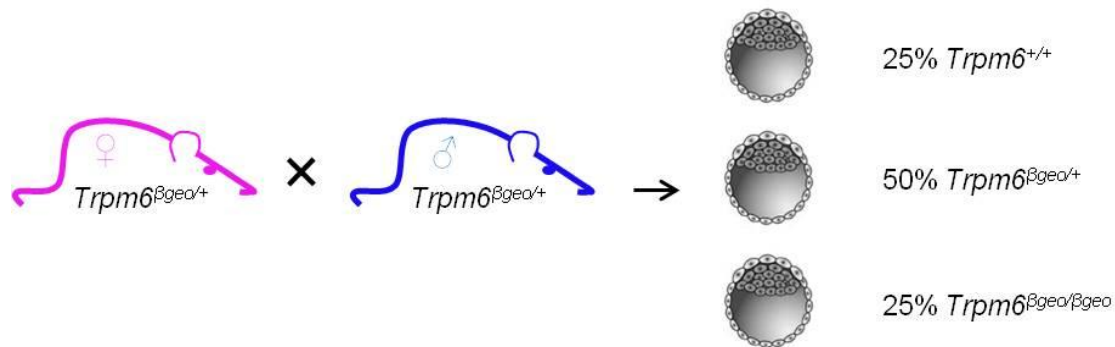


**Figure 4.9. Breeding schema used to isolate *Trpm6* gene deficient (*Trpm6*<sup>βgeo/βgeo</sup>) and WT (*Trpm6*<sup>+/+</sup>) e3.5 blastocysts.** Heterozygous *Trpm6*<sup>βgeo/+</sup> mice were crossed to produce 25% *Trpm6*<sup>+/+</sup>, 50% *Trpm6*<sup>βgeo/+</sup> and 25% *Trpm6*<sup>βgeo/βgeo</sup> blastocysts.

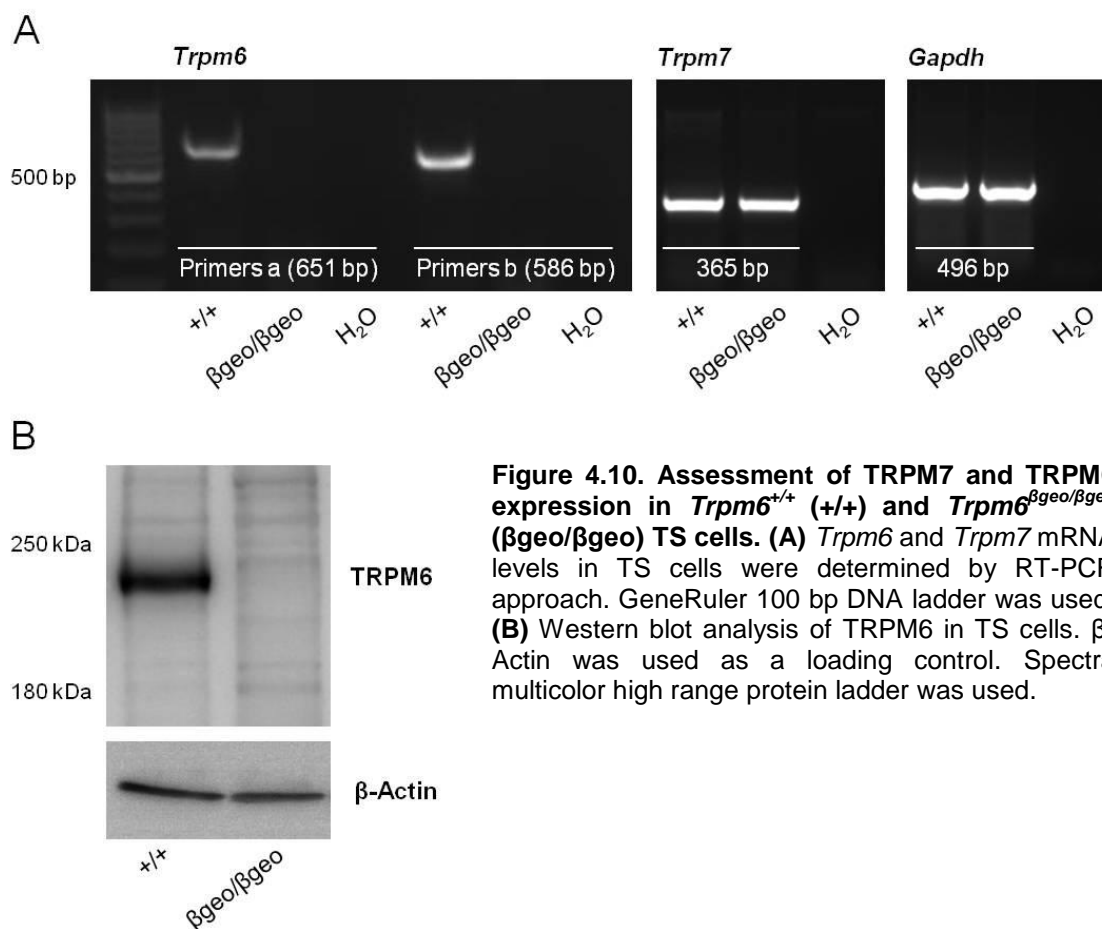


**Figure 4.10. Assessment of TRPM7 and TRPM6 expression in *Trpm6*<sup>+/+</sup> (+/+) and *Trpm6*<sup>βgeo/βgeo</sup> (βgeo/βgeo) TS cells.** (A) *Trpm6* and *Trpm7* mRNA levels in TS cells were determined by RT-PCR approach. GeneRuler 100 bp DNA ladder was used. (B) Western blot analysis of TRPM6 in TS cells. β-Actin was used as a loading control. Spectra multicolor high range protein ladder was used.

Next, in analogy to experiments with *Trpm7* deficient TS cells (Fig. 4.3), we investigated whether *Trpm6* deficient TS cells would require additional  $Mg^{2+}$  in the culture medium to proliferate. We observed that  $Mg^{2+}$ -supplemented WT and *Trpm6* deficient TS cells grew in tight colonies, characteristic for TS cells (Fig. 4.11A). In addition, a small portion of spontaneously differentiated cells were also present. In contrast to the situation with *Trpm7* deficient cells, we observed that KO TS cells could proliferate normally in the presence of physiological  $Mg^{2+}$  levels in the culture medium (Fig. 4.11B), indicating that inactivation of TRPM6 did not affect  $Mg^{2+}$  metabolism of mutant cells. Therefore, we performed our follow-up experiments with WT and mutant cells cultured in a regular cell culture medium.

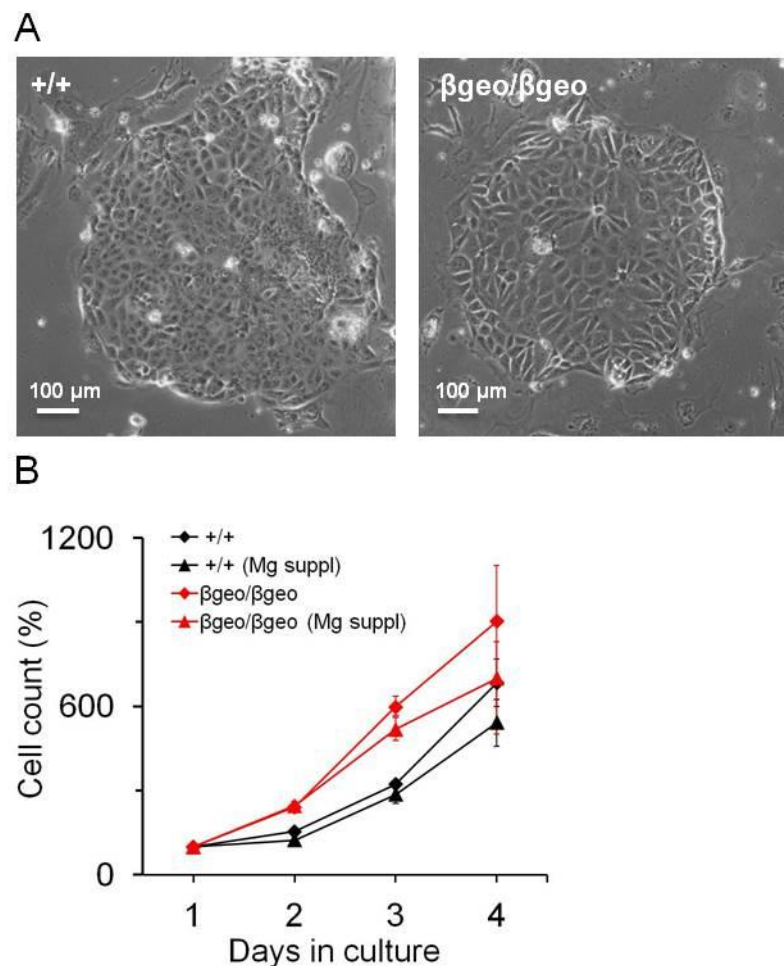


**Figure 4.11. Proliferation rates of *Trpm6*<sup>+/+</sup> (+/+) and *Trpm6*<sup>βgeo/βgeo</sup> (βgeo/βgeo) TS cells.**  $1 \times 10^5$  cells/well of WT and KO TS cells were seeded in 6-well plates in TS medium supplemented by 10 mM  $Mg^{2+}$ . After 24 h (day 1), the culture medium was replaced either with the regular or  $Mg^{2+}$ -supplemented media. **(A)** Images of living WT and KO TS cells taken after 3 days of the cell culture. **(B)** Growth curves of TS cells. Cell density at day 1 was accounted as 100%. Data represent the mean  $\pm$  SEM from three independent experiments.

#### 4.2.2. Assessment of native currents in *Trpm6* gene deficient TS cells

We employed patch-clamp technique in the whole-cell configuration to detect endogenous currents in *Trpm6* <sup>$\beta$ geo/ $\beta$ geo</sup> and *Trpm6*<sup>+/+</sup> TS cells. During recording, the cells were maintained in an extracellular solution containing 3 mM Ca<sup>2+</sup>. Similar to our previous experiments (Fig. 4.4), we were able to induce in WT TS cells TRPM7-like divalent cation currents by removal of intracellular Mg<sup>2+</sup> (Fig. 4.12). We noted that the currents in WT and mutant TS cells were developed with similar kinetics (Fig. 4.12A). Thus, immediately after establishment of the whole-cell configuration, TRPM7-like currents were absent, but they were gradually increased and reached a plateau after ~300 s of the measurements (Fig. 4.12A). We observed that TS cells of both genotypes displayed a similar TRPM7-like shape of I-V relationships (Fig. 4.12B). However, the outward currents measured at +80 mV in *Trpm6* <sup>$\beta$ geo/ $\beta$ geo</sup> cells displayed significantly lower current amplitudes as compared to WT cells (Fig. 4.12C).

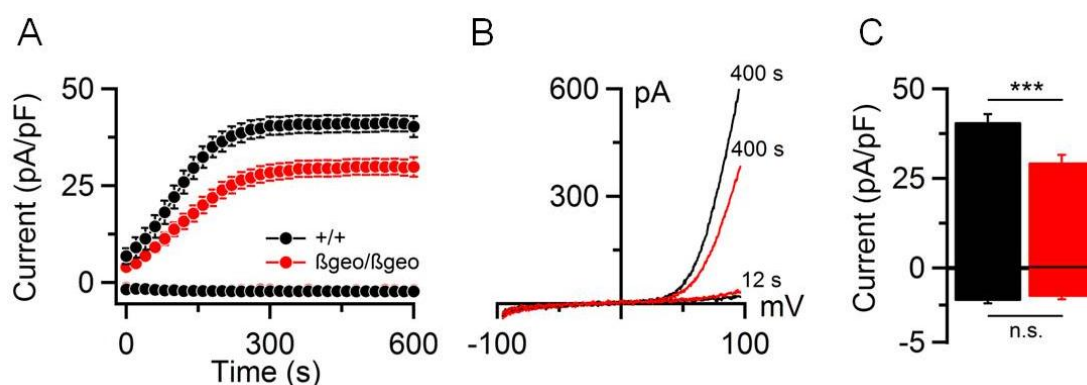


**Figure 4.12. Divalent cation-selective currents in *Trpm6*<sup>+/+</sup> (+/+) and *Trpm6* <sup>$\beta$ geo/ $\beta$ geo</sup> ( $\beta$ geo/ $\beta$ geo) TS cells induced by Mg<sup>2+</sup>-free intracellular solution. (A)** Whole-cell currents (mean  $\pm$  SEM) recorded in WT (n=22) and KO (n=22) TS cells. The currents were extracted at  $-80$  and  $+80$  mV, normalized to cell size and plotted versus time of the experiment. **(B)** Representative I-V relationships extracted from individual ramps at 400 s. **(C)** Bar graphs of averaged outward ( $+80$  mV, upper panel) and inward ( $-80$  mV, lower panel) current amplitudes (mean  $\pm$  SEM) obtained at 400 s (n.s., not significant; \*\*\*  $p \leq 0.001$ ). n, number of cells measured.

It is well documented [67, 72, 193] that extracellular divalent cations (Mg<sup>2+</sup> and Ca<sup>2+</sup>) act as a permeant blocker of the TRPM7 channel, resulting in very small inward currents at physiological membrane potentials ranging in mammalian cells from  $-40$  mV to  $-80$  mV. Accordingly, it is difficult to compare inward currents measured in WT versus KO TS cells (Fig. 4.12A). However, exposure of TRPM7 to divalent cation-free (DVF) external solution relieves the channel from the block resulting in a fast induction

of large inward currents at negative membrane potentials [67, 69]. Therefore, we used such experimental setting in our study (Fig. 4.13). We induced TRPM7-like currents using the standard intracellular solution and an external solution containing 1 mM  $\text{Ca}^{2+}$  and 2 mM  $\text{Mg}^{2+}$ . When TRPM7-like currents were fully induced (at ~500s), cells were exposed to DVF solution (Fig. 4.13A-C), which caused induction of large and linear inward currents carried by monovalent cations. In line with our previous measurements (Fig. 4.12), we found that *Trpm6* deficient cells exhibited significantly reduced inward and outward currents at these experimental conditions (Fig. 4.13D).

Taken together, we concluded that, unlike to *Trpm7*, inactivation of *Trpm6* caused a reduction of divalent cation-selective currents in TS cells.

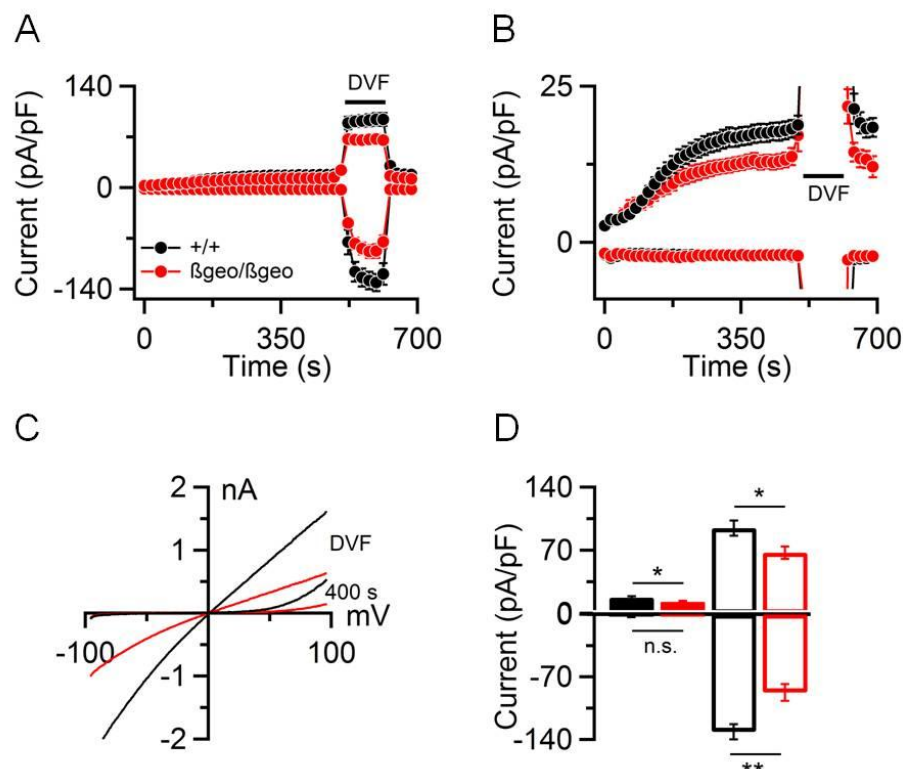


**Figure 4.13. Divalent cation-selective currents in *Trpm6*<sup>+/+</sup> (+/+) and *Trpm6* <sup>$\beta\text{geo}/\beta\text{geo}$</sup>  ( $\beta\text{geo}/\beta\text{geo}$ ) TS cells measured at DVF conditions. (A)** Whole-cell currents (mean  $\pm$  SEM) recorded in WT (n=16) and KO (n=14) TS cells. When currents were fully activated, the cells were perfused with a DVF solution as indicated by the black bars. The currents were extracted at  $-80$  and  $+80$  mV, normalized to cell size and plotted versus time of the experiment. **(B)** A magnification of currents shown in (A). **(C)** Representative I-V relationships obtained from individual ramps before (400 s) and during DVF application. **(D)** Bar graphs of averaged outward ( $+80$  mV, upper panel) and inward ( $-80$  mV, lower panel) current amplitudes (mean  $\pm$  SEM) obtained before (filled bars) and during (open bars) exposure to DVF (n.s., not significant; \*  $p \leq 0.05$ ; \*\*  $p \leq 0.01$ ). n, number of cells measured.

### 4.2.3. Effects of cytosolic $Mg^{2+}$ and Mg-ATP on currents in WT and *Trpm6* deficient TS cells

It is well known that the currents mediated by TRPM7 are inhibited by intracellular free  $Mg^{2+}$  ( $[Mg^{2+}]_i$ ) and Mg-ATP ( $[Mg\cdot ATP]_i$ ) [67, 69, 95]. Consequently, it was suggested that these inhibitory effects underline a physiological negative feedback on TRPM6 and TRPM7 activity enabling to adjust influx of  $Mg^{2+}$  according to cellular contents of  $Mg^{2+}$  and Mg-ATP. Therefore, we investigated concentration-response of TRPM7-like currents to  $[Mg^{2+}]_i$  in *Trpm6* <sup>$\beta$ geo/ $\beta$ geo</sup> and *Trpm6*<sup>+/+</sup> TS cells. We used Cs<sup>+</sup>-based pipette solutions containing different levels of free  $Mg^{2+}$  (Table 3.3). As shown in Fig. 4.14A, increasing  $[Mg^{2+}]_i$  caused a concentration-dependent inhibition of TRPM7-like currents in TS cells of both genotypes. The currents were fully inhibited by  $[Mg^{2+}]_i$  beyond 2 mM. The half-maximal inhibitory concentration ( $IC_{50}$ ) calculated from these datasets was 584  $\mu$ M for KO and 482  $\mu$ M for WT TS cells, suggesting that physiological levels of cytosolic  $Mg^{2+}$  concentrations (0.5-1 mM [93, 94]) regulate TRPM7-like currents similarly in *Trpm6* <sup>$\beta$ geo/ $\beta$ geo</sup> and *Trpm6*<sup>+/+</sup> cells.

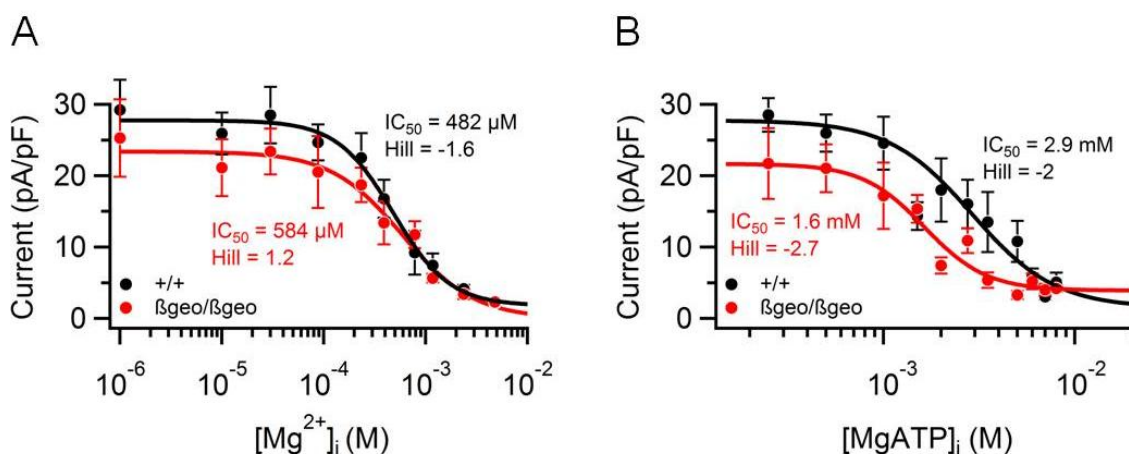


**Figure 4.14. Concentration-dependent inhibition of whole-cell currents by intracellular  $Mg^{2+}$  (A) and Mg-ATP (B) in *Trpm6*<sup>+/+</sup> (+/+) and *Trpm6* <sup>$\beta$ geo/ $\beta$ geo</sup> ( $\beta$ geo/ $\beta$ geo) TS cells.** Mean current amplitudes assessed at +80 mV and extracted at 400 s were used to fit the curves and calculate the indicated  $IC_{50}$  values (4-18 cells per concentration). Error bars indicate SEM.

Next, we investigated effects of Mg-ATP on TRPM7-like currents in *Trpm6* <sup>$\beta$ geo/ $\beta$ geo</sup> and *Trpm6*<sup>+/+</sup> TS cells. To determine concentration-response of TRPM7-like currents to  $[Mg\cdot ATP]_i$ , we used a Cs<sup>+</sup>-based intracellular solutions containing 2.7 mM EDTA, and different amount of Mg-ATP and MgCl<sub>2</sub> to achieve the desired Mg-ATP concentrations (Table 3.4). Internal free  $Mg^{2+}$  was set to 250  $\mu$ M at all concentrations of Mg-ATP

examined. As expected, TRPM7-like currents were suppressed by  $[\text{Mg}\cdot\text{ATP}]_i$  (Fig. 4.14B). Unlike to experiments with  $[\text{Mg}^{2+}]_i$ , we observed a leftward shift in concentration-dependent suppression of the currents in *Trpm6* deficient cells by  $[\text{Mg}\cdot\text{ATP}]_i$ . The calculated  $\text{IC}_{50}$  for *Trpm6* deficient and WT TS cells was 1.6 mM and 2.9 mM, respectively (Fig. 4.14B). These results suggested that TRPM6 alters the sensitivity of TRPM7-like currents to  $\text{Mg}\cdot\text{ATP}$  but not to  $\text{Mg}^{2+}$ .

#### 4.2.4. Assessment of constitutive channel activity in WT and *Trpm6* deficient TS cells

Currents conducted by the recombinant or native TRPM7 channels are usually not detectable immediately after break-in of the cell membrane by a patch microelectrode (i.e., upon establishment of the whole-cell configuration), but start to develop within a few seconds following depletion of intracellular  $\text{Mg}^{2+}$ . However, we noted that ~30% WT TS cells exhibited large TRPM7-like currents immediately after breaking of the cell membrane. I-V relationships of these pre-activated or constitutively active currents were indistinguishable from the shape of I-V characteristic of fully developed TRPM7-like currents. Typical examples of induced (dashed line) versus constitutively active (straight line) currents are illustrated in Fig. 4.15A. We also noted that *Trpm6* deficient cells display a lower number of cells with such pre-activated TRPM7-like currents. In order to quantify these findings in WT and mutant cells, we set up formal criteria to exclude from further analysis measurements contaminated by high background currents, which were unlikely conducted by TRPM6 or TRPM7. First, we excluded measurements if series resistance ( $R_s$ ) was more than 10 M $\Omega$  for at least 15 ramps. Second, we considered that pre-activated TRPM7-like currents should have the characteristic pronounced rectification of its I-V relationship at positive membrane potentials and small inward currents at negative membrane potentials, i.e., current amplitudes at -90 mV have to be 5 times smaller than at +90 mV. Finally, we considered that the cell exhibited pre-activated TRPM7-like currents if current amplitudes more than 60 pA/pF (at +80 mV) were observed immediately after the break-in of the membrane.

Using these thresholds, we established that 28.5% of WT TS cells exhibited pre-activated TRPM7-like currents, whereas only 13.1% of *Trpm6* deficient cells showed constitutive activity of TRPM7-like channels. Furthermore, we observed that the corresponding current amplitudes in mutant cells were significantly smaller than the

corresponding values measured in WT cells (Fig. 4.15C). Overall, our findings are consistent with the idea that TRPM6 enhances the basal divalent cation-selective currents.

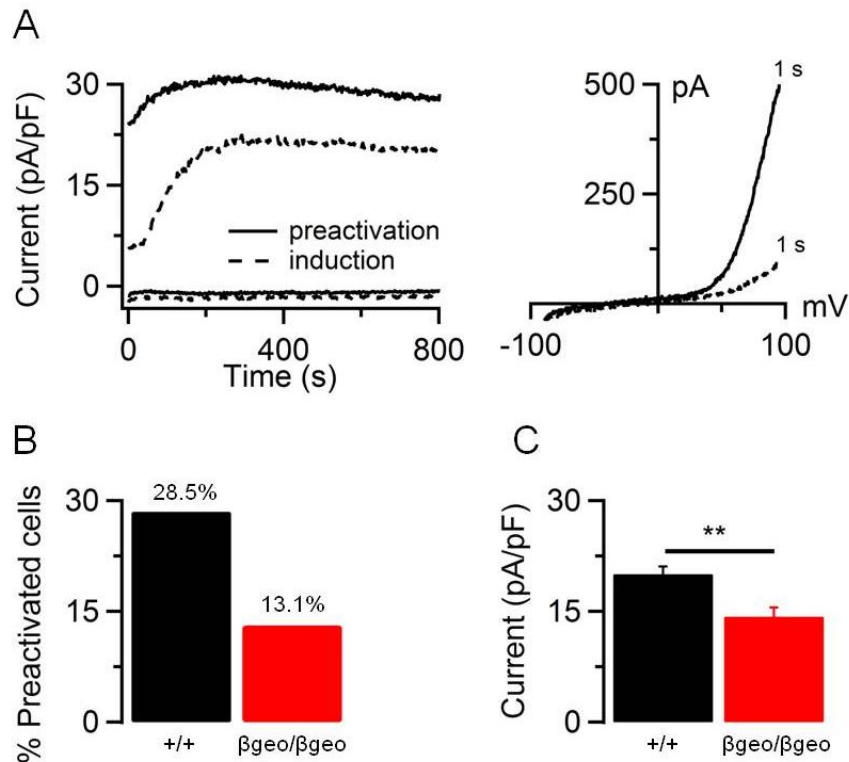


**Figure 4.15. Detection of pre-activated TRPM7-like currents in *Trpm6*<sup>+/+</sup> (+/+) and *Trpm6*<sup>βgeo/βgeo</sup> (βgeo/βgeo) TS cells. (A) *Left panel*: Representative traces of whole-cell currents measured in WT cell displaying pre-activated currents (straight line) as compared to WT cell with small initial currents (dashed line). *Right panel*: Representative I-V relationships of currents in *Left panel* at 1 s. (B) Percentage of WT and KO TS cells showed pre-activated currents. (C) Bar graphs represent the outward current amplitudes (+80 mV, mean ± SEM) in cohorts of WT and KO TS cells displaying pre-activated currents at break-in extracted at 1 s. WT (n=91) and KO (n=39) cells (\*\* p ≤ 0.01). n, number of cells measured.**

### 4.3. Characterization of recombinant mouse TRPM6

So far, only the human TRPM6 channel was characterized in heterologous expression systems and these experiments produced contradictory observations [68, 77, 82, 91]. Therefore, in the second part of the present study, we functionally characterized the recombinant mouse TRPM6 channel overexpressed in HEK 293 cells aiming to clarify whether its functional characteristics could help to explain the role of the native TRPM6 in TS cells.

#### 4.3.1. Heterologous expression of mouse TRPM6 cDNA in HEK 293 cells

Using molecular biology techniques, a full-length mouse TRPM6 cDNA has been cloned in our laboratory from RNA isolated from the mouse lung tissue [181]. The obtained TRPM6 cDNA encodes a 2028 aa protein containing a highly conserved in TRPM channels N-terminal domain followed by a channel segment and a C-terminal kinase domain (Fig. 1.3B). Based on experiments with TRPM7 [194], we could predict locations of residues essential for a catalytic activity of the TRPM6 kinase, for instance, K1810 (K1646 in mouse TRPM7 protein) [69, 195] and a threonine residue (T1730) autophosphorylated by the TRPM6 kinase domain (corresponding to S1567 in the mouse TRPM7 channel [86]) (Fig. 4.16A).

To examine these predictions, we used site-directed mutagenesis to generate a TRPM6 cDNA version containing a 'kinase-dead' (KD) mutation (TRPM6<sup>K1810R</sup>) and a variant lacking the predicted phosphorylation residue (TRPM6<sup>T1730A</sup>). Next, we transiently transfected HEK 293 cells with WT TRPM6, TRPM6<sup>K1810R</sup> and TRPM6<sup>T1730A</sup> constructs and assessed expression levels of the TRPM6 variants by Western blot using a rabbit polyclonal antibody specific for phosphorylated T1730 in TRPM6 ((p)T1730-specific antibody) and a commercially available anti-TRPM6 polyclonal antibodies (ab47017) to detect total TRPM6 content (Fig. 4.16B). We observed that ab47017 detected similar levels of 232 kDa WT TRPM6, TRPM6<sup>K1810R</sup> and TRPM6<sup>T1730A</sup>, whereas (p)T1730-specific antibody could detect only WT version of TRPM6 (Fig. 4.16B). These results indicate that the kinase domain of TRPM6 phosphorylates T1730 and that KD mutation blocks the kinase activity of TRPM6. Hence, heterologous expression of mouse TRPM6 cDNA constructs allowed us to express the full-length TRPM6 with the active kinase.

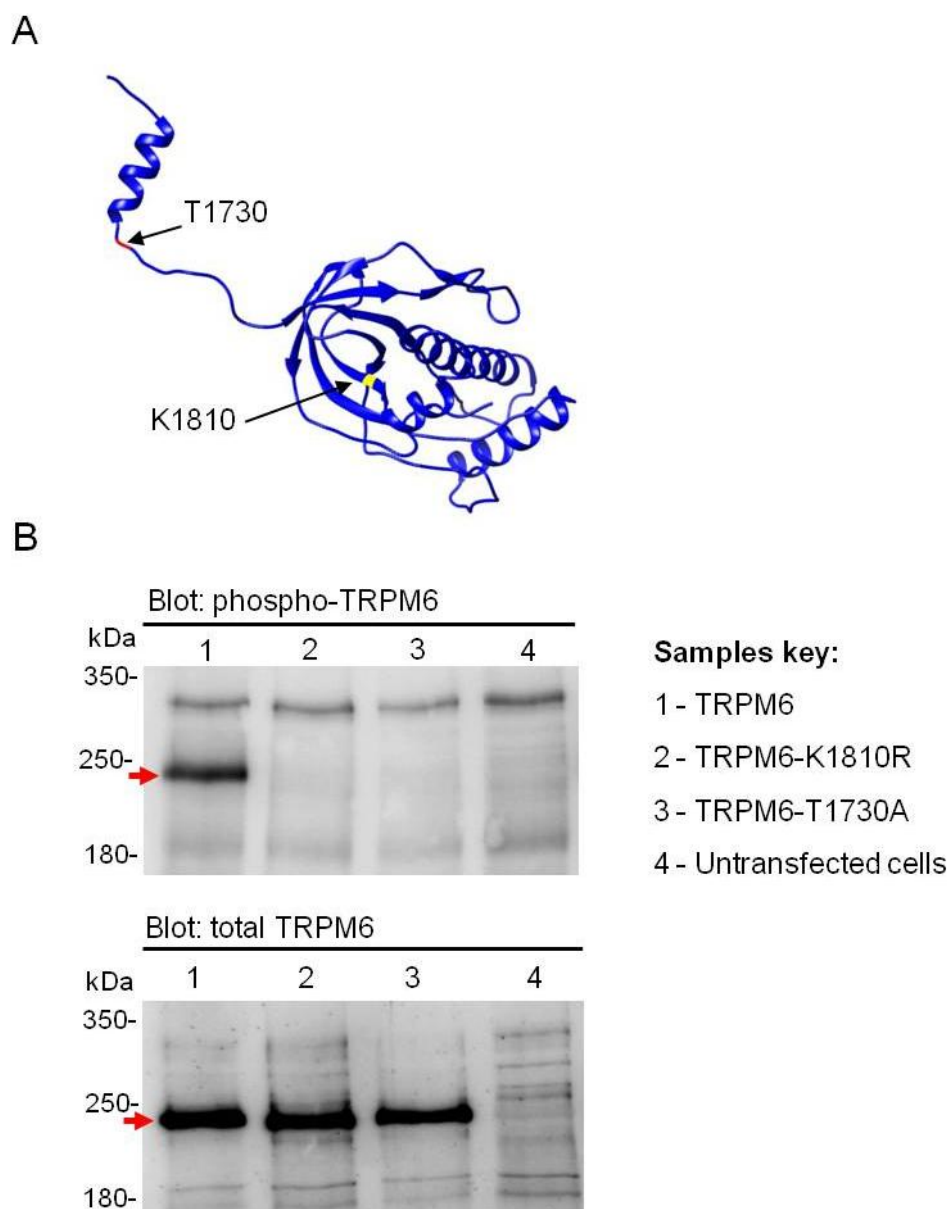


**Figure 4.16. Assessment of the mouse TRPM6 kinase activity.** (A) Kinase domain of the mouse TRPM6 protein. K1810 is a conserved residue of the catalytic site of the kinase domain. T1730 is a residue phosphorylated by the TRPM6 kinase. (B) Western blot analysis of WT and mutant TRPM6 expression constructs using the anti-(p)T1730 antibody. Western blot was repeated 3 times with analogous results.

#### 4.3.2. Patch-clamp analysis of HEK 293 cells expressing mouse TRPM6

For assessment of TRPM6 mediated currents, HEK 293 cells were transiently transfected with 2  $\mu$ g mouse TRPM6 or TRPM7 cDNA placed in pIRES2-EGFP plasmid, which enables to express simultaneously TRPM6 or TRPM7 and the enhanced green fluorescent protein (EGFP). Consequently, only EGFP-positive cells were studied in the patch-clamp experiments. Likewise to experiments with TS and HAP1 cells, the whole-cell currents were elicited by a voltage ramps from  $-80$  to  $+80$

mV, using the standard external solution containing 2 mM  $Mg^{2+}$  and 1 mM  $Ca^{2+}$  and the standard  $Mg^{2+}$ -free internal solution.

In a good agreement with previous studies [66, 67], characteristic TRPM7 currents were small immediately after establishment of the whole-cell configuration, however, they were quickly increased because of removal of internal  $Mg^{2+}$  and were fully developed at  $\sim 100$  s (Fig. 4.17A). TRPM6-expressing cells also displayed currents (Fig. 4.17A,B). Like TRPM7, TRPM6 currents were very small after break-in and fully developed after  $\sim 100$ s of recordings (Fig. 4.17A,B). However, TRPM6 exhibited some features well distinguishable from TRPM7. Firstly, TRPM6 current amplitudes were  $\sim 3$ -fold smaller (Fig. 4.17A,D). Secondly, TRPM6 currents were gradually suppressed after  $\sim 120$ s of recordings (Fig. 4.17B). Further analysis showed that TRPM6 displayed a TRPM7-like steeply outwardly rectifying I-V relationship (Fig. 4.17C).

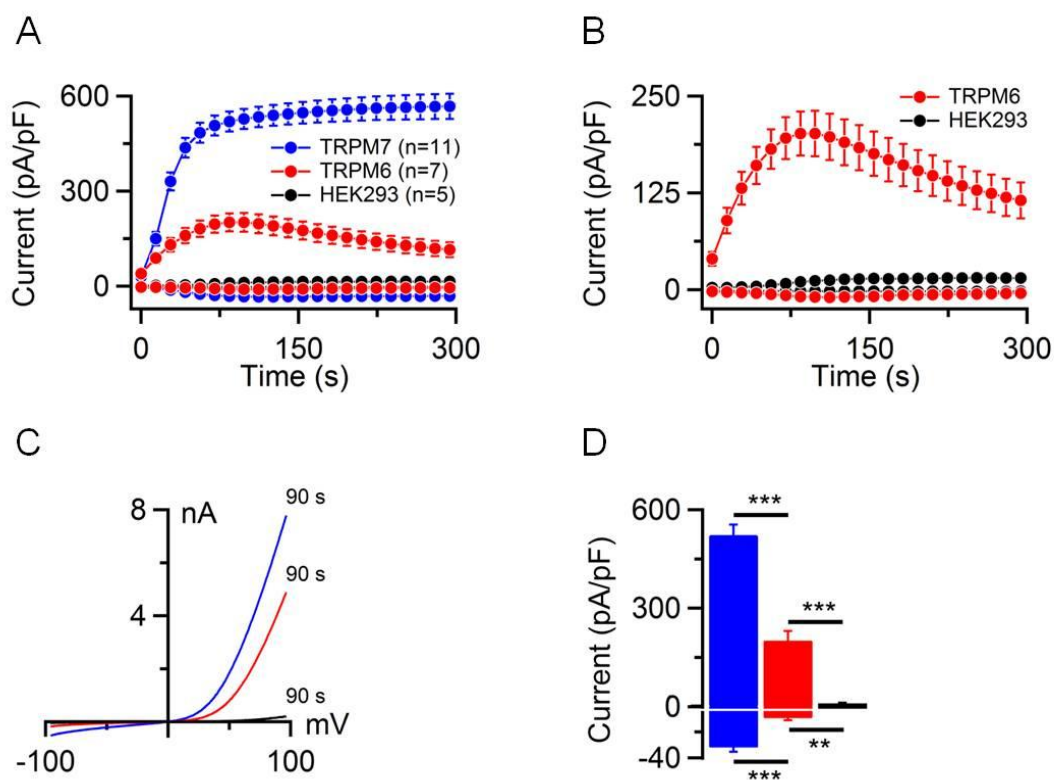


**Figure 4.17. Assessment of mouse TRPM6 and TRPM7 currents in HEK 293 cells. (A)** Whole-cell currents (mean  $\pm$  SEM) measured in TRPM6 (red), TRPM7 transfected (blue) and untransfected (black) cells ( $n$  = number of cells measured). The current amplitudes were acquired at  $-80$  and  $+80$  mV, normalized to cell size and plotted versus time of the experiment. **(B)** A magnification of TRPM6 and endogenous currents shown in (A). **(C)** Representative I-V relationships of currents shown in (A) extracted from individual ramps at 90s. **(D)** Bar graphs of averaged outward ( $+80$  mV, *upper panel*) and inward ( $-80$  mV, *lower panel*) currents (mean  $\pm$  SEM) obtained at 90 s (\*\*  $p \leq 0.01$ ; \*\*\*  $p \leq 0.001$ ).

It has been demonstrated that endogenous human TRPM7 is expressed in HEK 293 cells and that the native TRPM7 currents are well detectable in this cell line [67]. In fact, we could elicit endogenous TRPM7-like currents in untransfected HEK 293 cells (Fig. 4.17 A,B). However, these endogenous currents were not detectable immediately upon establishment of the whole-cell configuration, developed over a longer time period, and were ~10-fold smaller as compared to TRPM6 currents (Fig. 4.17 B,D). Hence, the endogenous TRPM7 channels could not contribute or significantly contaminate our recordings with TRPM6-expressing cells.

Next, we studied whether the recombinant TRPM6 channel activity could be functionally expressed in TS cells deficient in TRPM7. TRPM7 KO TS cells were electroporated with mouse TRPM6 cDNA and the patch-clamp measurements were performed 24 h after transfection. These measurements revealed whole-cell currents highly resembling TRPM6 currents observed in transfected HEK 293 cells (Fig. 4.18). Thus, transfection of different cell types with mouse TRPM6 cDNA allowed us to measure the TRPM6 channel activity.

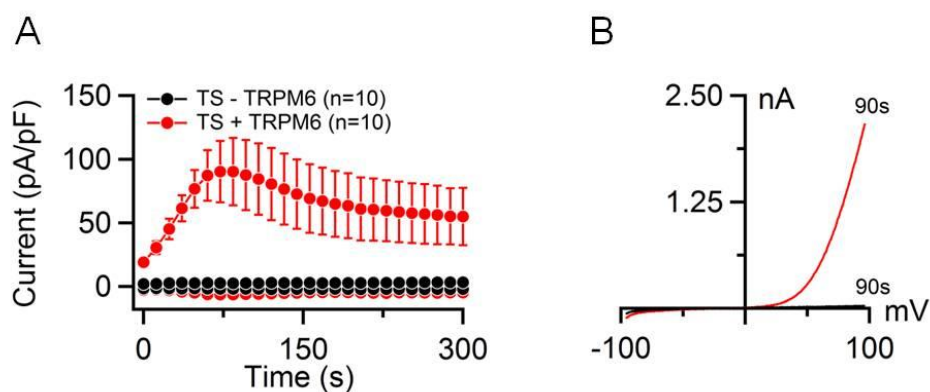


**Figure 4.18. Expression of mouse TRPM6 in TS cells.** *Trpm7* gene deficient TS cells were electroporated with TRPM6 cDNA and examined by patch-clamp technique. **(A)** Whole-cell currents (mean  $\pm$  SEM) measured in TRPM6-expressing (red) and untransfected (black) TS cells ( $n$  = number of cells measured). The current amplitudes were acquired at  $-80$  and  $+80$  mV, normalized to cell size and plotted versus time of the experiment. **(B)** Representative I-V relationships of the currents shown in (A) extracted from individual ramps at 90 s.

Zhang *et al.* [92] reported that transient overexpression of human TRPM6 cDNA enabled to produce a functional channel only if cDNA was inserted in a pCINeo-IRES-GFP expression vector. However, the same TRPM6 cDNA placed in several other plasmids could not produce functional channels [92]. This unexpected characteristic of human TRPM6 cDNA seems to be unique among known ion channels and remains to

be explained mechanistically. Therefore, we investigated whether functional expression of our mouse TRPM6 clone is also affected by plasmid backbone. We sub-cloned TRPM6 cDNA into a widely used pcDNA3.1 vector [77] and co-transfected this construct with a small amount of EGFP cDNA (pcDNA3.1) in HEK 293 cells. Patch-clamp measurements of EGFP-positive HEK 293 cells (Fig. 4.19) detected inward and outward currents recapitulating TRPM6 currents measured in HEK 293 cells transfected with pIRES2-EGFP-TRPM6 construct (Fig. 4.17). We concluded that the expression vectors are interchangeable for functional expression of mouse TRPM6 cDNA. Therefore, in our follow-up experiments we used only pIRES2-EGFP-TRPM6 vector.

Taken together, our results indicate that overexpression of the mouse TRPM6 protein results in formation of functional homomultimeric channel complexes with a moderate channels activity as compared to the recombinant TRPM7 channels.

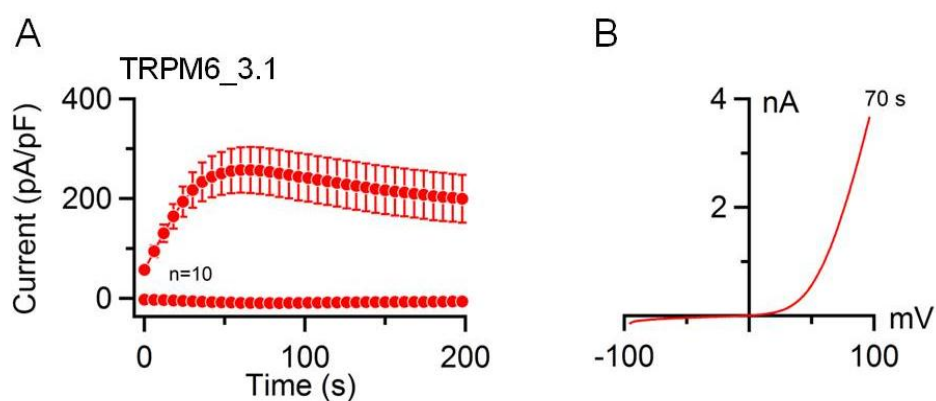


**Figure 4.19. Evaluation of HEK 293 cells transfected with mouse TRPM6 cDNA inserted in pcDNA3.1 vector.** TRPM6 cDNA in pcDNA3.1 was co-transfected with EGFP construct (pcDNA3.1) in HEK 293 cells. **(A)** Whole-cell currents (mean  $\pm$  SEM) measured in EGFP-positive cells ( $n$  = number of cells measured). The current amplitudes were acquired at  $-80$  (lower traces) and  $+80$  mV (upper traces), normalized to cell size and plotted versus time of the experiment. **(B)** Representative I-V relationships of the currents shown in (A) extracted from individual ramps at 70 s.

#### 4.3.3. Cation permeability of the mouse TRPM6 channel

TRPM7 has been characterized as a cation channel selective for divalent cations including  $\text{Ca}^{2+}$ ,  $\text{Mg}^{2+}$  and  $\text{Zn}^{2+}$  [67, 72]. To assess the cation permeation profile of mouse TRPM6, we examined a so-called divalent cation's permeation block of TRPM6 currents, a well-described channel characteristic of TRPM7. To this end, HEK 293 cells were transiently transfected with TRPM6 or TRPM7 cDNAs. Subsequently, EGFP-positive cells were induced by the standard  $\text{Mg}^{2+}$ -free intracellular solution. After a full

development of the currents, the cells were exposed to a divalent cation-free (DVF) external solution.

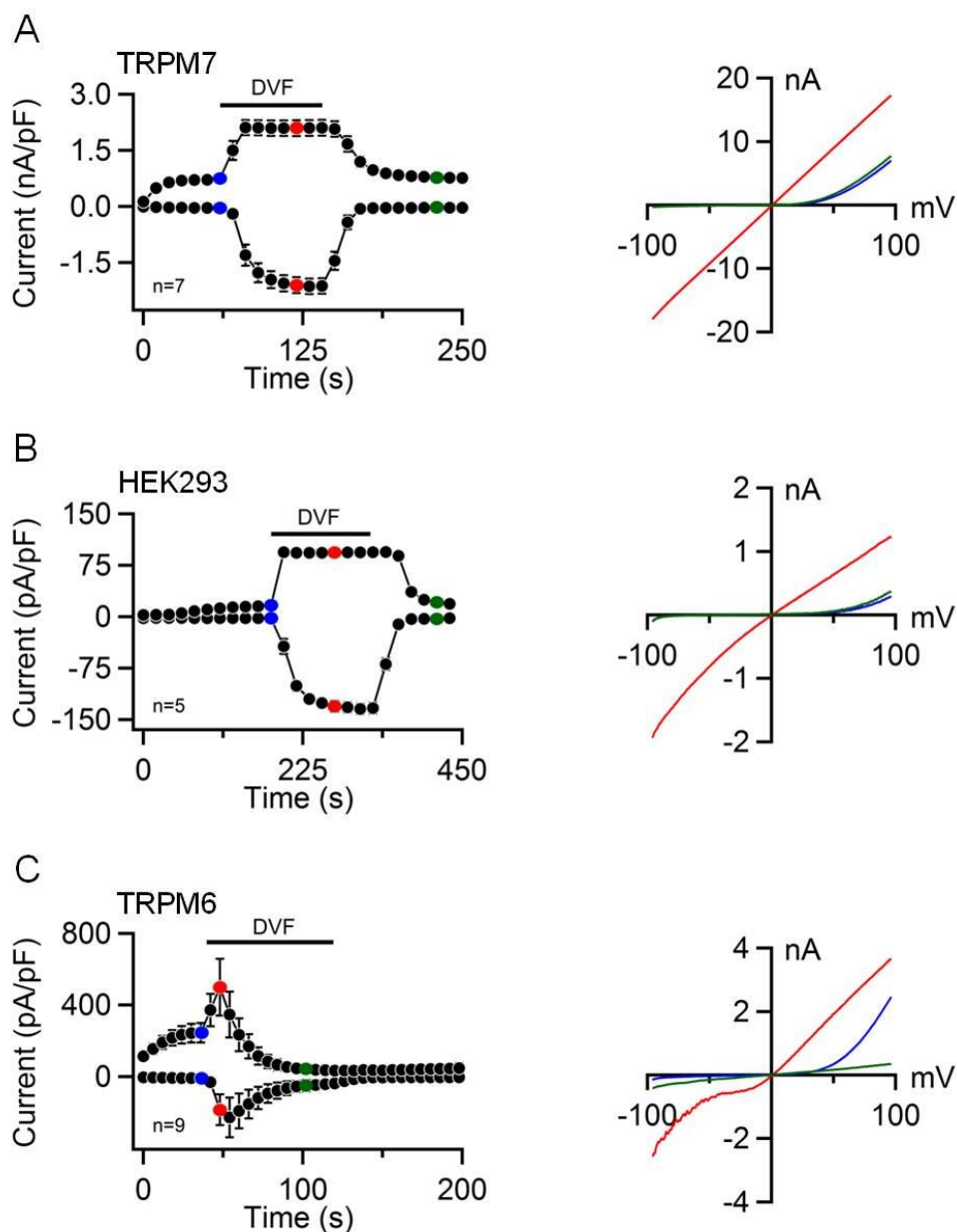


**Figure 4.20. Assessment of mouse TRPM6 and TRPM7 currents in DVF extracellular solution.** *Left panels:* Whole-cell currents (mean  $\pm$  SEM) measured in TRPM7 transfected (A), untransfected (B) and TRPM6 transfected (C) HEK 293 cells ( $n$  = number of cells measured). Currents were induced using the standard free  $[Mg^{2+}]_i$  intracellular solution and the standard external solution. When currents were fully developed, cells were perfused with the DVF solution. The current amplitudes were acquired at  $-80$  and  $+80$  mV, normalized to cell size and plotted versus time of the experiment. *Right panels:* Representative I-V relationships obtained from individual ramps before (blue), during (red) and after (green) DVF application as indicated in the *left panels* by coloured data points.

In line to other studies [67], exposure of TRPM7-expressing cells to DVF solution could abolish the permeation block of the channel and, consequently, entailed large monovalent cation currents with characteristic linear I-V relationships (Fig. 4.20A). These linearized monovalent currents were stable over exposure time. However, these alterations were fully reversed after wash-out of DVF solution (Fig. 4.20A). Native TRPM7 currents showed a similar response to application of DVF saline (Fig. 4.20B).

In contrast to TRPM7, TRPM6 transfected cells showed only initial response to the application of DVF solution characterized by transient increases of both outward and inward currents followed by a fast and irreversible inactivation of TRPM6 activity (Fig. 4.20C). Mechanisms underlying such fast inactivation of TRPM6 currents remain unclear and should be elucidated in the future. Thus, unlike to TRPM7, mouse TRPM6 is capable of developing monovalent currents only for a short time.

Next, we conducted experiments aiming to assess the relative divalent cation permeation profiles of TRPM6 in comparison to TRPM7. To determine the cation selectivity of TRPM7, two approaches were previously used: (i) by a comparison of reversal potentials of monovalent currents before and after application of external solutions containing distinct divalent cations [67, 72, 191], and (ii) by assessment of inward current amplitudes in cells exposed to external solutions containing individual divalent cations [67, 72, 191]. Since assessment of the reversal potential of monovalent TRPM6 currents was impossible (Fig. 4.20C), we focused on the second option (Fig. 4.21, 4.22). Whole-cell currents were induced in either TRPM6 or TRPM7 transfected HEK 293 cells using the standard internal and external solutions. When currents were developed, the cells were transiently exposed to a saline containing 10 mM of  $Zn^{2+}$ ,  $Ca^{2+}$  or  $Mg^{2+}$  and amplitudes of inward currents at  $-80$  mV were estimated. We tested 10 mM solutions since  $Zn^{2+}$  is poorly soluble above 10 mM at pH 7.0. To prevent a contamination of recordings by  $Na^+$  currents, external monovalent cations were replaced by non-permeant N-methyl-D-glucamine (NMDG). Finally, in order to offset variations in expression levels of TRPM6 and TRPM7, we normalized outward and inward currents (current amplitudes immediately before the application of divalent cation-based solutions were set to "1"). Our experiments revealed that the exposure of TRPM7 transfected cells to 10 mM  $Zn^{2+}$  led to a ~3-fold increase of inward currents (Fig. 4.21A). The perfusion of cells with 10 mM  $Mg^{2+}$  or 10 mM  $Ca^{2+}$  caused a moderate but statistically significant reduction of inward currents likely due to a negative effect of these cations on the channel gating (Fig. 4.21B,C). Thus, in accordance with published work [72], TRPM7 showed a higher permeability for  $Zn^{2+}$  in

comparison to  $\text{Mg}^{2+}$  and  $\text{Ca}^{2+}$ . In addition, TRPM7 showed an equal permeability for  $\text{Mg}^{2+}$  and  $\text{Ca}^{2+}$ .

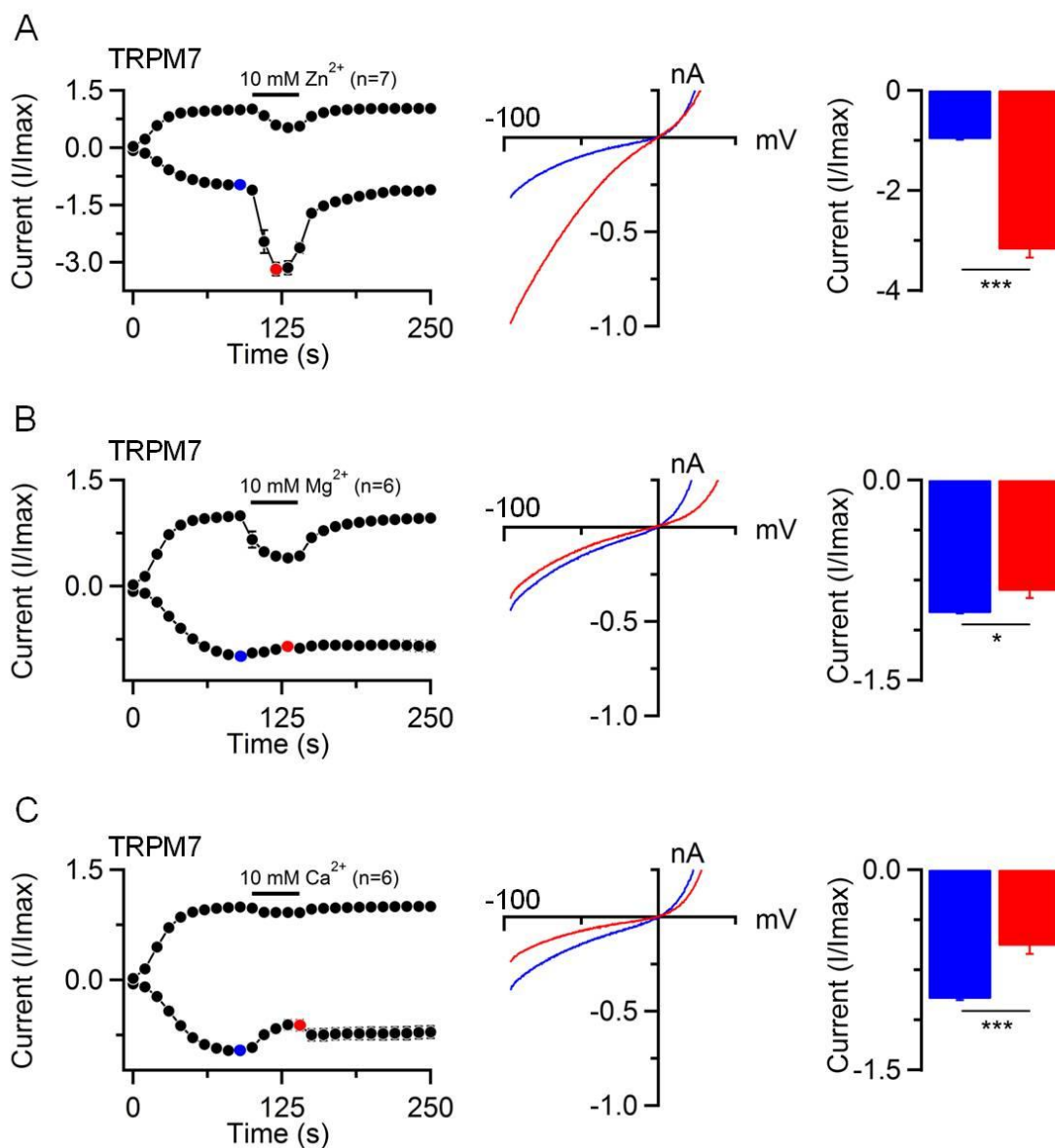


**Figure 4.21. Assessment of divalent cation permeability of mouse TRPM7.** *Left panels:* Whole-cell currents measured in TRPM7 transfected HEK 293 cells ( $n$  = number of cells measured). When currents were fully activated, the cells were exposed to an external solution containing 10 mM  $\text{Zn}^{2+}$  (**A**), 10 mM  $\text{Mg}^{2+}$  (**B**) or 10 mM  $\text{Ca}^{2+}$  (**C**). The currents were acquired at  $-80$  (lower traces) and  $+80$  mV (upper traces), normalized to cell size and plotted versus time of the experiment. Current amplitudes immediately before the application of the divalent cation-based solutions ( $I_{\text{max}}$ ) were set to “1” and normalized current amplitudes ( $I/I_{\text{max}} \pm \text{SEM}$ ) were calculated. *Middle panels:* Representative I-V relationships obtained from individual ramps before (blue) and during (red) application of the divalent cation as indicated in the *left panels*. *Right panels:* Bar graphs of averaged inward currents ( $-80$  mV,  $I/I_{\text{max}} \pm \text{SEM}$ ) obtained before (blue) and during (red) application of the divalent cation-based solutions as indicated in the *left panels* by coloured data points (\*  $p \leq 0.05$ , \*\*\*  $p \leq 0.001$ ).

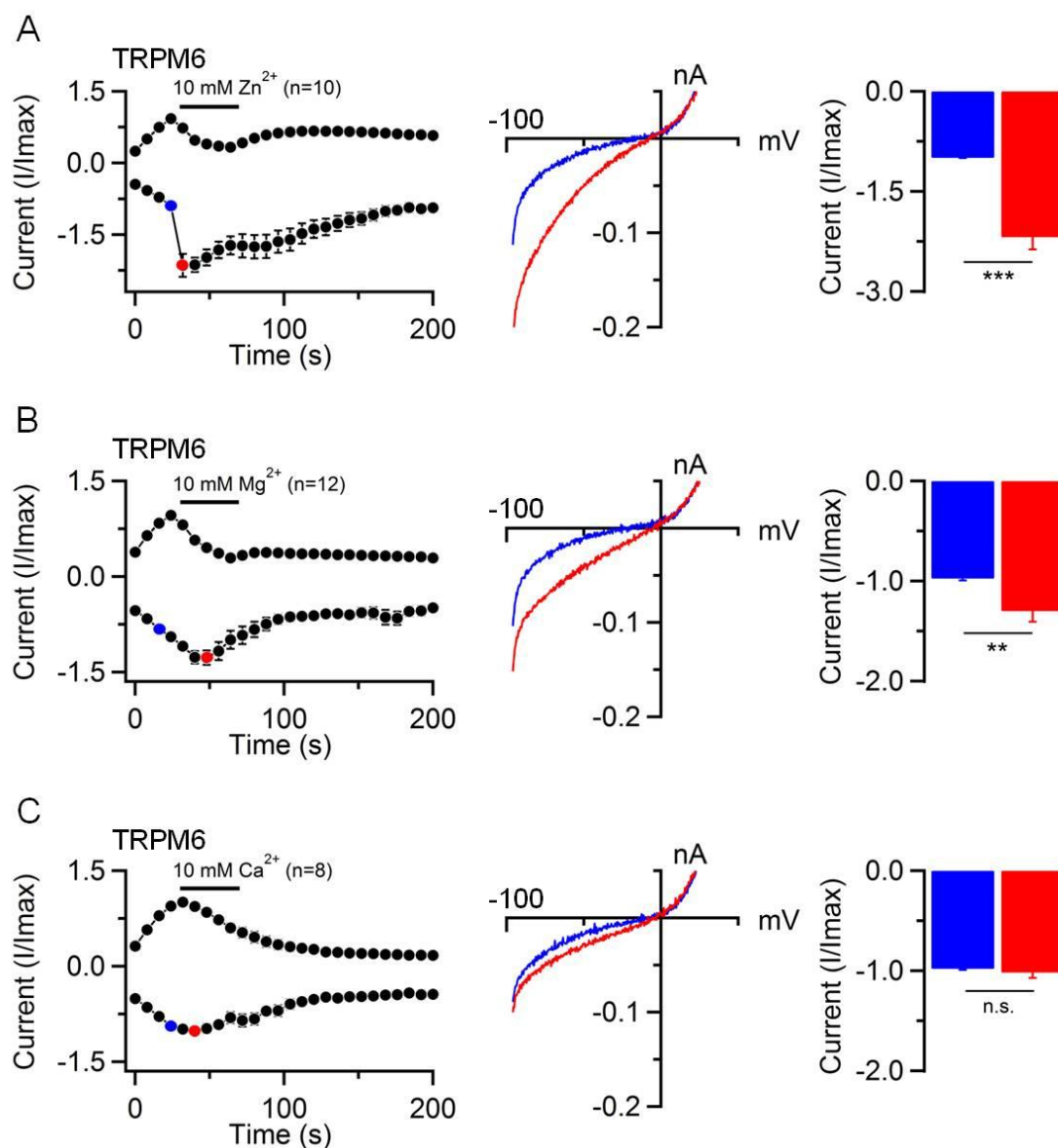


**Figure 4.22. Assessment of divalent cation permeability of mouse TRPM6.** *Left panels:* Whole-cell currents measured in TRPM6 transfected HEK 293 cells ( $n$  = number of cells measured). When currents were fully activated, the cells were exposed to an external solution containing 10 mM Zn<sup>2+</sup> (**A**), 10 mM Mg<sup>2+</sup> (**B**) or 10 mM Ca<sup>2+</sup> (**C**). The currents were acquired at  $-80$  and  $+80$  mV, normalized to cell size and plotted versus time of the experiment. Current amplitudes immediately before the application of the divalent cation-based solutions ( $I_{\text{max}}$ ) were set to “1” and normalized current amplitudes ( $I/I_{\text{max}} \pm \text{SEM}$ ) were calculated. *Middle panels:* Representative I-V relationships obtained from individual ramps before (blue) and during (red) application of the divalent cation as indicated in the *left panels*. *Right panels:* Bar graphs of averaged inward currents ( $-80$  mV,  $I/I_{\text{max}} \pm \text{SEM}$ ) obtained before (blue) and during (red) application of the divalent cation as indicated in the *left panels* by coloured data points (n.s., not significant; \*\*  $p \leq 0.01$ , \*\*\*  $p \leq 0.001$ ).

Next, we performed a similar assessment of TRPM6 currents. Like TRPM7, TRPM6 was found to be well permeable for  $Zn^{2+}$ , since the application of 10 mM  $Zn^{2+}$  caused a ~2-fold increase of inward currents (Fig. 4.22A). In contrast to TRPM7, inward currents of TRPM6 were increased in the presence of 10 mM  $Mg^{2+}$  (Fig. 4.22B) and were invariable by exposure of the cells to 10 mM  $Ca^{2+}$  (Fig. 4.22C). These results suggested that TRPM6 is more selective to  $Mg^{2+}$  as compared to  $Ca^{2+}$ . To summarize, we found that TRPM6 channel is highly permeable for divalent cations. However, the ion selectivity profile of TRPM6 is not identical to that of TRPM7.

#### 4.3.4. The mouse TRPM6 channel is highly sensitive to intracellular $Mg^{2+}$

As mentioned above (4.2.3), it has been proposed that  $[Mg^{2+}]_i$  and  $[Mg\cdot ATP]_i$  are endogenous regulators of TRPM7 and TRPM6 [67-69, 92, 95, 100]. To access the sensitivity of TRPM6 to  $[Mg^{2+}]_i$ , we attempted to compare a concentration-dependent response of TRPM6 versus TRPM7 currents using internal solutions containing different levels of free  $Mg^{2+}$ . In our initial experiments, we examined TRPM6 and TRPM7 transfected HEK 293 cells using either the standard  $Mg^{2+}$ -free intracellular pipette solution or a solution containing 1  $\mu M$  free  $[Mg^{2+}]_i$  (Fig. 4.23). In line with previous work [67, 69, 95], we observed that 1  $\mu M$  free  $[Mg^{2+}]_i$  did not elicit an inhibitory effect on TRPM7 (Fig. 4.23A,F) and caused only a minor suppression of endogenous TRPM7 currents in untransfected HEK 293 cells (Fig. 4.23B,F). Surprisingly, we found that the currents in TRPM6 transfected cells were not activated at all in the presence of 1  $\mu M$  free  $[Mg^{2+}]_i$  (Fig. 4.23C,F). Next, we attempted to perfuse TRPM6-expressing cells with a nominally  $Mg^{2+}$ -free intracellular solution (*n.f.*), i.e., a standard Cs-based  $Mg^{2+}$ -free internal solution lacking divalent chelators EDTA or EGTA. As demonstrated in Fig. 4.23D, TRPM6 currents could not be induced as well in these conditions.

It has been suggested that the catalytic activity of the TRPM7 kinase regulates the sensitivity of TRPM7 to  $Mg^{2+}$  and  $Mg\cdot ATP$  [69, 95]. Therefore, using 'kinase-dead' TRPM6<sup>K1810R</sup> version, we studied whether the kinase activity of TRPM6 interfered with the high sensitivity of TRPM6 to  $[Mg^{2+}]_i$ . However, our experiments showed that, like TRPM6, TRPM6<sup>K1810R</sup> is inactive in the presence of 1  $\mu M$  free  $[Mg^{2+}]_i$ , but could be activated with the standard  $Mg^{2+}$ -free solution (Fig. 4.23E,F).

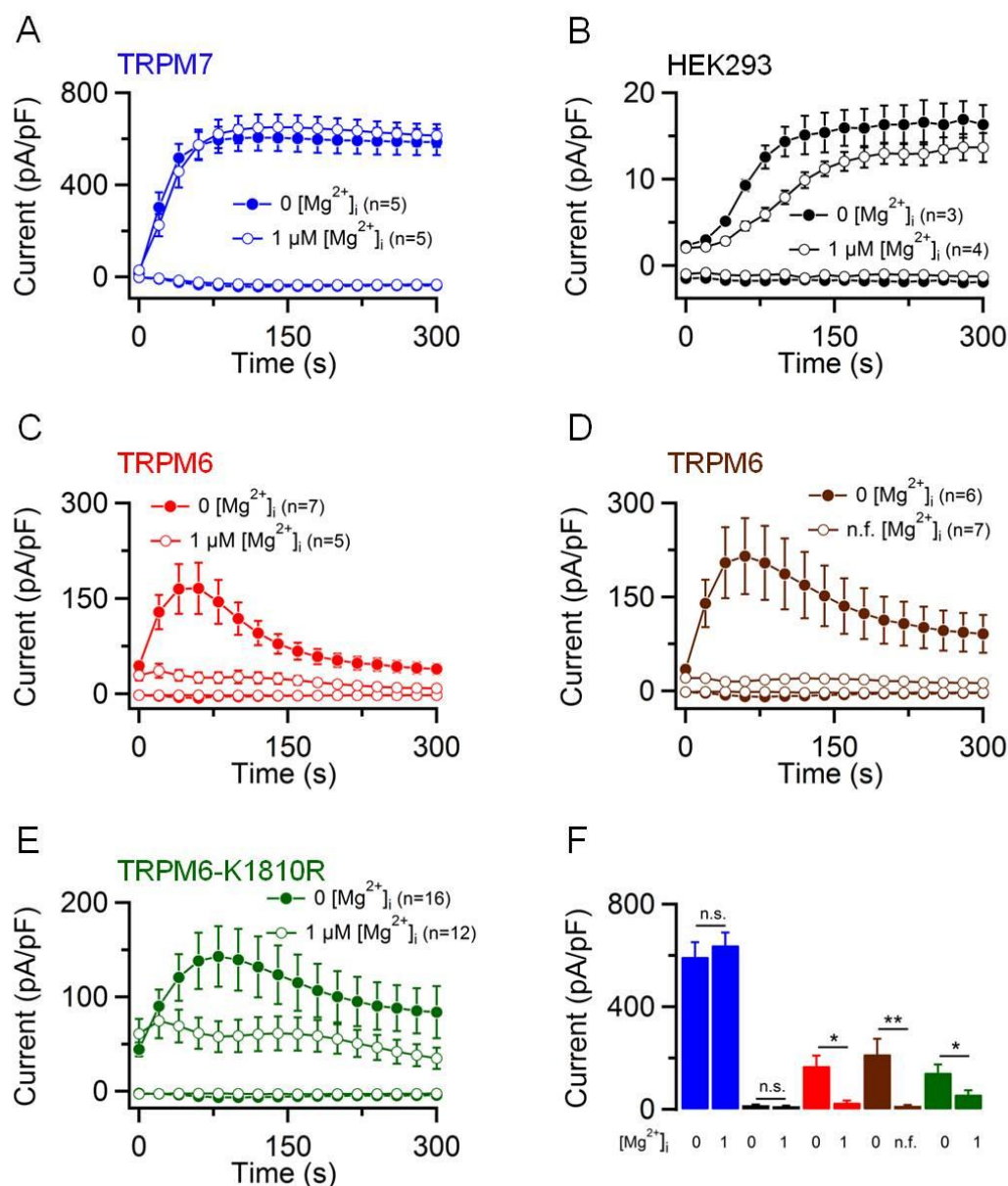


**Figure 4.23. Effects of intracellular Mg<sup>2+</sup> on mouse TRPM6 and TRPM7 currents.** (A-C) Whole-cell currents (mean ± SEM) measured in TRPM7 transfected (A), untransfected (B), or WT TRPM6 transfected (C) HEK 293 cells (n = number of cells measured). Cells were perfused either with the standard Mg<sup>2+</sup>-free intracellular solution (filled circles) or with a solution containing 1 μM free [Mg<sup>2+</sup>]<sub>i</sub> (open circles). The currents were acquired at -80 and +80 mV, normalized to cell size and plotted versus time of the experiment. (D) Measurements were performed with TRPM6 transfected cells as in (C) except that the nominally free [Mg<sup>2+</sup>]<sub>i</sub> solution (*n.f.*) was used. (E) Measurements were performed with TRPM6<sup>K1810R</sup> as in (C). (F) Bar graphs of averaged outward currents (+80 mV, mean ± SEM) shown in (A-E). Current amplitudes were extracted at time intervals when the currents were maximally induced by the Mg<sup>2+</sup>-free intracellular solution as follows: at 200s for TRPM7 (blue) and untransfected cells (black), 50s for WT TRPM6 (red), 80 s for TRPM6<sup>K1810R</sup> (green) (n.s., not significant; \* p ≤ 0.05; \*\* p ≤ 0.01).

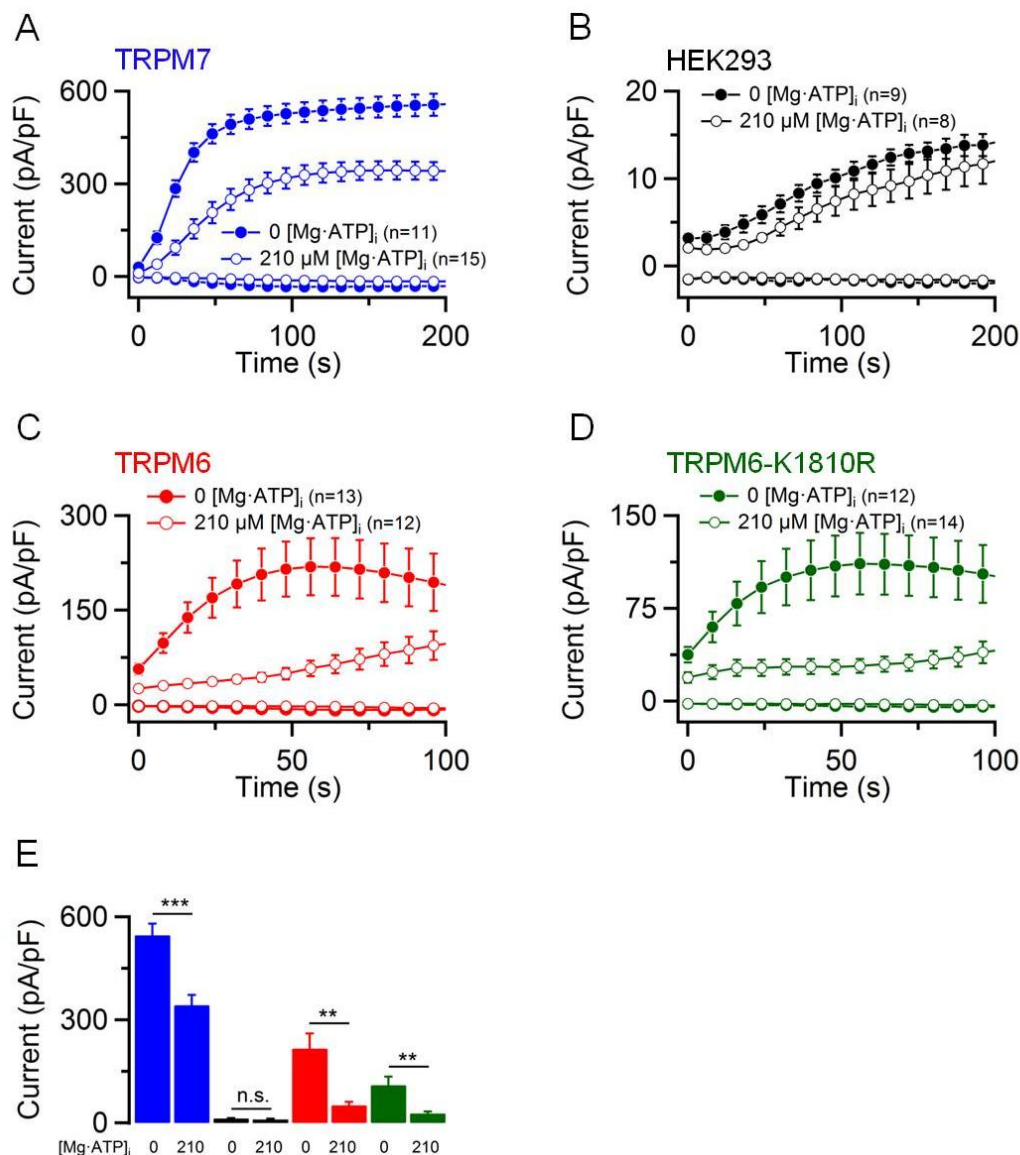


**Figure 4.24. Effects of intracellular Mg-ATP on mouse TRPM6 and TRPM7 currents. (A-D)** Whole-cell currents (mean  $\pm$  SEM) measured in TRPM7 transfected (A) and untransfected (B) HEK 293 cells, or cells transfected either with WT TRPM6 (C) or TRPM6<sup>K1810R</sup> (D) ( $n$  = number of cells measured). Cells were perfused either with the standard Mg<sup>2+</sup>-free intracellular solution (filled circles) or with a solution containing 210  $\mu$ M [Mg-ATP]<sub>i</sub> and 10  $\mu$ M free [Mg<sup>2+</sup>]<sub>i</sub> (open circles). The currents were acquired at  $-80$  and  $+80$  mV, normalized to cell size and plotted versus time of the experiment. **(F)** Bar graphs of averaged outward currents ( $+80$  mV, mean  $\pm$  SEM) shown in (A-D). Current amplitudes were extracted at time intervals when the currents were maximally induced by the Mg<sup>2+</sup>-free intracellular solution as follows: at 200s for TRPM7 (blue) and untransfected cells (black), 50s for WT TRPM6 (red) and TRPM6<sup>K1810R</sup> (green) (n.s., not significant; \*\*  $p < 0.01$ ; \*\*\*  $p < 0.001$ ).

In physiological saline, a  $K_d$  of Mg-ATP is  $\sim 60$   $\mu$ M (at pH 7.2, 37 °C). Hence, cytosolic levels of Mg-ATP (3-7 mM in most mammalian cells [93, 94]) will be in equilibrium with a certain amount of free Mg<sup>2+</sup>. Consequently, TRPM6 will likely remain inactive in the presence of Mg-ATP. To test this idea experimentally, we designed a pipette solution with very low content of Mg-ATP ( $\sim 210$   $\mu$ M) resulting in  $\sim 10$   $\mu$ M free Mg<sup>2+</sup>. Under these

conditions, TRPM7 currents were only modestly suppressed by 210  $\mu\text{M}$  Mg-ATP (Fig. 4.24A,E). Currents mediated by the native TRPM7 channels were also only slightly reduced (Fig. 4.24B,E). As expected, both WT TRPM6 and TRPM6<sup>K1810R</sup> variants were inactive in the presence of 210  $\mu\text{M}$  [Mg-ATP]<sub>i</sub> (Fig. 4.24C,D,E). Thus, TRPM6 revealed an exceptionally high sensitivity to cytosolic [Mg<sup>2+</sup>]<sub>i</sub>. Interestingly, this notable feature of TRPM6 is not dependent on the kinase activity of TRPM6.

#### 4.3.5. Modulation of TRPM6 and TRPM7 by pharmacological compounds

Recently, our group identified several small synthetic molecules acting as activators or inhibitors of the TRPM7 channel [110, 111]. NS8593 was found to be a potent inhibitor of TRPM7 [110]. Accordingly, we investigated whether NS8593 could elicit an inhibitory effect also on TRPM6. To this end, we activated whole-cell TRPM6 currents by our standard approach and applied externally 10  $\mu\text{M}$  NS8593. As TRPM6 currents undergo a gradual inactivation stage, a set of untreated cells was also measured to estimate better the inhibitory effect of NS8593. We found that 10  $\mu\text{M}$  NS8593 caused a rapid inhibition of the TRPM6 channel activity (Fig. 4.25A).

Next, we examined effects of naltriben [111], a potent agonist of the TRPM7 channel. It should be stressed that naltriben cannot exert its effect on TRPM7 if the channel is already induced by the Mg<sup>2+</sup>-free solution. Therefore, we studied the stimulatory effect of naltriben on TRPM7 currents using an intracellular solution containing 2 mM free [Mg<sup>2+</sup>]<sub>i</sub>. As expected, 50  $\mu\text{M}$  naltriben led to a fast activation of TRPM7 currents (Fig. 4.25B). To investigate a response of TRPM6, we used the standard Mg<sup>2+</sup>-free intracellular pipette solution and the solution containing 1  $\mu\text{M}$  free [Mg<sup>2+</sup>]<sub>i</sub> (Fig. 4.25C). However, unlike TRPM7, TRPM6 showed no response to 50  $\mu\text{M}$  naltriben.

2-Aminoethyl diphenylborinate (2-APB) was found to elicit an inhibitory effects on TRPM7 currents [91, 108]. It was reported that this compound potentiates the human TRPM6 channel [91, 92]. This prompted us to assess the effects of 2-APB on TRPM6 in comparison to TRPM7. Transiently transfected HEK 293 cells were perfused with the standard Mg<sup>2+</sup>-free intracellular pipette solution and exposed to 200  $\mu\text{M}$  2-APB when TRPM6 and TRPM7 currents reached the maximal amplitudes. In order to offset variability in expression levels of TRPM6 and TRPM7 of response to 2-APB, the currents were normalized as explained in Fig. 4.21. In good agreement with published work [91, 108], 200  $\mu\text{M}$  2-APB efficiently suppressed TRPM7 currents (Fig. 4.26A). We also found that the native TRPM7 currents were only modestly affected by 2-APB (Fig.

4.26B). Remarkably, 200  $\mu\text{M}$  2-APB was able to significantly potentiate TRPM6 currents in the absence of intracellular  $\text{Mg}^{2+}$  (Fig. 4.26C). It was found previously that 1  $\mu\text{M}$  free  $\text{Mg}^{2+}$  is sufficient to suppress TRPM6 (Fig. 4.23C). Therefore, we asked whether 200  $\mu\text{M}$  2-APB was able to counteract the inhibitory effect of  $\text{Mg}^{2+}$  on TRPM6. As shown in Fig. 4.26D, the increase in TRPM6 currents in the presence of 1  $\mu\text{M}$  free  $\text{Mg}^{2+}$  was more pronounced. Taken together, our data indicate that TRPM6 and TRPM7 have different sensitivity to naltriben and 2-APB.

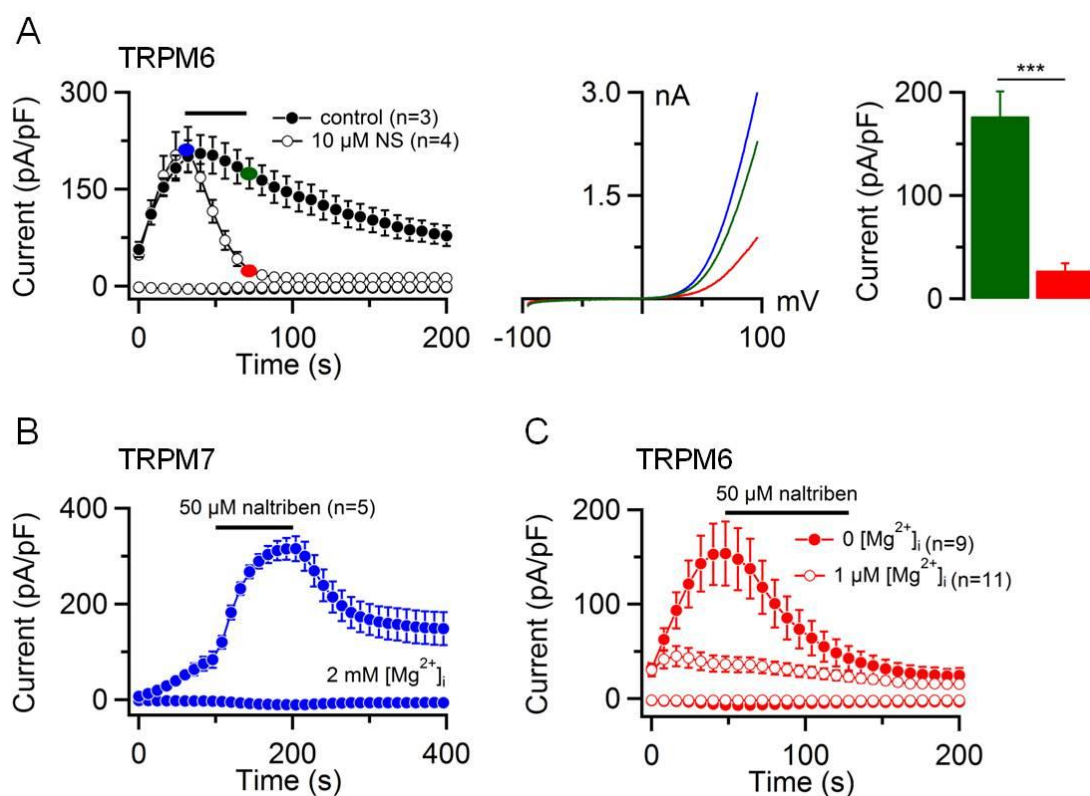


**Figure 4.25. Effects of NS8593 and naltriben on mouse TRPM6 currents.** (A) Inhibition of TRPM6 currents by NS8593. *Left panel:* Whole-cell currents (mean  $\pm$  SEM) measured in TRPM6 transfected HEK 293 cells ( $n$  = number of cells measured). Currents were induced using a standard  $\text{Mg}^{2+}$ -free intracellular solution and a standard external solution. When currents started to develop, the cells were exposed to 10  $\mu\text{M}$  of NS8593 (open circles). A subset of TRPM6-positive cells was examined without application of NS8593 (filled circles). The currents were acquired at  $-80$  and  $+80$  mV, normalized to cell size and plotted versus time of the experiment. *Middle panel:* Representative I-V relationships obtained from individual ramps before (blue) and during (red and green) application of NS8593 as indicated in the *left panel*. *Right panel:* Bar graphs of outward currents ( $+80$  mV, mean  $\pm$  SEM) obtained from untreated (green) and NS8593-treated cells (red) as indicated in the *left panel* (\*\*\*)  $p \leq 0.001$ ). (B) Stimulation of TRPM7 currents by naltriben ( $n$  = number of cells measured). Currents were induced using an intracellular solution containing 2 mM free  $[\text{Mg}^{2+}]_i$  and the standard external solution. The cells were exposed to 50  $\mu\text{M}$  of naltriben. The currents were acquired at  $-80$  and  $+80$  mV, normalized to cell size and plotted versus time of the experiment. (C) Assessment of 50  $\mu\text{M}$  naltriben effects on TRPM6 currents. Measurements were performed similarly to (B) using either the standard  $\text{Mg}^{2+}$ -free intracellular solution (filled circles) or solution containing 1  $\mu\text{M}$  free  $[\text{Mg}^{2+}]_i$  (open circles).

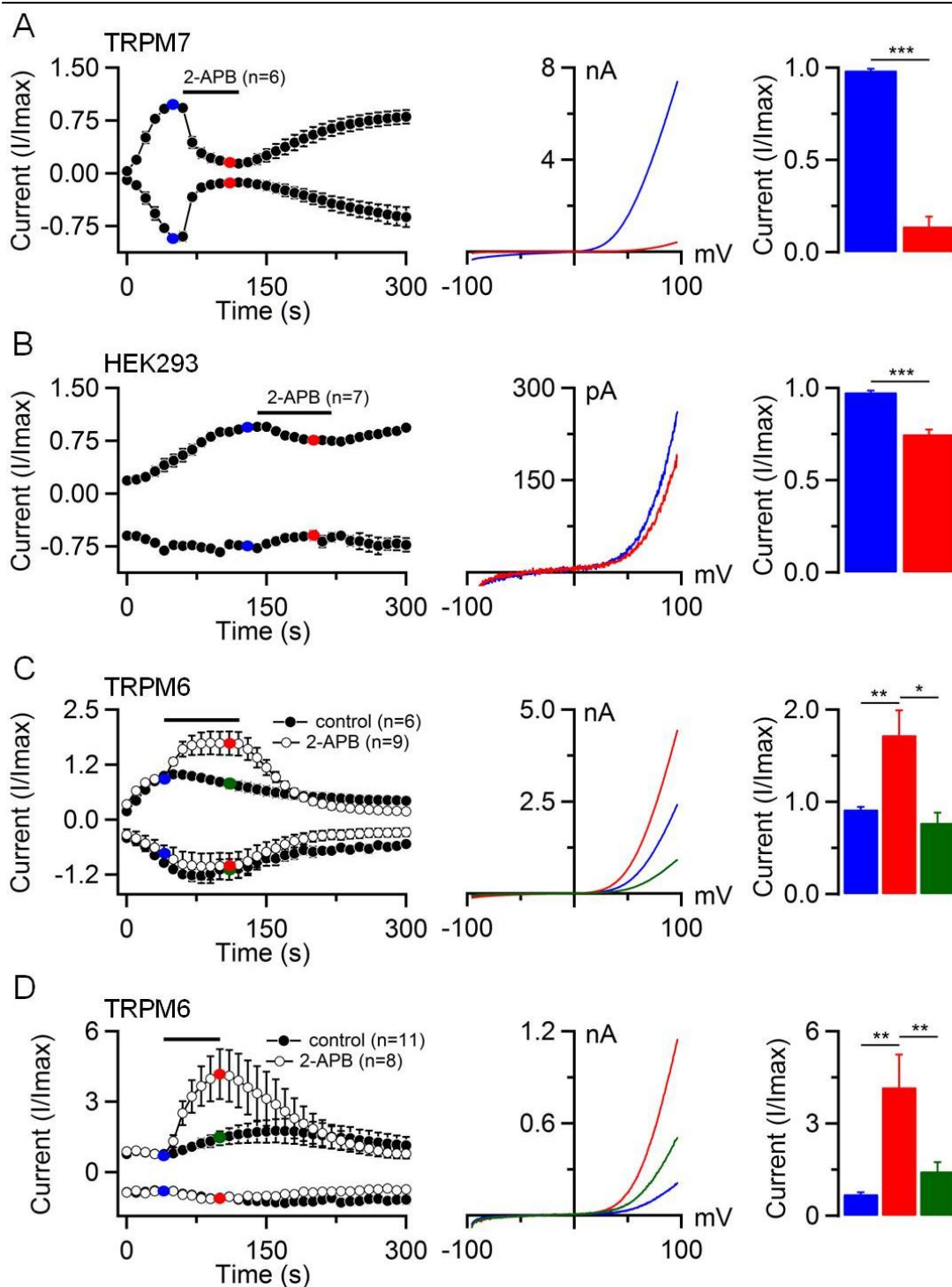


**Figure 4.26. Effects of 2-APB on mouse TRPM6 and TRPM7 currents.** (A, B) *Left panels:* Whole-cell currents measured in TRPM7 transfected (A) and untransfected HEK 293 cells (B) ( $n$  = number of cells measured). When currents were fully activated, the cells were exposed to 200  $\mu\text{M}$  2-APB. The currents were acquired at  $-80$  and  $+80$  mV, normalized to cell size and plotted versus time of the experiment, and shown as  $I/I_{\text{max}} \pm \text{SEM}$ . *Middle panels:* Representative I-V relationships obtained from individual ramps before (blue) and during (red) application of 2-APB as indicated in the *left panels* by coloured dots. *Right panels:* Bar graphs of outward currents ( $+80$  mV,  $I/I_{\text{max}} \pm \text{SEM}$ ) obtained from coloured data-points (i.e. blue, red or green) as indicated in the *left panels* (\*\* $p \leq 0.001$ ). (C, D) Measurements were performed with TRPM6 transfected cells similarly to (A) except that a subset of cells were examined without application of 200  $\mu\text{M}$  2-APB (control). Recordings were performed using either the standard free  $[\text{Mg}^{2+}]_i$  intracellular solution (C) or the solution containing 1  $\mu\text{M}$  free  $[\text{Mg}^{2+}]_i$  (D) (\*  $p \leq 0.05$ ; \*\*  $p \leq 0.01$ ).

Next, we asked whether 2-APB stabilizes TRPM6 monovalent currents which are quickly decayed in DVF saline (Fig. 4.20C). To address this question, HEK 293 cells expressing TRPM6 were exposed to 200  $\mu$ M 2-APB in DVF solution. We found that co-application of 2-APB and DVF allowed to induce large and stable TRPM6 monovalent currents with a characteristic linear I-V relationship (Fig. 4.27A). In contrast to mouse TRPM6, native TRPM7 currents were reduced in the presence of 2-APB in DFV conditions (Fig. 4.27B). Taken together, we concluded that 2-APB positively regulates TRPM6 and inhibits TRPM7.

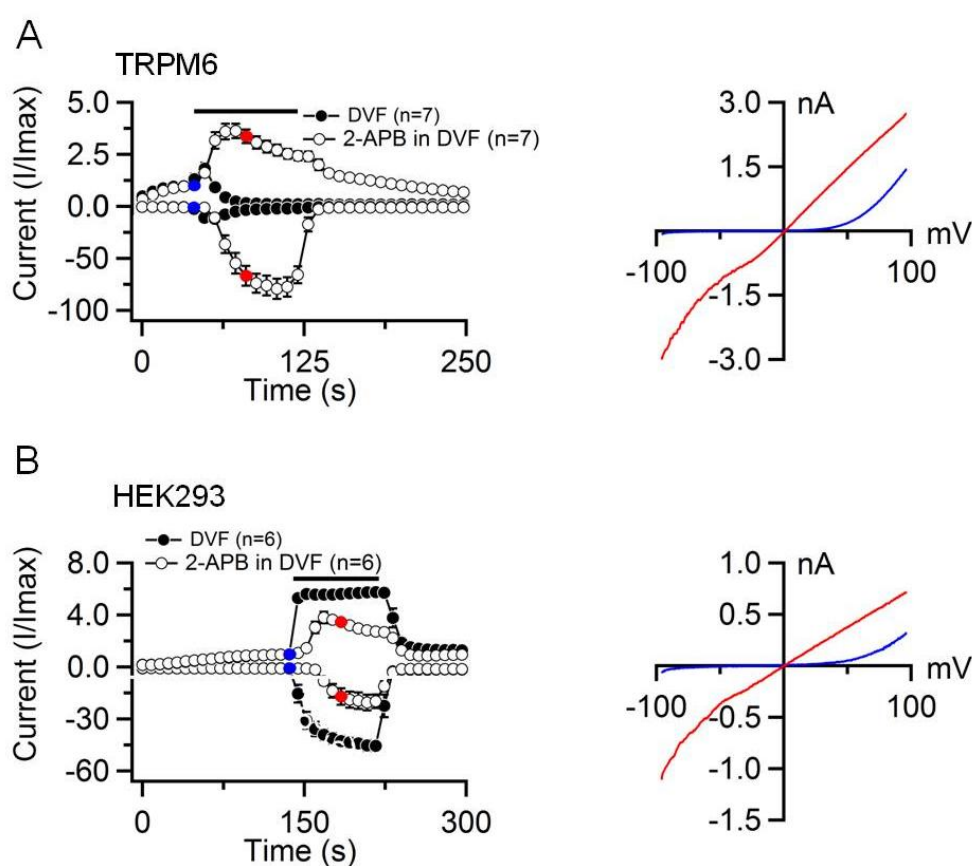


**Figure 4.27. Effects of 2-APB on mouse TRPM6 in the absence of extracellular divalent cations.** *Left panels:* whole-cell currents measured in TRPM6 transfected (**A**) and untransfected (**B**) HEK 293 cells ( $n$  = number of cells measured). When currents were fully activated, the cells were perfused with DVF solution without (filled circles) or with 2-APB (open circles). The currents were acquired at  $-80$  and  $+80$  mV, normalized to cell size and plotted versus time of the experiment, and shown as  $I/I_{\max} \pm$  SEM. *Right panels:* Representative I-V relationships obtained from individual ramps before (blue) and during (red) application as indicated in the *left panels* by coloured dots.

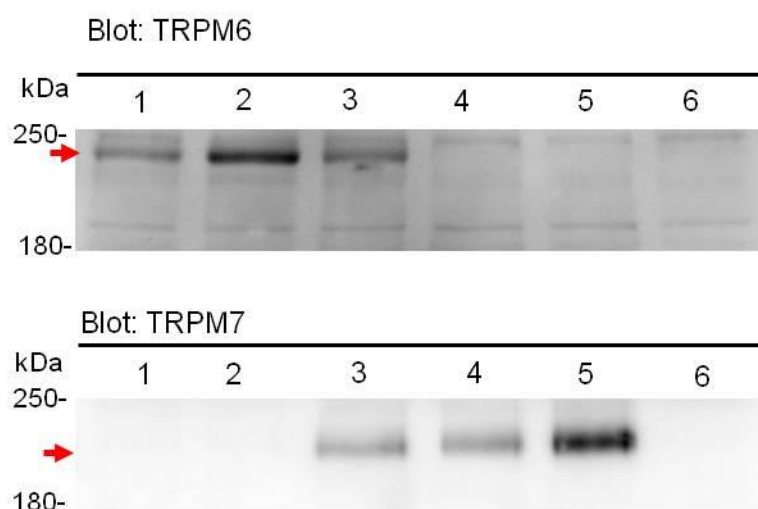
#### 4.3.6. Assessment of heteromeric TRPM6/M7 channel complexes

Our patch-clamp experiments with the recombinant TRPM6 protein suggested that overexpressed TRPM6 is able to form homomeric TRPM6 channels, which are extremely sensitive to internal  $Mg^{2+}$  and, thereby, will remain inactive in the presence of cytosolic free  $Mg^{2+}$  levels (0.5-1 mM in mammalian cells [93, 94]). This finding raises a question as how TRPM6 would function in the physiological conditions. It has been suggested by our group [77, 79] that the native TRPM6 protein primarily exist as a subunit of heteromeric channel complexes formed by TRPM6 and TRPM7 (TRPM6/M7). Accordingly, we asked whether such paradoxical  $Mg^{2+}$  sensitivity of TRPM6 could be altered in TRPM6/M7 complexes. To this end, HEK 293 cells were co-transfected with 1  $\mu$ g TRPM6 and 1  $\mu$ g TRPM7 plasmids. In control experiments, 2  $\mu$ g cDNAs were used to transfect the cells. Of note, Western blot analysis revealed that co-expression of TRPM6 had no effect on expression levels of TRPM7 (Fig. 4.28).

Next, we performed patch-clamp experiments with cell expressing only TRPM7 or co-expressing TRPM6 and TRPM7. We found that TRPM6/M7 transfected cells exhibited significantly higher amplitudes compared to cells transfected only with TRPM7 (Fig. 4.29A). Moreover, it is noteworthy that all cells expressing TRPM6/M7 displayed large currents immediately after establishment of the whole-cell configuration (Fig. 4.29B). These pre-activated currents showed a characteristic TRPM7-like I-V relationships (Fig. 4.29B). In contrast, TRPM7 currents were small after break-in in all measured cells (Fig. 4.29B). Further analysis revealed that amplitudes of TRPM6/M7 pre-activated currents were ~10-fold larger than the corresponding values of TRPM7 (Fig. 4.29B). Remarkably, such constitutive channel activity was not observed in experiments with untransfected HEK 293 cells (Fig. 4.17B) or in the cells transfected only with TRPM6 (Fig. 4.17A,B), suggesting that the association of TRPM6 and TRPM7 in TRPM6/M7 channel complexes results in a new channel type, which is, unlike TRPM6 or TRPM7, constitutively active in resting cells, i.e., in the presence of physiological levels of  $Mg^{2+}$  and Mg-ATP.

Accordingly, in the next set of experiments, we defined the concentration-dependent suppression of TRPM6/M7 currents by  $[Mg^{2+}]_i$ . To address this question, HEK 293 cells were transfected by TRPM6/M7 or TRPM7 and examined using internal solutions containing different free  $[Mg^{2+}]_i$  (Table 3.5). As shown in Fig. 4.29C, we observed only a minor rightward shift in the concentration-response curve of TRPM6/M7 as compared to TRPM7. However, cells expressing TRPM6/M7 exhibited larger current amplitudes over the whole range of  $[Mg^{2+}]_i$  examined (Fig. 4.29C). These results support a notion

that TRPM7 offsets the high sensitivity of TRPM6 to  $Mg^{2+}$  in heteromeric TRPM6/M7 complexes.



**Samples key:**

- 1 - TRPM6 (1  $\mu$ g)
- 2 - TRPM6 (2  $\mu$ g)
- 3 - TRPM6 (1  $\mu$ g) + TRPM7 (1  $\mu$ g)
- 4 - TRPM7 (1  $\mu$ g)
- 5 - TRPM7 (2  $\mu$ g)
- 6 - Untransfected cells

**Figure 4.28. Western blot analysis of HEK 293 cells expressing mouse TRPM6, TRPM7 and TRPM6/M7.** HEK 293 cells were transiently transfected with TRPM6 or/and TRPM7 cDNA constructs and cell lysates were studied using either anti-TRPM6 (**A**) or anti-TRPM7 (**B**) antibodies. Representative blots are shown. The experiment was repeated twice with the similar results.

Finally, we asked whether TRPM6/M7 would be active in the presence of  $Mg\cdot ATP$ . In most mammalian cells, physiological concentrations of intracellular  $Mg\cdot ATP$  vary in a range of 3-7 mM [93, 94]. In the first experiment, we tested effects of a relatively high level of  $Mg\cdot ATP$ . We found that 9 mM  $[Mg\cdot ATP]_i$  caused a nearly full suppression of TRPM7 (Fig. 4.30A). Surprisingly, TRPM6/M7 currents were only modestly suppressed by 9 mM  $[Mg\cdot ATP]_i$  (Fig. 4.30A). Similarly to the experiments showed in Fig. 4.29B, TRPM6/M7-expressing cells displayed very large currents immediately after break-in (Fig. 4.30B).

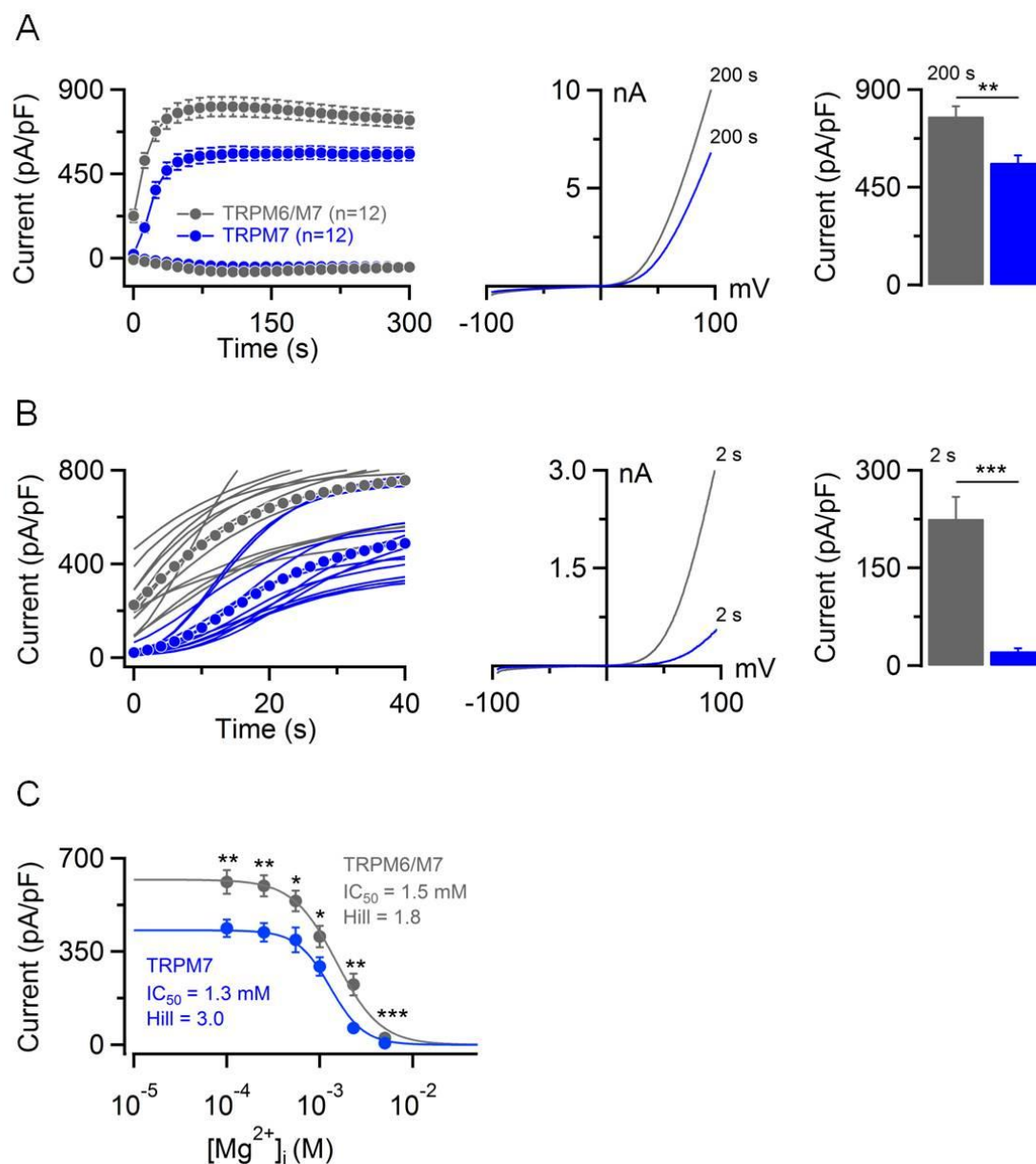


**Figure 4.29. Assessment of mouse TRPM6/M7 currents.** (A) *Left panel:* Whole-cell currents (mean  $\pm$  SEM) measured in TRPM7 (blue) and TRPM6/M7 (gray) transfected HEK 293 cells (n = number of cells measured). Currents were induced using a standard  $Mg^{2+}$ -free intracellular solution and a standard external solution. The currents were acquired at  $-80$  and  $+80$  mV, normalized to cell size and plotted versus time of the experiment. *Middle panel:* Representative I-V relationships of currents illustrated in the *left panel* extracted from individual ramps at 200s. *Right panel:* Bar graphs of averaged outward currents ( $+80$  mV, mean  $\pm$  SEM) shown in the *left panel* obtained at 200 s (\*\* p < 0.01). (B) A magnification of currents illustrated in (A). *Left panel:* Outward current amplitudes ( $+80$  mV) acquired from individual cells with the corresponding means (dots). *Middle panel:* Representative I-V relationships of currents extracted at 2 s shown in the *left panel*. *Right panel:* Bar graphs of averaged outward currents ( $+80$  mV, mean  $\pm$  SEM) shown in the *left panel* obtained at 2 s (\*\*\* p < 0.001). (C) Concentration-dependent inhibition of currents by  $[Mg^{2+}]_i$ . Mean current amplitudes assessed at  $+80$  mV and extracted at 200 s were used to fit the curves and calculate the indicated  $IC_{50}$  values (10-12 cells per concentration) (\* p  $\leq$  0.05; \*\* p  $\leq$  0.01; \*\*\* p  $\leq$  0.001). Error bars indicate SEM.

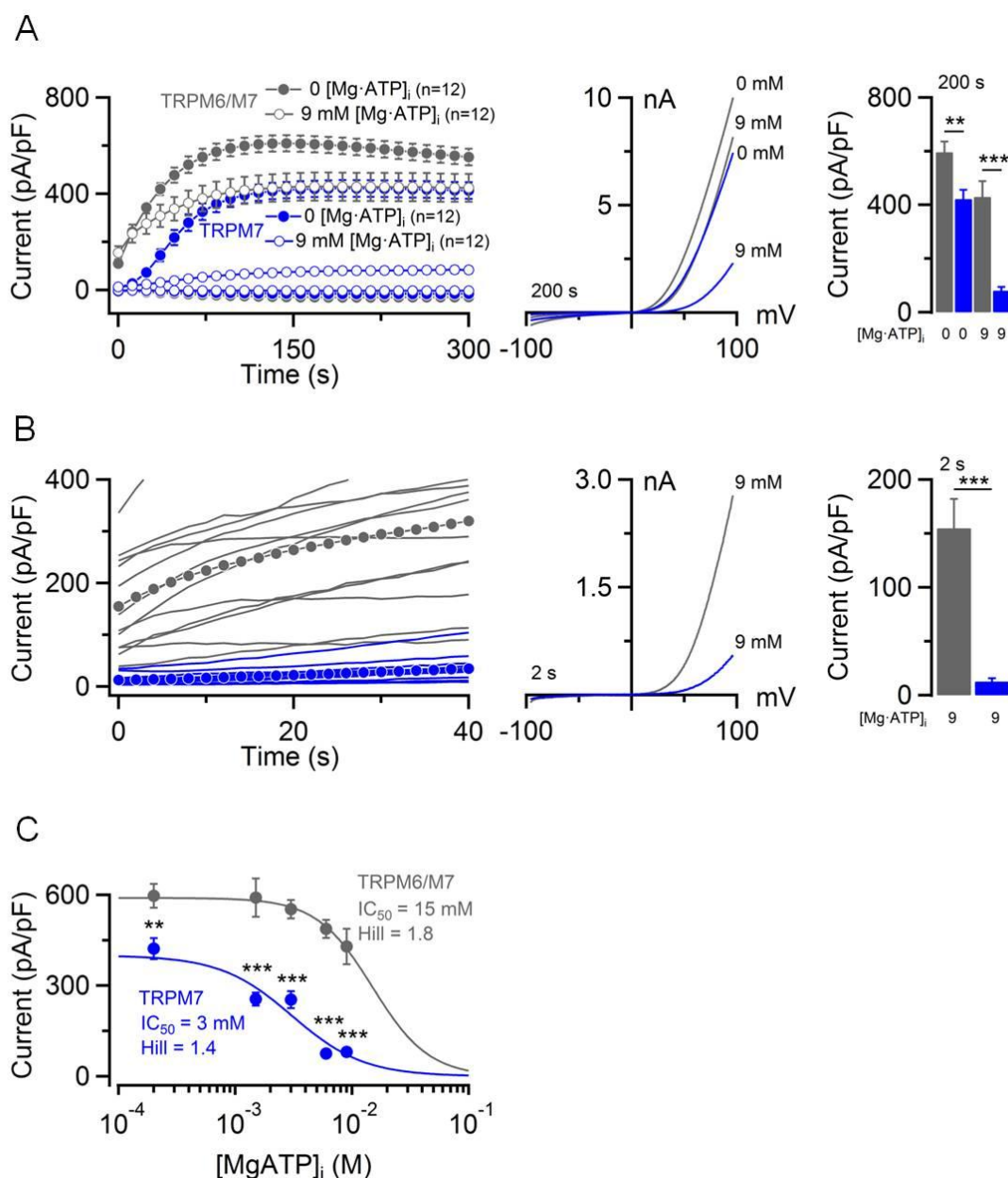


**Figure 4.30. Sensitivity of mouse TRPM6/M7 currents to cytosolic Mg-ATP. (A) Left panel:** Whole-cell currents (mean ± SEM) measured in TRPM7 (blue) and TRPM6/M7 (gray) transfected HEK 293 cells (n = number of cells measured). Currents were induced using either an internal solution containing 9 mM [Mg·ATP]<sub>i</sub> and 250 μM free [Mg<sup>2+</sup>]<sub>i</sub> (open circles) or only 250 μM free [Mg<sup>2+</sup>]<sub>i</sub> (filled circles). The currents were acquired at −80 and +80 mV, normalized to cell size and plotted versus time of the experiment. **Middle panel:** Representative I-V relationships of currents illustrated in the left panel extracted from individual ramps at 200s. **Right panel:** Bar graphs of averaged outward currents (+80 mV, mean ± SEM) shown in the left panel obtained at 200 s (\*\* p < 0.01; \*\*\* p < 0.001). **(B)** A magnification of currents illustrated in (A). **Left panel:** Outward current amplitudes (+80 mV) acquired from individual cells with the corresponding means (dots). **Middle panel:** Representative I-V relationships of currents extracted at 2 s shown in the left panel. **Right panel:** Bar graphs of averaged outward currents (+80 mV, mean ± SEM) shown in the left panel obtained at 2 s (\*\* p < 0.001). **(C)** Concentration-dependent inhibition of currents by [Mg·ATP]<sub>i</sub> (250 μM free [Mg<sup>2+</sup>]<sub>i</sub>). Mean current amplitudes assessed at +80 mV and extracted at 200 s were used to fit the curves and calculate the indicated IC<sub>50</sub> values (9-12 cells per concentration) (\*\* p ≤ 0.01; \*\*\* p ≤ 0.001). Error bars indicate SEM.

In the second set of experiments, we compared concentration-dependent suppression of TRPM6/M7 and TRPM7 currents by  $[\text{Mg}\cdot\text{ATP}]_i$  (Table 3.6). Because of experimental limitations, effects of  $[\text{Mg}\cdot\text{ATP}]_i$  beyond 10 mM could not be reliably examined. We found that  $[\text{Mg}\cdot\text{ATP}]_i$  caused a suppression of TRPM7 currents with  $\text{IC}_{50}$  3.0 mM (Fig. 4.30C). However, TRPM6/M7 currents showed a remarkably low sensitivity to  $[\text{Mg}\cdot\text{ATP}]_i$  at all concentrations examined (Fig. 4.30C). Such weak effect of  $[\text{Mg}\cdot\text{ATP}]_i$  on TRPM6/M7 currents precluded us from a reliable calculation of  $\text{IC}_{50}$ . Nevertheless, fitting of a concentration-response curve suggested that  $\sim 15$  mM  $[\text{Mg}\cdot\text{ATP}]_i$  would cause 50% reduction of TRPM6/M7 currents (Fig. 4.30C). Thus, we could conclude that physiological levels of  $[\text{Mg}\cdot\text{ATP}]_i$  would elicit only a very minor effect on the mouse TRPM6/M7 channel complexes.

The kinase domain of the human TRPM6 is thought to be involved in the regulation of Mg-ATP sensitivity of the TRPM6/M7 heteromeric channel complexes [92]. Accordingly, we investigated whether the kinase-dead mutation (K1810R) in the mouse TRPM6 is able to affect the response of TRPM6 to Mg-ATP. To this end, we co-transfected HEK 293 cells with TRPM6<sup>K1810R</sup> and WT TRPM7. Our results demonstrated that TRPM6<sup>K1810R</sup> behaved similar to WT TRPM6 (Fig. 4.31). Thus, our data suggested the catalytic activity of the mouse TRPM6 kinase domain is not involved in this regulatory mechanism.

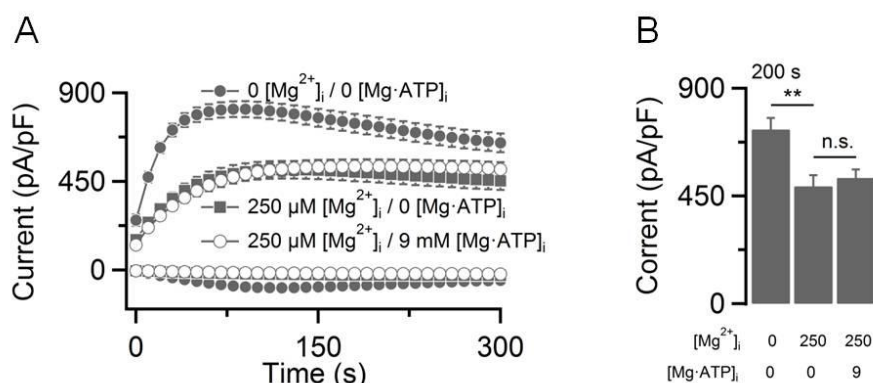


**Figure 4.31. Assessment of mouse TRPM6<sup>K1810R</sup> and WT TRPM7.** (A) Whole-cell currents (mean $\pm$ SEM) recorded in HEK 293 cells co-expressing TRPM6<sup>K1810R</sup> and WT TRPM7. The currents were induced using a standard  $[\text{Mg}^{2+}]_i$  free internal solution (filled circles,  $n=12$ ) and solutions containing either 250  $\mu\text{M}$  free  $[\text{Mg}^{2+}]_i$  (filled squares,  $n=11$ ) or 9 mM  $[\text{Mg}\cdot\text{ATP}]_i$  and 250  $\mu\text{M}$  free  $[\text{Mg}^{2+}]_i$  (open circles,  $n=12$ ). The currents were extracted at  $-80$  and  $+80$  mV, normalized to cell size and plotted versus time of the experiment. (B) Bar graph of averaged outward currents ( $+80$  mV, mean  $\pm$  SEM) shown in (A) (n.s., not significant; \*\*  $p \leq 0.01$ ). n, number of cells measured.

## 5. Discussion

The kinase-coupled channels TRPM6 and TRPM7 were suggested to play an essential role in the organismal  $Mg^{2+}$  balance by regulating  $Mg^{2+}$  influx in the cell [69-71]. However, this concept is intensively debated in the scientific literature. For instance, it was suggested that TRPM7 regulates different cellular processes in a  $Mg^{2+}$ -independent manner [25]. Functional characteristics of the TRPM6 channel are also discussed differently [68, 77, 92]. In the present study, we provide new mechanistic evidence supporting the concept that a functional interplay of TRPM6 and TRPM7 underlines a cellular uptake of  $Mg^{2+}$ , what in turn determinates the physiological roles of these proteins in organismal  $Mg^{2+}$  homeostasis.

### 5.1. TRPM7 controls cellular $Mg^{2+}$ metabolism

It is commonly accepted that TRPM7 forms a homotetrameric channel, which is selective for divalent cations such as  $Zn^{2+}$ ,  $Ca^{2+}$  and  $Mg^{2+}$ . However, there are ongoing debates in the literature whether TRPM7-mediated influx of  $Mg^{2+}$  or  $Ca^{2+}$  is relevant for the numerous cellular processes regulated by TRPM7. In the pioneering study, Nadler *et al.* used DT40 B cells with a targeted deletion of *Trpm7* gene [67]. The homology recombination approach allowed an efficient production of clones heterozygous for TRPM7 null mutation, but no clones were obtained with loss-of-function mutations in both alleles, suggesting that TRPM7 is essential for the cell viability [67]. In follow-up experiments, Schmitz *et al.* have shown that TRPM7 deficient DT40 cells cultured in a standard cell culture medium exhibited a profound decreases in total  $Mg^{2+}$  content [69]. Moreover, they found that addition of 10 mM  $Mg^{2+}$  (but not  $Ca^{2+}$ ,  $Mn^{2+}$ , or  $Zn^{2+}$ ) in the culture medium allowed these KO cells to grow and proliferate similarly to their parental cells, indicating that TRPM7 function is indispensable for the cellular  $Mg^{2+}$  homeostasis [69]. The  $Mg^{2+}$ -dependent proliferation defect of DT40 B cells could be also rescued by ectopic expression of mammalian proteins, which are presumed to function as  $Mg^{2+}$  channels or transporters such as SLC41A1 [155, 156], SLC41A2 [157, 158] or MagT1 [153]. More recently, Ryazanova *et al.* have demonstrated that *Trpm7* gene deficient mouse embryonic stem (ES) cells developed a phenotype resembling TRPM7 deficient DT40 cells [113], supporting the notion that the ubiquitously expressed TRPM7 channel controls  $Mg^{2+}$  uptake in vertebrate cells. However, it has to be stressed that several other studies pointed out that TRPM7 functions primarily as  $Ca^{2+}$ -permeable channel

and, accordingly, that TRPM7 regulates  $\text{Ca}^{2+}$ -dependent signaling pathways in the cell [124, 128, 196-198]. Finally, it was speculated that TRPM7-dependent  $\text{Zn}^{2+}$  entry may also play a physiological role [106, 199-201].

Here, we assessed the cellular role of TRPM7 in three distinct cell types. Specifically, we examined consequences of a complete deletion of TRPM7 protein on the endogenous TRPM7 currents and the ability of mutant cells to proliferate in a standard culture medium or in a medium supplemented with  $\text{Mg}^{2+}$ .

Recently, our group has established that the embryonic development of mice is critically dependent from TRPM6 activity in placental trophoblasts [144]. Accordingly, we asked whether placental cells, such as trophoblast stem (TS) cells, can be used as new experimental model to examine the cellular function of the kinase-linked channels. To address this question, we produced *Trpm7* deficient TS cells from e3.5 blastocysts derived from a cross of *Trpm7* <sup>$\Delta 17/+$</sup>  mice. We found that WT TS cells express TRPM6 and TRPM7 proteins. Patch-clamp experiments revealed that WT TS cells display relatively large divalent cation-selective currents sensitive to intracellular  $\text{Mg}^{2+}$ . Very similar currents were previously measured in many other cell lines and primary isolated cells. These currents were referred to as  $\text{Mg}^{2+}$ -inhibited cation (MIC) currents [97, 98], magnesium nucleotide-regulated metal ion (MagNuM) currents [67, 99] or TRPM7-like currents [144]. We found that the genetic deletion of *Trpm7* in TS cells abrogated completely these TRPM7-like currents. We also found that maintaining *Trpm7* deficient TS cells in a standard cell culture medium leads to suppressed proliferation of these KO cells. Furthermore, we demonstrated that viability of KO TS cells can be rescued by addition of  $\text{Mg}^{2+}$  to the culture medium. These findings support the idea that TRPM7 currents are essential for the  $\text{Mg}^{2+}$  uptake and viability of TS cells [69, 77, 113].

To recapitulate our findings with TS cells, we made use of an alternative in vitro model. In these experiments, we focused on a functional assessment of haploid human leukemia haploid (HAP1) cells [186, 187]. The *TRPM7* deficient (KO) clone was acquired from Horizon Genomics using CRISPR/Cas9 system [144]. Noteworthy, like TS cells, WT HAP1 cells express TRPM6 and TRPM7. WT HAP1 cells harbor moderate levels of endogenous TRPM7-like currents. Analogously to TS cells, the genetic deletion of *TRPM7* completely abolished these currents. As expected, KO HAP1 cells could proliferate only if the cell culture medium contained additional  $\text{Mg}^{2+}$ , supporting the concept that TRPM7 plays a vital role in  $\text{Mg}^{2+}$  uptake, which is required for cell proliferation. Interestingly, similar to the situation with TS cells, this TRPM7 function could not be compensated by TRPM6.

TRPM7 is highly expressed in different types of non-proliferating blood cells [180]. Recently, a screen for new inherited forms of macrothrombocytopenia resulted in the identification of two human families harbouring loss-of-function point mutations in *TRPM7* [180]. The affected individuals displayed impaired thrombopoiesis due to altered cellular  $Mg^{2+}$  homeostasis and cytoskeletal architecture [180]. We wondered whether megakaryocytes (MKs) derived from a mice strain with a conditional inactivation of *Trpm7* specifically in megakaryocytes can recapitulate alterations observed in human MKs of the above-mentioned patients. MKs are large progenitor cells in the bone marrow responsible for the generation of blood thrombocytes (platelets) [180]. MKs extend long cytoplasmic processes into bone marrow sinusoids, called proplatelets, which to release platelets [180]. In a collaboration with Dr. Attila Braun's group, we found that these mutant mice are able to generate MKs and platelets *in vivo*. In our patch-clamp experiments, we could show that mutant MKs completely lack native TRPM7 currents. In line with this finding, TRPM7 deficient platelets were moderately depleted in  $Mg^{2+}$  [180]. Taken together, we concluded that TRPM7 regulates  $Mg^{2+}$  metabolism in this cell type as well.

To summarize, our experiments with three independent cell types (extraembryonic stem cells, tumor-derived cells and non-proliferating cells) support a model that TRPM7 mediates the endogenous divalent cation-selective currents, which are critically implicated in  $Mg^{2+}$  cellular metabolism.

## 5.2. TRPM6 cooperates with TRPM7 in TS cells

Mutations in human *TRPM6* gene were linked to the familial hypomagnesemia with secondary hypocalcemia (HSH), an autosomal recessive disease characterized by low  $Mg^{2+}$  and  $Ca^{2+}$  serum levels [70, 71]. However, the first attempt to elucidate pathomechanisms of HSH in animal model resulted in unexpected findings. Walder *et al.* [142] found that a constitutive inactivation of *Trpm6* results in embryonic death at day e12.5. Recently, our group [144] could define a role of *Trpm6* in the prenatal survival of mice. Our laboratory provided the comprehensive evidence that the embryonic mortality of *Trpm6* deficient mice is caused by the loss of TRPM6 activity in the placental trophoblasts in syncytiotrophoblast layer I (SynT-I) [144]. Accordingly, we used a conditional mutagenesis to show that the epiblast-restricted inactivation of *Trpm6* enables to produce viable adult mice lacking TRPM6 in the whole body [144]. We also found that TRPM6 deficiency in the prenatal or adult organisms is associated

to systemic  $Mg^{2+}$  deprivation. Taken together, we propose a new model for a role of *Trpm6* in the prenatal development of mice. According to this model, *Trpm6* is required for  $Mg^{2+}$  transport via syncytiotrophoblast layers of the placenta. Consequently, the genetic inactivation of *Trpm6* leads to  $Mg^{2+}$  deficiency and secondary embryonic phenotypes such as the growth failure [144].

Currently, there is no consensus regarding the cellular function of TRPM6. As already mentioned, TRPM6 has been shown to be expressed mainly in the transporting epithelial cells of the kidney and intestine [70, 71], whereas TRPM7 is ubiquitously expressed [67]. Thus, TRPM6 is always co-expressed with TRPM7, and it remains to be answered why a loss of TRPM6 function in HSH patients and KO mice could not be compensated by TRPM7. The critical role of *Trpm6* in the placental trophoblasts prompted us to use TS cells as an in vitro experimental model to address this question.

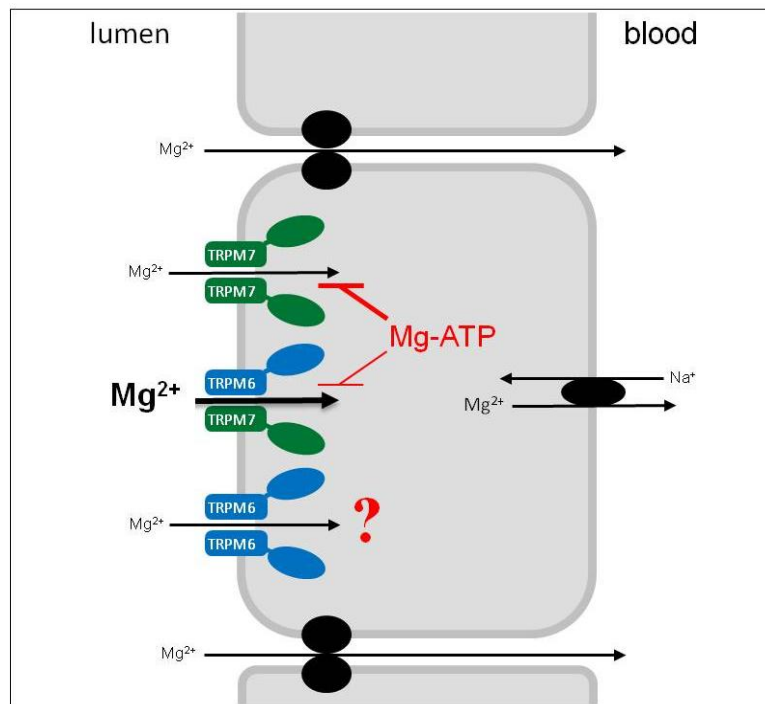


**Figure 5.1. A proposed model representing the role of TRPM6/M7 channels for transcellular  $Mg^{2+}$  transport in the epithelial cells.** Figure modified from [177].

Analogously to *Trpm7* KO TS cells, we derived *Trpm6* gene deficient and corresponding WT TS cells from *Trpm6*<sup>geo/+</sup> parents. In contrast to *Trpm7* deficient TS cells, TS cells lacking TRPM6 were able to proliferate in standard cell culture medium (not fortified by additional  $Mg^{2+}$ ). Similarly to the previous patch-clamp experiments, our analysis of WT TS revealed high density of TRPM7-like currents cells induced by

depletion of intracellular  $Mg^{2+}$ . However, in contrast to *Trpm7* deficient cells characterized by a complete lack of the endogenous TRPM7-like currents, we observed that *Trpm6* deficient cells displayed only a partial reduction of the current amplitudes. These findings are fully compatible with a previously suggested model [77, 144] that native TRPM6 functions as a subunit of heteromeric TRPM6/M7 channel complexes (Fig. 5.1). In line with this idea, the deletion of TRPM6 and TRPM7 elicits different impacts on the endogenous currents and, consequently,  $Mg^{2+}$ -dependent proliferation of TS cells: ablation of TRPM7 removes TRPM7 and TRPM6/M7 channel complexes, whereas inactivation of TRPM6 impairs only TRPM6/M7 channels.

Based on such assumption, we compared effects of intracellular  $Mg^{2+}$  and Mg-ATP on currents in TRPM6 KO cells (expressing only TRPM7 channels) versus WT cells (containing TRPM7 and TRPM6/M7 channels). As mentioned above,  $Mg^{2+}$  and Mg-ATP were suggested as physiological regulators of TRPM6 and TRPM7 [67-69, 92, 95, 100]. We found that TRPM7-like currents were similarly inhibited by  $Mg^{2+}$  in TS cells of the both genotypes, i.e., TRPM7 and TRPM6/M7 channels likely display the similar sensitivity to intracellular  $Mg^{2+}$ . However, we observed that the currents in *Trpm6* deficient cells were substantially more sensitive to Mg-ATP as compared to WT cells. This finding is consistent with a recent report [92] showing a very low sensitivity of recombinant TRPM6/M7 channels overexpressed in HEK 293 cells. We concluded that association of native TRPM6 with TRPM7 alters the sensitivity of TRPM6/M7 channel complexes to Mg-ATP. Consequently, TRPM6/M7 channels will be more active in the presence of cytosolic levels of Mg-ATP (Fig. 5.1). Finally, our experiments showed that WT TS cells exhibit a significantly higher fraction of cells with spontaneous channel activity detectable before a depletion of internal  $Mg^{2+}$  occurs. Such high constitutive activity of the endogenous TRPM7-like currents may be attributed to the reduced sensitivity of TRPM6/M7 channels to Mg-ATP in the resting cells (prior to a removal of internal  $Mg^{2+}$  by perfusion of cell by the pipette solution). Thus, TRPM6 alters quantitative and qualitative characteristics of the native TRPM7-like currents what will likely enhance entry of  $Mg^{2+}$  in cells co-expressing TRPM6 and TRPM7. Apparently, this role of TRPM6 is not essential for cell autonomous functions since TRPM7 remains active. However, such an extra  $Mg^{2+}$  entry path may drive a vectored transcellular  $Mg^{2+}$  transport (Fig. 5.1). Accordingly, such model is well compatible with findings that the *in vivo* role of TRPM6 cannot be maintained by TRPM7 alone.

### 5.3. Interplay of TRPM6 and TRPM7 channels determines the sensitivity of TRPM6/M7 channels to cytosolic $Mg^{2+}$ and Mg-ATP

In the next step of the present work, we investigated the role of channel and kinase domains of TRPM6 for the sensitivity of TRPM6/M7 channels to  $[Mg^{2+}]_i$  and  $[Mg\cdot ATP]_i$ . Because the functional consequences of the heterologous expression of human TRPM6 is surrounded by considerable controversy [68, 77, 92], we functionally characterized a newly cloned mouse TRPM6 cDNA.

In the past, our laboratory extensively investigated the recombinant human TRPM6 protein in HEK 293 cells, *Xenopus* oocytes and other expression systems [77]. It was found that human TRPM6 is retained in intracellular membrane compartments and that co-expression of TRPM6 and TRPM7 caused co-trafficking of TRPM6/M7 to the cell surface [77]. In addition, the interaction of TRPM6 with TRPM7 was shown by fluorescence resonance energy transfer (FRET) technique and co-immunoprecipitation approaches [77]. Currents mediated by TRPM6/M7 channels were higher than TRPM7 currents [77].

However, it should be noted that other laboratories suggested that the recombinant human TRPM6 is able to function independently from TRPM7 [68, 92]. This idea was based on the observation that transient transfection of human TRPM6 in pCINeo-IRES-GFP plasmid (but not other expression vectors) enables to induce TRPM6 currents without co-expression of TRPM7 [68, 92]. Of note, experiments with human TRPM6 in pCINeo-IRES-GFP vector produced different observations regarding the sensitivity of TRPM6 to intracellular levels of  $Mg^{2+}$  and  $[Mg\cdot ATP]_i$ . One laboratory demonstrated that TRPM6 is inhibited by  $[Mg^{2+}]_i$  and  $[Mg\cdot ATP]_i$  with  $IC_{50}$  of 510  $\mu M$  and 1.3 mM, respectively [68, 100]. However, another group reported that human TRPM6 cDNA inserted in pCINeo-IRES-GFP allowed to elicit currents, which were insensitive to 3-9 mM  $[Mg\cdot ATP]_i$  and highly sensitive to  $[Mg^{2+}]_i$  with  $IC_{50}$  of 29  $\mu M$  [92]. Mechanistically, these discrepancies remain to be explained. Specifically, it is unclear why only pCINeo-IRES-hTRPM6-GFP plasmid enables to succeed a functional expression of TRPM6.

Because the characteristics of human TRPM6 cDNA are rather controversial, in the present work we investigated a newly generated murine TRPM6 cDNA. We found that mouse TRPM6 cDNA could be functionally expressed irrespective of the vector backbone. Thus, an overexpression system did not completely recapitulated the characteristics of the native TRPM6 protein, since endogenous TRPM6 was active only

in the presence of TRPM7. Nevertheless, such experimental approach may be instrumental for dissecting functional impacts of the kinase versus channel activity of TRPM6 on regulatory features of the TRPM6/M7 channels. We observed that overexpression of mouse TRPM6 cDNA in HEK 293 cells allowed to detect TRPM6 currents, which were substantially smaller than TRPM7 currents, suggesting that the formation of functional TRPM6 homomeric channels was considerably less efficient than TRPM7 channels. Furthermore, unlike TRPM7, TRPM6 currents were quickly inactivated. We also observed that, similar to TRPM7, TRPM6 is more permeable for  $Zn^{2+}$  as compared to  $Mg^{2+}$  and  $Ca^{2+}$ . Most remarkably, the mouse TRPM6 channel was very sensitive to internal levels of  $Mg^{2+}$ . TRPM6 was not active in the presence of nominally  $Mg^{2+}$  free buffer, indicating that TRPM6 homomers, if formed, will be blocked in the presence of physiological levels of  $Mg^{2+}$ . We also found that the TRPM6 kinase is not involved in the extraordinary  $Mg^{2+}$  sensitivity of TRPM6. Our data show that, similarly to TRPM7 [110], TRPM6 activity is suppressed by the small organic molecule NS8593. Unlike TRPM7 [111], TRPM6 is complete insensitive to naltriben. In good agreement with [91], TRPM7 currents are inhibited by 2-APB, while TRPM6 currents are increased by this compound. Thus, the two channels exhibit a different response to pharmacological modulator.

Next, we studied how TRPM6 alters the response of TRPM7 to  $[Mg^{2+}]_i$  and  $[Mg\cdot ATP]_i$ . We found that cells expressing TRPM6 and TRPM7 develop currents significantly bigger than cells transfected with only TRPM7, hence, recapitulating the situation in TS cells. TRPM6/M7 channels showed very high activity after break-in, indicating that these channels were active in the presence of cytosolic levels of  $Mg^{2+}$  and  $Mg\cdot ATP$ . In line with this idea, we found that, unlike TRPM7, TRPM6/M7 currents were only modestly suppressed by physiological concentrations of  $Mg\cdot ATP$  (3-9 mM) and were more active in the presence of physiological levels  $Mg^{2+}$  (0.5-1 mM). Finally, we observed that the TRPM6 kinase does not influence the low response of the TRPM6/M7 channels to internal  $Mg\cdot ATP$ .

To summarize, we found that TRPM6 and TRPM7 contribute differentially to key regulatory features of the TRPM6/M7 channels. Assembly of TRPM6 and TRPM7 produce a new type of cation channel that is active in the presence of physiological levels of cytosolic  $Mg^{2+}$  and  $Mg\cdot ATP$ . Accordingly, TRPM6/M7 channels will allow for a constant uptake of  $Mg^{2+}$  independent on the actual metabolic state of epithelial cells. In contrast, the TRPM7 channels are tightly controlled by  $[Mg^{2+}]_i$  and  $[Mg\cdot ATP]_i$  and, consequently, TRPM7 activity will be closely linked to cellular  $Mg^{2+}$  metabolism. This

model provides a plausible answer for the question as to why in transporting epithelia TRPM6 cannot be replaced by TRPM7.

## 6. Conclusions

1. The native TRPM7 channel mediates  $Mg^{2+}$  and Mg-ATP sensitive divalent cation currents in TS, HAP1 and MKs cells. Genetic inactivation of TRPM7 in these cells leads to  $Mg^{2+}$  deficiency associated with a proliferation defect of TS and HAP1 cells, indicating that TRPM7 channel is required for  $Mg^{2+}$  uptake into cells.
2. In TS cells, the native TRPM6 protein functions primarily as a subunit of heteromeric TRPM6/M7 channel complexes. The association of TRPM6 with TRPM7 increases constitutive activity and reduces the sensitivity to cytosolic Mg-ATP of TRPM6/M7 channels.
3. Recombinant mouse TRPM6 and TRPM7 overexpressed in HEK 293 cells recapitulate key characteristics of endogenous TRPM6 and TRPM7 channels. Specifically, recombinant mouse TRPM6 associates with TRPM7 to form heteromeric channel complexes, which remain active in the presence of physiological level of cytosolic  $Mg^{2+}$  and Mg-ATP. Such functional interplay of TRPM6 with TRPM7 may explain the nonredundant role of TRPM6 in  $Mg^{2+}$  transport by epithelial cell.

---

# References

1. **Venkatachalam, K.** and C. Montell, *TRP channels*. *Annu Rev Biochem*, 2007. 76: p. 387-417.
2. **Montell, C.**, *Physiology, phylogeny, and functions of the TRP superfamily of cation channels*. *Sci STKE*, 2001. 2001(90): p. re1.
3. **Ramsey, I.S.**, M. Delling, and D.E. Clapham, *An introduction to TRP channels*. *Annu Rev Physiol*, 2006. 68: p. 619-47.
4. **Owsianik, G.**, et al., *Permeation and selectivity of TRP channels*. *Annu Rev Physiol*, 2006. 68: p. 685-717.
5. **Montell, C.**, *The TRP superfamily of cation channels*. *Sci STKE*, 2005. 2005(272): p. re3.
6. **Vriens, J.**, et al., *Invertebrate TRP proteins as functional models for mammalian channels*. *Pflugers Arch*, 2004. 449(3): p. 213-26.
7. **Hoenderop, J.G.**, et al., *Homo- and heterotetrameric architecture of the epithelial Ca<sup>2+</sup> channels TRPV5 and TRPV6*. *EMBO J*, 2003. 22(4): p. 776-85.
8. **Kuzhikandathil, E.V.**, et al., *Functional analysis of capsaicin receptor (vanilloid receptor subtype 1) multimerization and agonist responsiveness using a dominant negative mutation*. *J Neurosci*, 2001. 21(22): p. 8697-706.
9. **Moiseenkova-Bell, V.Y.**, et al., *Structure of TRPV1 channel revealed by electron cryomicroscopy*. *Proc Natl Acad Sci U S A*, 2008. 105(21): p. 7451-5.
10. **Liao, M.**, et al., *Structure of the TRPV1 ion channel determined by electron cryo-microscopy*. *Nature*, 2013. 504(7478): p. 107-12.
11. **Cao, E.**, et al., *TRPV1 structures in distinct conformations reveal activation mechanisms*. *Nature*, 2013. 504(7478): p. 113-8.
12. **Zubcevic, L.**, et al., *Cryo-electron microscopy structure of the TRPV2 ion channel*. *Nat Struct Mol Biol*, 2016. 23(2): p. 180-186.
13. **Huynh, K.W.**, et al., *Structure of the full-length TRPV2 channel by cryo-EM*. *Nat Commun*, 2016. 7: p. 11130.
14. **Saotome, K.**, et al., *Crystal structure of the epithelial calcium channel TRPV6*. *Nature*, 2016. 534(7608): p. 506-11.

15. **Shen, P.S.**, et al., *The Structure of the Polycystic Kidney Disease Channel PKD2 in Lipid Nanodiscs*. Cell, 2016. 167(3): p. 763-773 e11.
16. **Wilkes, M.**, et al., *Molecular insights into lipid-assisted Ca<sup>2+</sup> regulation of the TRP channel Polycystin-2*. Nat Struct Mol Biol, 2017. 24(2): p. 123-130.
17. **Paulsen, C.E.**, et al., *Structure of the TRPA1 ion channel suggests regulatory mechanisms*. Nature, 2015. 520(7548): p. 511-7.
18. **Mio, K.**, et al., *The TRPC3 channel has a large internal chamber surrounded by signal sensing antennas*. J Mol Biol, 2007. 367(2): p. 373-83.
19. **Jin, P.**, et al., *Electron cryo-microscopy structure of the mechanotransduction channel NOMPC*. Nature, 2017. 547(7661): p. 118-122.
20. **Sedgwick, S.G.** and S.J. Smerdon, *The ankyrin repeat: a diversity of interactions on a common structural framework*. Trends Biochem Sci, 1999. 24(8): p. 311-6.
21. **Clapham, D.E.**, *TRP channels as cellular sensors*. Nature, 2003. 426(6966): p. 517-24.
22. **Erler, I.**, et al., *Trafficking and assembly of the cold-sensitive TRPM8 channel*. J Biol Chem, 2006. 281(50): p. 38396-404.
23. **Mei, Z.Z.**, et al., *Intracellular coiled-coil domain engaged in subunit interaction and assembly of melastatin-related transient receptor potential channel 2*. J Biol Chem, 2006. 281(50): p. 38748-56.
24. **Tsuruda, P.R.**, D. Julius, and D.L. Minor, Jr., *Coiled coils direct assembly of a cold-activated TRP channel*. Neuron, 2006. 51(2): p. 201-12.
25. **Fleig, A.** and V. Chubanov, *Trpm7*. Handb Exp Pharmacol, 2014. 222: p. 521-46.
26. **Montell, C.** and G.M. Rubin, *Molecular characterization of the Drosophila trp locus: a putative integral membrane protein required for phototransduction*. Neuron, 1989. 2(4): p. 1313-23.
27. **Phillips, A.M.**, A. Bull, and L.E. Kelly, *Identification of a Drosophila gene encoding a calmodulin-binding protein with homology to the trp phototransduction gene*. Neuron, 1992. 8(4): p. 631-42.
28. **Xu, X.Z.**, et al., *TRPgamma, a drosophila TRP-related subunit, forms a regulated cation channel with TRPL*. Neuron, 2000. 26(3): p. 647-57.

29. **Hardie**, R.C. and B. Minke, *The trp gene is essential for a light-activated Ca<sup>2+</sup> channel in Drosophila photoreceptors*. Neuron, 1992. 8(4): p. 643-51.
30. **Clapham**, D.E., L.W. Runnels, and C. Strubing, *The TRP ion channel family*. Nat Rev Neurosci, 2001. 2(6): p. 387-96.
31. **Vennekens**, R., et al., *Current understanding of mammalian TRP homologues*. Cell Calcium, 2002. 31(6): p. 253-64.
32. **Caterina**, M.J., et al., *The capsaicin receptor: a heat-activated ion channel in the pain pathway*. Nature, 1997. 389(6653): p. 816-24.
33. **Jaquemar**, D., T. Schenker, and B. Trueb, *An ankyrin-like protein with transmembrane domains is specifically lost after oncogenic transformation of human fibroblasts*. J Biol Chem, 1999. 274(11): p. 7325-33.
34. **Jordt**, S.E., et al., *Mustard oils and cannabinoids excite sensory nerve fibres through the TRP channel ANKTM1*. Nature, 2004. 427(6971): p. 260-5.
35. **Bandell**, M., et al., *Noxious cold ion channel TRPA1 is activated by pungent compounds and bradykinin*. Neuron, 2004. 41(6): p. 849-57.
36. **Walker**, R.G., A.T. Willingham, and C.S. Zuker, *A Drosophila mechanosensory transduction channel*. Science, 2000. 287(5461): p. 2229-34.
37. **Mochizuki**, T., et al., *PKD2, a gene for polycystic kidney disease that encodes an integral membrane protein*. Science, 1996. 272(5266): p. 1339-42.
38. **Nomura**, H., et al., *Identification of PKDL, a novel polycystic kidney disease 2-like gene whose murine homologue is deleted in mice with kidney and retinal defects*. J Biol Chem, 1998. 273(40): p. 25967-73.
39. **Wu**, G., et al., *Identification of PKD2L, a human PKD2-related gene: tissue-specific expression and mapping to chromosome 10q25*. Genomics, 1998. 54(3): p. 564-8.
40. **Veldhuisen**, B., et al., *Genes homologous to the autosomal dominant polycystic kidney disease genes (PKD1 and PKD2)*. Eur J Hum Genet, 1999. 7(8): p. 860-72.
41. **Guo**, L., et al., *Identification and characterization of a novel polycystin family member, polycystin-L2, in mouse and human: sequence, expression, alternative splicing, and chromosomal localization*. Genomics, 2000. 64(3): p. 241-51.

42. **Sun, M.**, et al., *Mucopolipidosis type IV is caused by mutations in a gene encoding a novel transient receptor potential channel*. Hum Mol Genet, 2000. 9(17): p. 2471-8.
43. **Bassi, M.T.**, et al., *Cloning of the gene encoding a novel integral membrane protein, mucopolipidin-and identification of the two major founder mutations causing mucopolipidosis type IV*. Am J Hum Genet, 2000. 67(5): p. 1110-20.
44. **Bargal, R.**, et al., *Identification of the gene causing mucopolipidosis type IV*. Nat Genet, 2000. 26(1): p. 118-23.
45. **Duncan, L.M.**, et al., *Down-regulation of the novel gene melastatin correlates with potential for melanoma metastasis*. Cancer Res, 1998. 58(7): p. 1515-20.
46. **Xu, X.Z.**, et al., *Regulation of melastatin, a TRP-related protein, through interaction with a cytoplasmic isoform*. Proc Natl Acad Sci U S A, 2001. 98(19): p. 10692-7.
47. **Grimm, C.**, et al., *Molecular and functional characterization of the melastatin-related cation channel TRPM3*. J Biol Chem, 2003. 278(24): p. 21493-501.
48. **Held, K.**, T. Voets, and J. Vriens, *TRPM3 in temperature sensing and beyond*. Temperature (Austin), 2015. 2(2): p. 201-13.
49. **Naylor, J.**, et al., *Pregnenolone sulphate- and cholesterol-regulated TRPM3 channels coupled to vascular smooth muscle secretion and contraction*. Circ Res, 2010. 106(9): p. 1507-15.
50. **Vriens, J.**, et al., *TRPM3 is a nociceptor channel involved in the detection of noxious heat*. Neuron, 2011. 70(3): p. 482-94.
51. **Oberwinkler, J.**, et al., *Alternative splicing switches the divalent cation selectivity of TRPM3 channels*. J Biol Chem, 2005. 280(23): p. 22540-8.
52. **Dembla, S.**, et al., *Anti-nociceptive action of peripheral mu-opioid receptors by G-beta-gamma protein-mediated inhibition of TRPM3 channels*. Elife, 2017. 6.
53. **Quallo, T.**, et al., *G protein betagamma subunits inhibit TRPM3 ion channels in sensory neurons*. Elife, 2017. 6.
54. **Badheka, D.**, et al., *Inhibition of Transient Receptor Potential Melastatin 3 ion channels by G-protein betagamma subunits*. Elife, 2017. 6.
55. **Csanady, L.**, *A new target for G protein signaling*. Elife, 2017. 6.

- 
56. **Launay, P.**, et al., *TRPM4 is a Ca<sup>2+</sup>-activated nonselective cation channel mediating cell membrane depolarization*. *Cell*, 2002. 109(3): p. 397-407.
  57. **Hofmann, T.**, et al., *TRPM5 is a voltage-modulated and Ca(2+)-activated monovalent selective cation channel*. *Curr Biol*, 2003. 13(13): p. 1153-8.
  58. **Perez, C.A.**, et al., *A transient receptor potential channel expressed in taste receptor cells*. *Nat Neurosci*, 2002. 5(11): p. 1169-76.
  59. **Zhang, Y.**, et al., *Coding of sweet, bitter, and umami tastes: different receptor cells sharing similar signaling pathways*. *Cell*, 2003. 112(3): p. 293-301.
  60. **Sano, Y.**, et al., *Immunocyte Ca<sup>2+</sup> influx system mediated by LTRPC2*. *Science*, 2001. 293(5533): p. 1327-30.
  61. **Perraud, A.L.**, et al., *ADP-ribose gating of the calcium-permeable LTRPC2 channel revealed by Nudix motif homology*. *Nature*, 2001. 411(6837): p. 595-9.
  62. **Hara, Y.**, et al., *LTRPC2 Ca<sup>2+</sup>-permeable channel activated by changes in redox status confers susceptibility to cell death*. *Mol Cell*, 2002. 9(1): p. 163-73.
  63. **Wehage, E.**, et al., *Activation of the cation channel long transient receptor potential channel 2 (LTRPC2) by hydrogen peroxide. A splice variant reveals a mode of activation independent of ADP-ribose*. *J Biol Chem*, 2002. 277(26): p. 23150-6.
  64. **Peier, A.M.**, et al., *A TRP channel that senses cold stimuli and menthol*. *Cell*, 2002. 108(5): p. 705-15.
  65. **McKemy, D.D.**, W.M. Neuhausser, and D. Julius, *Identification of a cold receptor reveals a general role for TRP channels in thermosensation*. *Nature*, 2002. 416(6876): p. 52-8.
  66. **Runnels, L.W.**, L. Yue, and D.E. Clapham, *TRP-PLIK, a bifunctional protein with kinase and ion channel activities*. *Science*, 2001. 291(5506): p. 1043-7.
  67. **Nadler, M.J.**, et al., *LTRPC7 is a Mg.ATP-regulated divalent cation channel required for cell viability*. *Nature*, 2001. 411(6837): p. 590-5.
  68. **Voets, T.**, et al., *TRPM6 forms the Mg<sup>2+</sup> influx channel involved in intestinal and renal Mg<sup>2+</sup> absorption*. *J Biol Chem*, 2004. 279(1): p. 19-25.
  69. **Schmitz, C.**, et al., *Regulation of vertebrate cellular Mg<sup>2+</sup> homeostasis by TRPM7*. *Cell*, 2003. 114(2): p. 191-200.

70. **Walder**, R.Y., et al., *Mutation of TRPM6 causes familial hypomagnesemia with secondary hypocalcemia*. Nat Genet, 2002. 31(2): p. 171-4.
71. **Schlingmann**, K.P., et al., *Hypomagnesemia with secondary hypocalcemia is caused by mutations in TRPM6, a new member of the TRPM gene family*. Nat Genet, 2002. 31(2): p. 166-70.
72. **Monteilh-Zoller**, M.K., et al., *TRPM7 provides an ion channel mechanism for cellular entry of trace metal ions*. J Gen Physiol, 2003. 121(1): p. 49-60.
73. **Runnels**, L.W., L. Yue, and D.E. Clapham, *The TRPM7 channel is inactivated by PIP(2) hydrolysis*. Nat Cell Biol, 2002. 4(5): p. 329-36.
74. **Xie**, J., et al., *Phosphatidylinositol 4,5-bisphosphate (PIP(2)) controls magnesium gatekeeper TRPM6 activity*. Sci Rep, 2011. 1: p. 146.
75. **Riazanova**, L.V., et al., *[Novel type of signaling molecules: protein kinases covalently linked to ion channels]*. Mol Biol (Mosk), 2001. 35(2): p. 321-32.
76. **Ryazanov**, A.G., *Elongation factor-2 kinase and its newly discovered relatives*. FEBS Lett, 2002. 514(1): p. 26-9.
77. **Chubanov**, V., et al., *Disruption of TRPM6/TRPM7 complex formation by a mutation in the TRPM6 gene causes hypomagnesemia with secondary hypocalcemia*. Proc Natl Acad Sci U S A, 2004. 101(9): p. 2894-9.
78. **Chubanov**, V. and T. Gudermann, *Trpm6*. Handb Exp Pharmacol, 2014. 222: p. 503-20.
79. **Chubanov**, V., et al., *Hypomagnesemia with secondary hypocalcemia due to a missense mutation in the putative pore-forming region of TRPM6*. J Biol Chem, 2007. 282(10): p. 7656-67.
80. **Fonfria**, E., et al., *Tissue distribution profiles of the human TRPM cation channel family*. J Recept Signal Transduct Res, 2006. 26(3): p. 159-78.
81. **Kunert-Keil**, C., et al., *Tissue-specific expression of TRP channel genes in the mouse and its variation in three different mouse strains*. BMC Genomics, 2006. 7: p. 159.
82. **Schmitz**, C., et al., *The channel kinases TRPM6 and TRPM7 are functionally nonredundant*. J Biol Chem, 2005. 280(45): p. 37763-71.

83. **Fujiwara**, Y. and D.L. Minor, Jr., *X-ray crystal structure of a TRPM assembly domain reveals an antiparallel four-stranded coiled-coil*. J Mol Biol, 2008. 383(4): p. 854-70.
84. **Drennan**, D. and A.G. Ryazanov, *Alpha-kinases: analysis of the family and comparison with conventional protein kinases*. Prog Biophys Mol Biol, 2004. 85(1): p. 1-32.
85. **Ryazanov**, A.G., K.S. Pavur, and M.V. Dorovkov, *Alpha-kinases: a new class of protein kinases with a novel catalytic domain*. Curr Biol, 1999. 9(2): p. R43-5.
86. **Matsushita**, M., et al., *Channel function is dissociated from the intrinsic kinase activity and autophosphorylation of TRPM7/ChaK1*. J Biol Chem, 2005. 280(21): p. 20793-803.
87. **Dorovkov**, M.V. and A.G. Ryazanov, *Phosphorylation of annexin I by TRPM7 channel-kinase*. J Biol Chem, 2004. 279(49): p. 50643-6.
88. **Clark**, K., et al., *TRPM7, a novel regulator of actomyosin contractility and cell adhesion*. EMBO J, 2006. 25(2): p. 290-301.
89. **Perraud**, A.L., et al., *The channel-kinase TRPM7 regulates phosphorylation of the translational factor eEF2 via eEF2-k*. Cell Signal, 2011. 23(3): p. 586-93.
90. **Deason-Towne**, F., A.L. Perraud, and C. Schmitz, *Identification of Ser/Thr phosphorylation sites in the C2-domain of phospholipase C gamma2 (PLCgamma2) using TRPM7-kinase*. Cell Signal, 2012. 24(11): p. 2070-5.
91. **Li**, M., J. Jiang, and L. Yue, *Functional characterization of homo- and heteromeric channel kinases TRPM6 and TRPM7*. J Gen Physiol, 2006. 127(5): p. 525-37.
92. **Zhang**, Z., et al., *The TRPM6 kinase domain determines the Mg.ATP sensitivity of TRPM7/M6 heteromeric ion channels*. J Biol Chem, 2014. 289(8): p. 5217-27.
93. **Romani**, A.M. and A. Scarpa, *Regulation of cellular magnesium*. Front Biosci, 2000. 5: p. D720-34.
94. **Romani**, A.M., *Cellular magnesium homeostasis*. Arch Biochem Biophys, 2011. 512(1): p. 1-23.
95. **Demeuse**, P., R. Penner, and A. Fleig, *TRPM7 channel is regulated by magnesium nucleotides via its kinase domain*. J Gen Physiol, 2006. 127(4): p. 421-34.

96. **Kozak**, J.A. and M.D. Cahalan, *MIC channels are inhibited by internal divalent cations but not ATP*. *Biophys J*, 2003. 84(2 Pt 1): p. 922-7.
97. **Prakriya**, M. and R.S. Lewis, *Separation and characterization of currents through store-operated CRAC channels and Mg<sup>2+</sup>-inhibited cation (MIC) channels*. *J Gen Physiol*, 2002. 119(5): p. 487-507.
98. **Kozak**, J.A., H.H. Kerschbaum, and M.D. Cahalan, *Distinct properties of CRAC and MIC channels in RBL cells*. *J Gen Physiol*, 2002. 120(2): p. 221-35.
99. **Hermosura**, M.C., et al., *Dissociation of the store-operated calcium current I(CRAC) and the Mg-nucleotide-regulated metal ion current MagNuM*. *J Physiol*, 2002. 539(Pt 2): p. 445-58.
100. **Thebault**, S., et al., *Role of the alpha-kinase domain in transient receptor potential melastatin 6 channel and regulation by intracellular ATP*. *J Biol Chem*, 2008. 283(29): p. 19999-20007.
101. **Jiang**, J., M. Li, and L. Yue, *Potentiation of TRPM7 inward currents by protons*. *J Gen Physiol*, 2005. 126(2): p. 137-50.
102. **Li**, M., et al., *Molecular determinants of Mg<sup>2+</sup> and Ca<sup>2+</sup> permeability and pH sensitivity in TRPM6 and TRPM7*. *J Biol Chem*, 2007. 282(35): p. 25817-30.
103. **Kozak**, J.A., et al., *Charge screening by internal pH and polyvalent cations as a mechanism for activation, inhibition, and rundown of TRPM7/MIC channels*. *J Gen Physiol*, 2005. 126(5): p. 499-514.
104. **Abiria**, S.A., et al., *TRPM7 senses oxidative stress to release Zn<sup>2+</sup> from unique intracellular vesicles*. *Proc Natl Acad Sci U S A*, 2017. 114(30): p. E6079-E6088.
105. **Desai**, B.N., et al., *Cleavage of TRPM7 releases the kinase domain from the ion channel and regulates its participation in Fas-induced apoptosis*. *Dev Cell*, 2012. 22(6): p. 1149-62.
106. **Krapivinsky**, G., et al., *The TRPM7 chanzyme is cleaved to release a chromatin-modifying kinase*. *Cell*, 2014. 157(5): p. 1061-72.
107. **Krapivinsky**, G., et al., *Histone phosphorylation by TRPM6's cleaved kinase attenuates adjacent arginine methylation to regulate gene expression*. *Proc Natl Acad Sci U S A*, 2017. 114(34): p. E7092-E7100.

108. **Hanano**, T., et al., *Involvement of TRPM7 in cell growth as a spontaneously activated Ca<sup>2+</sup> entry pathway in human retinoblastoma cells*. J Pharmacol Sci, 2004. 95(4): p. 403-19.
109. **Zierler**, S., et al., *Waixenicin A inhibits cell proliferation through magnesium-dependent block of transient receptor potential melastatin 7 (TRPM7) channels*. J Biol Chem, 2011. 286(45): p. 39328-35.
110. **Chubanov**, V., et al., *Natural and synthetic modulators of SK (K<sub>Ca</sub>)<sub>2</sub> potassium channels inhibit magnesium-dependent activity of the kinase-coupled cation channel TRPM7*. Br J Pharmacol, 2012. 166(4): p. 1357-76.
111. **Hofmann**, T., et al., *Activation of TRPM7 channels by small molecules under physiological conditions*. Pflugers Arch, 2014. 466(12): p. 2177-89.
112. **Schäfer**, S., et al., *Mibefradil represents a new class of benzimidazole TRPM7 channel agonists*. Pflugers Arch, 2016. 468(4): p. 623-34.
113. **Ryazanova**, L.V., et al., *TRPM7 is essential for Mg(2+) homeostasis in mammals*. Nat Commun, 2010. 1: p. 109.
114. **Sahni**, J. and A.M. Scharenberg, *TRPM7 ion channels are required for sustained phosphoinositide 3-kinase signaling in lymphocytes*. Cell Metab, 2008. 8(1): p. 84-93.
115. **Su**, L.T., et al., *TRPM7 regulates cell adhesion by controlling the calcium-dependent protease calpain*. J Biol Chem, 2006. 281(16): p. 11260-70.
116. **Wei**, C., et al., *Calcium flickers steer cell migration*. Nature, 2009. 457(7231): p. 901-5.
117. **Oancea**, E., J.T. Wolfe, and D.E. Clapham, *Functional TRPM7 channels accumulate at the plasma membrane in response to fluid flow*. Circ Res, 2006. 98(2): p. 245-53.
118. **Numata**, T., T. Shimizu, and Y. Okada, *Direct mechano-stress sensitivity of TRPM7 channel*. Cell Physiol Biochem, 2007. 19(1-4): p. 1-8.
119. **Brauchi**, S., et al., *TRPM7 facilitates cholinergic vesicle fusion with the plasma membrane*. Proc Natl Acad Sci U S A, 2008. 105(24): p. 8304-8.
120. **Aarts**, M., et al., *A key role for TRPM7 channels in anoxic neuronal death*. Cell, 2003. 115(7): p. 863-77.

121. **Touyz, R.M.**, *Transient receptor potential melastatin 6 and 7 channels, magnesium transport, and vascular biology: implications in hypertension.* Am J Physiol Heart Circ Physiol, 2008. 294(3): p. H1103-18.
122. **Hermosura, M.C.**, et al., *A TRPM7 variant shows altered sensitivity to magnesium that may contribute to the pathogenesis of two Guamanian neurodegenerative disorders.* Proc Natl Acad Sci U S A, 2005. 102(32): p. 11510-5.
123. **Tseveleki, V.**, et al., *Comparative gene expression analysis in mouse models for multiple sclerosis, Alzheimer's disease and stroke for identifying commonly regulated and disease-specific gene changes.* Genomics, 2010. 96(2): p. 82-91.
124. **Du, J.**, et al., *TRPM7-mediated Ca<sup>2+</sup> signals confer fibrogenesis in human atrial fibrillation.* Circ Res, 2010. 106(5): p. 992-1003.
125. **Jiang, J.**, et al., *Transient receptor potential melastatin 7-like current in human head and neck carcinoma cells: role in cell proliferation.* Cancer Res, 2007. 67(22): p. 10929-38.
126. **Kim, B.J.**, et al., *Suppression of transient receptor potential melastatin 7 channel induces cell death in gastric cancer.* Cancer Sci, 2008. 99(12): p. 2502-9.
127. **Guilbert, A.**, et al., *Evidence that TRPM7 is required for breast cancer cell proliferation.* Am J Physiol Cell Physiol, 2009. 297(3): p. C493-502.
128. **Jin, J.**, et al., *Deletion of Trpm7 disrupts embryonic development and thymopoiesis without altering Mg<sup>2+</sup> homeostasis.* Science, 2008. 322(5902): p. 756-60.
129. **Jin, J.**, et al., *The channel kinase, TRPM7, is required for early embryonic development.* Proc Natl Acad Sci U S A, 2012. 109(5): p. E225-33.
130. **Sah, R.**, et al., *Timing of myocardial trpm7 deletion during cardiogenesis variably disrupts adult ventricular function, conduction, and repolarization.* Circulation, 2013. 128(2): p. 101-14.
131. **Sah, R.**, et al., *Ion channel-kinase TRPM7 is required for maintaining cardiac automaticity.* Proc Natl Acad Sci U S A, 2013. 110(32): p. E3037-46.
132. **Kaitsuka, T.**, et al., *Inactivation of TRPM7 kinase activity does not impair its channel function in mice.* Sci Rep, 2014. 4: p. 5718.

133. **Ryazanova, L.V.**, et al., *Elucidating the role of the TRPM7 alpha-kinase: TRPM7 kinase inactivation leads to magnesium deprivation resistance phenotype in mice*. Sci Rep, 2014. 4: p. 7599.
134. **Zierler, S.**, et al., *TRPM7 kinase activity regulates murine mast cell degranulation*. J Physiol, 2016. 594(11): p. 2957-70.
135. **Antunes, T.T.**, et al., *Transient Receptor Potential Melastatin 7 Cation Channel Kinase: New Player in Angiotensin II-Induced Hypertension*. Hypertension, 2016. 67(4): p. 763-73.
136. **Apa, H.**, et al., *A case of hypomagnesemia with secondary hypocalcemia caused by Trpm6 gene mutation*. Indian J Pediatr, 2008. 75(6): p. 632-4.
137. **Esteban-Oliva, D.**, G. Pintos-Morell, and M. Konrad, *Long-term follow-up of a patient with primary hypomagnesaemia and secondary hypocalcaemia due to a novel TRPM6 mutation*. Eur J Pediatr, 2009. 168(4): p. 439-42.
138. **Guran, T.**, et al., *Clinical and molecular characterization of Turkish patients with familial hypomagnesaemia: novel mutations in TRPM6 and CLDN16 genes*. Nephrol Dial Transplant, 2012. 27(2): p. 667-73.
139. **Habeb, A.M.**, H. Al-Harbi, and K.P. Schlingmann, *Resolving basal ganglia calcification in hereditary hypomagnesemia with secondary hypocalcemia due to a novel TRPM6 gene mutation*. Saudi J Kidney Dis Transpl, 2012. 23(5): p. 1038-42.
140. **Schlingmann, K.P.**, et al., *Novel TRPM6 mutations in 21 families with primary hypomagnesemia and secondary hypocalcemia*. J Am Soc Nephrol, 2005. 16(10): p. 3061-9.
141. **Zhao, Z.**, et al., *Novel TRPM6 mutations in familial hypomagnesemia with secondary hypocalcemia*. Am J Nephrol, 2013. 37(6): p. 541-8.
142. **Walder, R.Y.**, et al., *Mice defective in Trpm6 show embryonic mortality and neural tube defects*. Hum Mol Genet, 2009. 18(22): p. 4367-75.
143. **Woudenberg-Vrenken, T.E.**, et al., *Transient receptor potential melastatin 6 knockout mice are lethal whereas heterozygous deletion results in mild hypomagnesemia*. Nephron Physiol, 2011. 117(2): p. p11-9.
144. **Chubanov, V.**, et al., *Epithelial magnesium transport by TRPM6 is essential for prenatal development and adult survival*. Elife, 2016. 5.

145. **Copp**, A.J. and N.D. Greene, *Genetics and development of neural tube defects*. J Pathol, 2010. 220(2): p. 217-30.
146. **Swaminathan**, R., *Magnesium metabolism and its disorders*. Clin Biochem Rev, 2003. 24(2): p. 47-66.
147. **Saris**, N.E., et al., *Magnesium. An update on physiological, clinical and analytical aspects*. Clin Chim Acta, 2000. 294(1-2): p. 1-26.
148. **Altura**, B.M. and B.T. Altura, *Role of magnesium in patho-physiological processes and the clinical utility of magnesium ion selective electrodes*. Scand J Clin Lab Invest Suppl, 1996. 224: p. 211-34.
149. **Wolf**, F.I., et al., *Cell physiology of magnesium*. Mol Aspects Med, 2003. 24(1-3): p. 11-26.
150. **Quamme**, G.A., *Molecular identification of ancient and modern mammalian magnesium transporters*. Am J Physiol Cell Physiol, 2010. 298(3): p. C407-29.
151. **Simon**, D.B., et al., *Paracellin-1, a renal tight junction protein required for paracellular Mg<sup>2+</sup> resorption*. Science, 1999. 285(5424): p. 103-6.
152. **Hou**, J., et al., *Claudin-16 and claudin-19 interaction is required for their assembly into tight junctions and for renal reabsorption of magnesium*. Proc Natl Acad Sci U S A, 2009. 106(36): p. 15350-5.
153. **Goytain**, A. and G.A. Quamme, *Identification and characterization of a novel mammalian Mg<sup>2+</sup> transporter with channel-like properties*. BMC Genomics, 2005. 6: p. 48.
154. **Smith**, R.L., L.J. Thompson, and M.E. Maguire, *Cloning and characterization of MgtE, a putative new class of Mg<sup>2+</sup> transporter from Bacillus firmus OF4*. J Bacteriol, 1995. 177(5): p. 1233-8.
155. **Wabakken**, T., et al., *The human solute carrier SLC41A1 belongs to a novel eukaryotic subfamily with homology to prokaryotic MgtE Mg<sup>2+</sup> transporters*. Biochem Biophys Res Commun, 2003. 306(3): p. 718-24.
156. **Goytain**, A. and G.A. Quamme, *Functional characterization of human SLC41A1, a Mg<sup>2+</sup> transporter with similarity to prokaryotic MgtE Mg<sup>2+</sup> transporters*. Physiol Genomics, 2005. 21(3): p. 337-42.
157. **Goytain**, A. and G.A. Quamme, *Functional characterization of the mouse [corrected] solute carrier, SLC41A2*. Biochem Biophys Res Commun, 2005. 330(3): p. 701-5.

158. **Sahni**, J., B. Nelson, and A.M. Scharenberg, *SLC41A2 encodes a plasma-membrane Mg<sup>2+</sup> transporter*. *Biochem J*, 2007. 401(2): p. 505-13.
159. **de Baaij**, J.H., et al., *Identification of SLC41A3 as a novel player in magnesium homeostasis*. *Sci Rep*, 2016. 6: p. 28565.
160. **Mastrototaro**, L., et al., *Solute carrier 41A3 encodes for a mitochondrial Mg(2+) efflux system*. *Sci Rep*, 2016. 6: p. 27999.
161. **Wang**, C.Y., et al., *Molecular cloning and characterization of a novel gene family of four ancient conserved domain proteins (ACDP)*. *Gene*, 2003. 306: p. 37-44.
162. **Wang**, C.Y., et al., *Molecular cloning and characterization of the mouse Acdp gene family*. *BMC Genomics*, 2004. 5(1): p. 7.
163. **Gibson**, M.M., et al., *Magnesium transport in Salmonella typhimurium: the influence of new mutations conferring Co<sup>2+</sup> resistance on the CorA Mg<sup>2+</sup> transport system*. *Mol Microbiol*, 1991. 5(11): p. 2753-62.
164. **Goytain**, A. and G.A. Quamme, *Functional characterization of ACDP2 (ancient conserved domain protein), a divalent metal transporter*. *Physiol Genomics*, 2005. 22(3): p. 382-9.
165. **Butler**, M.G., *Prader-Willi syndrome: current understanding of cause and diagnosis*. *Am J Med Genet*, 1990. 35(3): p. 319-32.
166. **Nicholls**, R.D. and J.L. Knepper, *Genome organization, function, and imprinting in Prader-Willi and Angelman syndromes*. *Annu Rev Genomics Hum Genet*, 2001. 2: p. 153-75.
167. **Goytain**, A., et al., *NIPA1(SPG6), the basis for autosomal dominant form of hereditary spastic paraplegia, encodes a functional Mg<sup>2+</sup> transporter*. *J Biol Chem*, 2007. 282(11): p. 8060-8.
168. **Goytain**, A., R.M. Hines, and G.A. Quamme, *Functional characterization of NIPA2, a selective Mg<sup>2+</sup> transporter*. *Am J Physiol Cell Physiol*, 2008. 295(4): p. C944-53.
169. **Goytain**, A. and G.A. Quamme, *Identification and characterization of a novel family of membrane magnesium transporters, MMgT1 and MMgT2*. *Am J Physiol Cell Physiol*, 2008. 294(2): p. C495-502.

170. **Wiesenberger**, G., M. Waldherr, and R.J. Schweyen, *The nuclear gene MRS2 is essential for the excision of group II introns from yeast mitochondrial transcripts in vivo*. J Biol Chem, 1992. 267(10): p. 6963-9.
171. **Bui**, D.M., et al., *The bacterial magnesium transporter CorA can functionally substitute for its putative homologue Mrs2p in the yeast inner mitochondrial membrane*. J Biol Chem, 1999. 274(29): p. 20438-43.
172. **Zsurka**, G., J. Gregan, and R.J. Schweyen, *The human mitochondrial Mrs2 protein functionally substitutes for its yeast homologue, a candidate magnesium transporter*. Genomics, 2001. 72(2): p. 158-68.
173. **Kolisek**, M., et al., *Mrs2p is an essential component of the major electrophoretic Mg<sup>2+</sup> influx system in mitochondria*. EMBO J, 2003. 22(6): p. 1235-44.
174. **Konrad**, M., K.P. Schlingmann, and T. Gudermann, *Insights into the molecular nature of magnesium homeostasis*. Am J Physiol Renal Physiol, 2004. 286(4): p. F599-605.
175. **Ayuk**, J. and N.J. Gittoes, *Contemporary view of the clinical relevance of magnesium homeostasis*. Ann Clin Biochem, 2014. 51(Pt 2): p. 179-88.
176. **de Baaij**, J.H., J.G. Hoenderop, and R.J. Bindels, *Magnesium in man: implications for health and disease*. Physiol Rev, 2015. 95(1): p. 1-46.
177. **Dietrich**, A., V. Chubanov, and T. Gudermann, *Renal TRP channels*. J Am Soc Nephrol, 2010. 21(5): p. 736-44.
178. **Dilworth**, M.R. and C.P. Sibley, *Review: Transport across the placenta of mice and women*. Placenta, 2013. 34 Suppl: p. S34-9.
179. **Simmons**, D.G. and J.C. Cross, *Determinants of trophoblast lineage and cell subtype specification in the mouse placenta*. Dev Biol, 2005. 284(1): p. 12-24.
180. **Stritt**, S., et al., *Defects in TRPM7 channel function deregulate thrombopoiesis through altered cellular Mg(2+) homeostasis and cytoskeletal architecture*. Nat Commun, 2016. 7: p. 11097.
181. **Feroli**, S., et al., *TRPM6 and TRPM7 differentially contribute to the relief of heteromeric TRPM6/7 channels from inhibition by cytosolic Mg<sup>2+</sup> and Mg.ATP*. Sci Rep, 2017. 7(1): p. 8806.
182. **Hayashi**, S., T. Tenzen, and A.P. McMahon, *Maternal inheritance of Cre activity in a Sox2Cre deleter strain*. Genesis, 2003. 37(2): p. 51-3.

183. **Tanaka**, S., et al., *Promotion of trophoblast stem cell proliferation by FGF4*. Science, 1998. 282(5396): p. 2072-5.
184. **Erlebacher**, A., K.A. Price, and L.H. Glimcher, *Maintenance of mouse trophoblast stem cell proliferation by TGF-beta/activin*. Dev Biol, 2004. 275(1): p. 158-69.
185. **Natale**, D.R., et al., *Activin promotes differentiation of cultured mouse trophoblast stem cells towards a labyrinth cell fate*. Dev Biol, 2009. 335(1): p. 120-31.
186. **Carette**, J.E., et al., *Ebola virus entry requires the cholesterol transporter Niemann-Pick C1*. Nature, 2011. 477(7364): p. 340-3.
187. **Essletzbichler**, P., et al., *Megabase-scale deletion using CRISPR/Cas9 to generate a fully haploid human cell line*. Genome Res, 2014. 24(12): p. 2059-65.
188. **Blomen**, V.A., et al., *Gene essentiality and synthetic lethality in haploid human cells*. Science, 2015. 350(6264): p. 1092-6.
189. **Wang**, T., et al., *Identification and characterization of essential genes in the human genome*. Science, 2015. 350(6264): p. 1096-101.
190. **Tiedt**, R., et al., *Pf4-Cre transgenic mice allow the generation of lineage-restricted gene knockouts for studying megakaryocyte and platelet function in vivo*. Blood, 2007. 109(4): p. 1503-6.
191. **Mederos y Schnitzler**, M., et al., *Evolutionary determinants of divergent calcium selectivity of TRPM channels*. FASEB J, 2008. 22(5): p. 1540-51.
192. **Godfrey**, K.M., *The role of the placenta in fetal programming-a review*. Placenta, 2002. 23 Suppl A: p. S20-7.
193. **Kerschbaum**, H.H., J.A. Kozak, and M.D. Cahalan, *Polyvalent cations as permeant probes of MIC and TRPM7 pores*. Biophys J, 2003. 84(4): p. 2293-305.
194. **Yamaguchi**, H., et al., *Crystal structure of the atypical protein kinase domain of a TRP channel with phosphotransferase activity*. Mol Cell, 2001. 7(5): p. 1047-57.
195. **Chubanov**, V., et al., *Emerging roles of TRPM6/TRPM7 channel kinase signal transduction complexes*. Naunyn Schmiedebergs Arch Pharmacol, 2005. 371(4): p. 334-41.

- 
196. **Visser, D.**, et al., *TRPM7 triggers Ca<sup>2+</sup> sparks and invadosome formation in neuroblastoma cells*. *Cell Calcium*, 2013. 54(6): p. 404-15.
  197. **Wong, R.**, et al., *Activation of TRPM7 by naltriben enhances migration and invasion of glioblastoma cells*. *Oncotarget*, 2017.
  198. **Bernhardt, M.L.**, et al., *Store-operated Ca<sup>2+</sup> entry is not required for fertilization-induced Ca<sup>2+</sup> signaling in mouse eggs*. *Cell Calcium*, 2017.
  199. **Inoue, K.**, D. Branigan, and Z.G. Xiong, *Zinc-induced neurotoxicity mediated by transient receptor potential melastatin 7 channels*. *J Biol Chem*, 2010. 285(10): p. 7430-9.
  200. **Leng, T.D.**, et al., *Local anesthetic lidocaine inhibits TRPM7 current and TRPM7-mediated zinc toxicity*. *CNS Neurosci Ther*, 2015. 21(1): p. 32-9.
  201. **Kim, Y.**, et al., *Stress hormone potentiates Zn(2+)-induced neurotoxicity via TRPM7 channel in dopaminergic neuron*. *Biochem Biophys Res Commun*, 2016. 470(2): p. 362-7.

# Acknowledgments

This work was performed in the laboratories of Prof. Dr. Thomas Gudermann at the Walther-Straub-Institute of Pharmacology and Toxicology of the Ludwig-Maximilians-University in Munich. This thesis would not have been possible without the professional and moral assistance and support of various people, to whom I would like to express my profound gratitude.

First at all, I wish to acknowledge my principal supervisor (“zweiter Gutachter”), **Prof. Dr. Thomas Gudermann**, for providing me the opportunity to realize the PhD in his laboratory, for critically reading of this work, and for the scientific support as part of my thesis committee.

I would also like to sincerely thank my supervisor from the biology faculty (“erster Gutachter”), **Prof. Dr. Barbara Conradt**, for her willingness to be part of my thesis committee, and **PD. Dr. Eric Lambie** for the accurate evaluation of this work.

I would like to express my gratitude to **Dr. Vladimir Chubanov** for supervising this thesis, for assigning to me exiting research projects and for his scientific guidance. I particularly appreciate his trust in my capabilities, his massive support in hard times and his precious scientific suggestions. Thanks to him, I could enhance my scientific knowledge and technical skills.

I would like to take the opportunity to thank **Dr. Susanna Zierler** for providing me a rapid and comprehensive introduction into electrophysiological technique, for extremely helpful professional advice and useful comments on my work. I greatly appreciate her patience and time that she invested in my projects, and the care in answering all my questions.

I am deeply indebted to all my past and present colleagues: **Banu Akdogan, Serap Erdogmus, Sebastian Schäfer, Lorenz Mittermeier, Benjamin Stadlbauer, Miyuki Egawa**, and **Annika Wisnowsky** for the friendly working atmosphere in the laboratory, for their support, encouragement and advice. A special thank goes to Banu, who became a very good friend in the last two years, for supporting me in tough time, for her unlimited patience to listen all my problems and for encouraging words in stressful times. I strongly hope, I gave her as much support as she gave me.

For the valuable technical assistance in the laboratory and the excellent experimental contribution, I am deeply grateful to **Joanna Zaißerer**, **Renate Heilmair**, **Ludmila Sytik** and **Sheila Geiger**. In particular, I am really thankful to Joanna not just for the preparation of most part of my experiments, but also for patiently supporting me and for her encouragement during troubling times. Many thanks also to all members of the animal facility for the good organization, especially to **Petra Eigner**.

I would also to extend my thanks to all members of secretariat team for the outstanding administrative support, especially to **Jutta Schreier**, for her unlimited help in the complicated world of german bureaucracy.

**Prof. Harald Mückter** deserves an enormous thank for the lunchtimes spent together in the kitchen, for the interested conversations, for his help and support.

On a personal level, I cannot omit to thank my beloved friends from Italy: **Elena Alvoni**, **Marcella Forni** and **Emanuella Santovito**, who supported me in my decision to move to Germany to pursue a PhD and always trusted my professional abilities.

My darling parents, **Francesco Ferioli** and **Cosetta Goretti**, deserve my deepest gratitude for their financial and moral support during my studies and for encouraging me to start this PhD in Germany. A special thanks goes to my sister, **Sara Ferioli**, who always gave me help and advice whenever I needed.

Last but not least, I want to thank **Łukasz Kłos**, my boyfriend and father of my little precious treasure **Maja**, who really showed an indefinite patience in listening all my work problems and trying to give me a proper support during work-related ups and downs. *Kocham cię...*

---

# Curriculum vitae

## **Personal data:**

Name: Silvia Ferioli  
Birth date: 15.04.1984  
Birth place: Cento (FE), Italy  
Citizenship: Italian  
Address: Stahlgruber-Wohnpark 3, 85586 Poing  
Mobile phone: +49 0176 38654172  
E-mail: silviaferioli@hotmail.com

## **Scientific education:**

03/2012 – present     Dissertation at Walther-Straub-Institute of Pharmacology and Toxicology, Ludwig Maximilians University of Munich, Germany  
Doctoral thesis: Cellular functions of the kinase-coupled TRPM6/TRPM7 channels  
Supervisors: Prof. Dr. med. Thomas Gudermann, Prof. Dr. Barbara Conradt, Dr. Vladimir Chubanov

10/2007 - 04/2011     Master of Science in Biology (Major: health promotion) at University of Modena and Reggio Emilia, Italy  
Master's thesis: Effects of CYP19A1 mutations on aromatase expression in vitro  
Supervisors: Prof. Manuela Simoni, Dr. Elisa Pignatti  
Final grade: 110/110 *cum laude*

09/2003 - 07/2007     Bachelor of Science in Biology (Major: molecular cell biology) at University of Modena and Reggio Emilia, Italy  
Bachelor's thesis: FISH in the diagnosis of myelodysplastic syndrome in onco-hematology  
Supervisors: Dr. Paola Temperani, Dr. Francesca Giacobbi  
Final grade: 110/110 *cum laude*

## **Secondary education:**

09/2003 - 07/2007     High school diploma (Abitur) at Liceo Cevolani of Cento (FE), Italy.  
Final grade: 86/100

**Publications:**

- 1) **Ferioli S**, Zierler S, Zaißerer J, Schredelseker J, Gudermann T, Chubanov V. TRPM6 and TRPM7 differentially contribute to the relief of heteromeric TRPM6/7 channels from inhibition by cytosolic Mg<sup>2+</sup> and Mg-ATP. *Sci Rep.* 2017 Aug 18;7(1):8806.
- 2) Chubanov V, **Ferioli S**, Gudermann T. Assessment of TRPM7 functions by drug-like small molecules. *Cell Calcium.* 2017 Mar 14. pii: S0143-4160(17)30051-9. Review.
- 3) Chubanov V, **Ferioli S**, Wisnowsky A, Simmons DG, Leitzinger C, Einer C, Jonas W, Shymkiv Y, Bartsch H, Braun A, Akdogan B, Mittermeier L, Sytik L, Torben F, Jurinovic V, van der Vorst EP, Weber C, Yildirim ÖA, Sotlar K, Schürmann A, Zierler S, Zischka H, Ryazanov AG, Gudermann T. Epithelial magnesium transport by TRPM6 is essential for prenatal development and adult survival. *Elife.* 2016 Dec 19;5. pii: e20914.
- 4) Stritt S, Nurden P, Favier R, Favier M, **Ferioli S**, Gotru SK, van Eeuwijk JM, Schulze H, Nurden AT, Lambert MP, Turro E, Burger-Stritt S, Matsushita M, Mittermeier L, Ballerini P, Zierler S, Laffan MA, Chubanov V, Gudermann T, Nieswandt B. Defects in TRPM7 channel function deregulate thrombopoiesis through altered cellular Mg<sup>2+</sup> homeostasis and cytoskeletal architecture. *Nat Commun.* 2016 Mar 29;7:11097.
- 5) Schäfer S, **Ferioli S**, Hofmann T, Zierler S, Gudermann T, Chubanov V. Mibefradil represents a new class of benzimidazole TRPM7 channel agonists. *Pflugers Arch.* 2016 Apr;468(4):623-34.
- 6) Chubanov V, Schäfer S, **Ferioli S**, Gudermann T. Natural and Synthetic Modulators of the TRPM7 Channel. *Cells.* 2014 Nov 27;3(4):1089-101. Review.

**Conferences:**

- 1) **Ferioli S**, Egawa M, Mittermeier L, Zierler S, Gudermann T, Chubanov V. Genetic and pharmacological inactivation of TRPM7 in human leukemia cells. Deutschen Gesellschaft für experimentelle und klinische Pharmakologie und Toxikologie (DGPT), 6th-9th March 2017. Heidelberg, Germany. Poster.
- 2) **Ferioli S**, Zierler S, Gudermann T, Chubanov V. Functional interplay of TRPM6 and TRPM7 in trophoblast stem cells. Third Leuven TRP Symposium, 16th-18th September 2015. Leuven, Belgium. Oral presentation.
- 3) **Ferioli S**, Zierler S, Sytik L, Gudermann T, Chubanov V. Functional interplay of TRPM6 and TRPM7 in trophoblast stem cells. Deutschen Gesellschaft für experimentelle und klinische Pharmakologie und Toxikologie (DGPT), 10th-12th March 2015. Kiel, Germany. Poster.
- 4) **Ferioli S**, Zierler S, Gudermann T, Chubanov V. Functional interplay of TRPM6 and TRPM7 in trophoblast stem cells. 5th International Postgraduate Symposium in Biomedical Sciences, 3rd-5th November 2014. The School of Biomedical Sciences, the University of Queensland, Australia. Oral presentation.

- 5) **Feroli S**, Wisnowsky A, Simmons D, Trotzenko I, Sytik L, Heilmair R, Hofmann T, Gudermann T, Chubanov. Genetic delineation of the kinase and channel functions of TRPM7 in embryonic development and postnatal life of mice. Deutschen Gesellschaft für experimentelle und klinische Pharmakologie und Toxikologie (DGPT), 5th-7th March 2013. Halle, Germany. Poster.